國立成功大學太空與電漿科學研究所

碩士論文

均勻電漿中的自由電子流之模擬

Simulation of free-streaming electrons in a uniform plasma

研究生：楊宗桓

指導教授：張博宇博士

中華民國一〇七年七月

國立成功大學

碩士論文

均勻電漿中的自由電子流之模擬

Simulation of free-streaming electrons in a uniform plasma

研究生：楊宗桓

本論文業經審查及口試合格特此證明

論文考試委員：

藍 永 張

談永頤

張博宇

指導教授：張博宇

系(所)主管：陳炳志

電漿所 所長 陳炳志

中 華 民 國 107 年 7 月 19 日

摘要

本論文旨在透過數值模擬來探討均勻電漿中的自由電子流的不穩定性。自由電子流可以被我們正在建造的平行板電容(Parallel-plate capacitor bank)脈衝系統(Pulsed-power system)產生，而均勻電漿可以利用輝光放電產生。伏拉索夫解法器通常是種用動力學理論來模擬電漿現象的方法，因此，我們使用伏拉索夫解法器來模擬自由電子流。我們先透過模擬雙流不穩定性來驗證我們開發的伏拉索夫解法器是否正確，雙流不穩定性的能量守恆會被確認，而模擬中的不穩定成長率也會被拿來和理論比較。我們所模擬的自由電子流的熱速度為 $v_{th}=1$，電子束平均速度 v_b 分別設為 $v_b=2$、3、4、5，自由電子流與背景電子數量密度的比值 γ 則分別設為 $\gamma=0.5$、1、2。因此，會有 12 種不同的初始條件。我們發現，不穩定性的成長會發生在 $v_b=3$ 和 $v_b=4$ 的時候，$v_b=2$ 和 $v_b=5$ 時則不會。在 $v_b=2$ 時，分佈函數因受熱運動影響而擴散開，在 $v_b=5$ 時，背景電漿和電子流間的相對速度太大以至於無法互相影響。$v_b=3$ 和 $v_b=4$ 時的最高成長率發生在 $\gamma=1$ 時，但是成長率在不同的 γ 中都未超過 10%。

關鍵詞：自由電子流，伏拉索夫解法器，動能理論，雙流不穩定性

Abstract

This thesis is to study the free-streaming electrons moving in a uniform background plasma in numerical simulation. Free-streaming electrons can be generated in our parallel plate capacitor bank (PPCB) system under construction. Uniform plasma can be generated by glow discharge. The simulation code of free-streaming electrons is implemented via Vlasov solver. Vlasov solver is usually used to simulate plasma phenomena in kinetic regime. Two-stream instability is used to benchmark the code. The energy conservation is checked and energy growth rate of two-stream instability calculated from simulation results and theory are compared. The free-streaming electrons is simulated with thermal velocity $v_{th} = 1$, beam velocity $v_b = 2, 3, 4, 5$, respectively. Ratios between the number density of the free streaming electrons and the background electron density $\gamma = 0.5, 1, 2$, respectively. Therefore, there are 12 different initial conditions were simulated. Instabilities occur when beam velocity $v_b = 3$ and $v_b = 4$. No instability occurs for $v_b = 2$ and $v_b = 5$. In $v_b = 2$, instability v_b is diffused by electron of thermal motions. In $v_b = 5$, the relative velocity between electrons and the background plasma is too large so that they don't interact with each other. The growth rate is the highest when $\gamma = 1$. Nevertheless, the growth rate in different γ doesn't change over 10% between different γ we simulated.

Keywords: Free-streaming electrons, Vlasov solver, Kinetic regime, Two-stream instability

Acknowledgment

首先我想感謝張博宇教授,在這段時間以來不厭其煩的指導我,在課業上教了我許多知識,並且做了良好的規劃,讓我可以一步步的完成研究,而且在想法上也給了我許多不同以往的啟發,能跟著張博宇教授做研究是件很幸運的事情。接著感謝口試委員們願意幫我口試。另外也要感謝我同個研究室的同學,感謝你們替我買便當和陪我度過許多歡樂的日子,並讓我可以順利的度過研究所生活。最後要感謝我的家人的支持,我才能順利的完成這份學業。

Table of Contents

List of tables

List of figures

Chapter 1 Introduction

This thesis is to study free-streaming electrons in a uniform background plasma in simulations. The distribution function of electrons is very different from Maxwellian. Therefore, the phenomenon happens in kinetic regime. Vlasov equation will be solved numerically. In experiment, to generate free-streaming electron beams, a pulsed-power system is used. A pulsed-power system called parallel plate capacitor bank (PPCB) is being built in our group. It can generate a current up to ~800kA with a rise time of ~700ns. It can potentially generate a free-streaming electron beam with kinetic energy up to 80kV. In order to study the free-streaming electrons in a uniform plasma, a DC glow discharge will be used. The potential experimental setup is shown in Figure 1-1. Therefore, we are simulating the experiments of such electron beams in a background plasmas that will be conducted in the future.

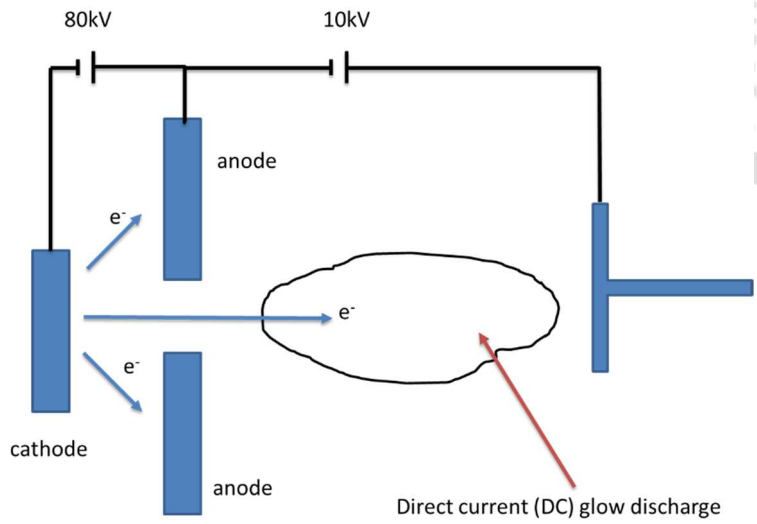

Figure 1-1 Schematic of experiment setup of generating free-streaming electrons.

1.1 Parallel plate capacitor bank

A pulsed-power system is a device that stores energy first and releases it in a short period of time to provide high power output. The system is built in a parallel plate capacitor bank (PPCB). The side view and top view of PPCB system are shown in Figure 1-2 and Figure 1-3 respectively, and Figure 1-4 shows the 3D configuration of PPCB system. The configuration of PPCB is introduced below. It consists of 20 capacitors. Each capacitor has 1μF capacitance. Two capacitors connected in series is called one stage. Ten stages are connected in parallel. Therefore, one stage has 0.5μF capacitance and ten stages connected in parallel have totally 5μF capacitance. Figure 1-5 is the circuit diagram of PPCB system. When PPCB system is charged to 80kV, it stores 16kJ energy. On the other hand, when it is discharged, it provides a current with ~800kA. Parameters of PPCB system are shown in Table 1-1.

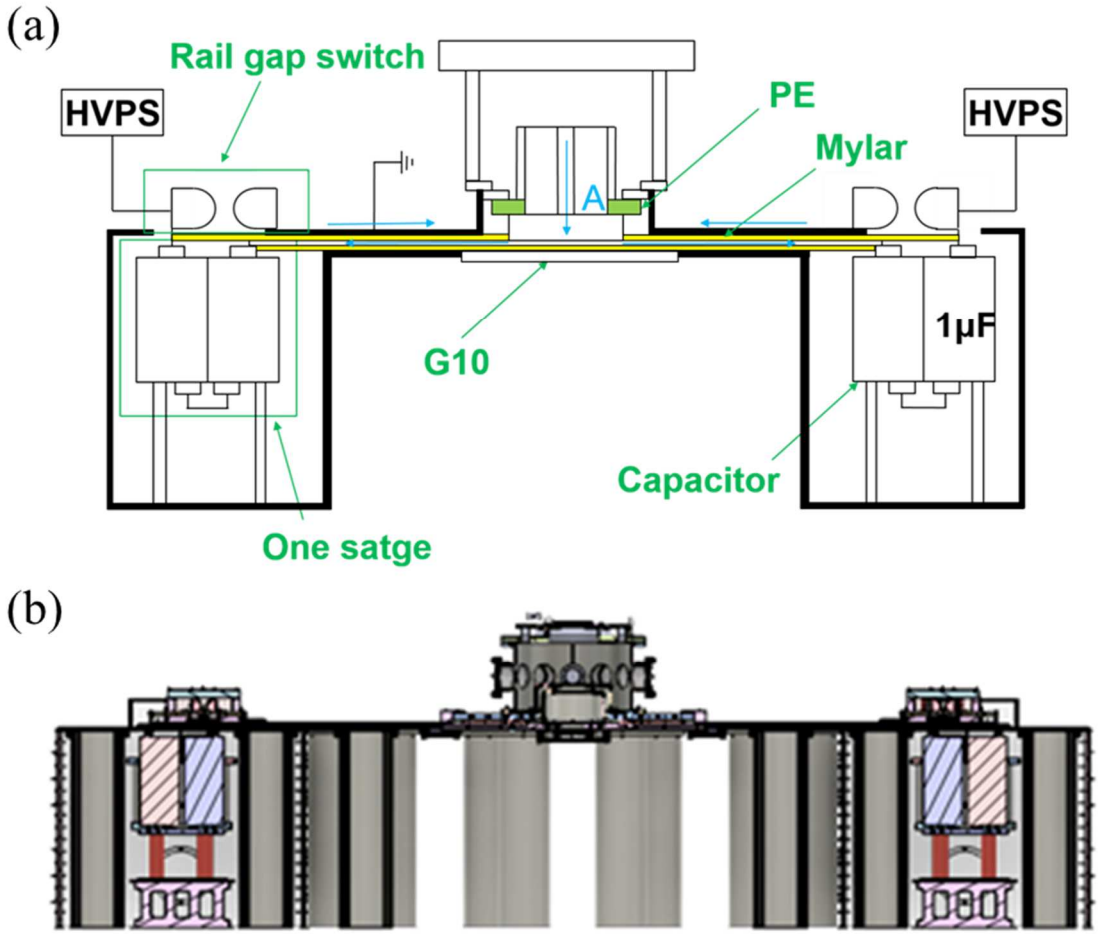

Figure 1-2 (a) Side view of the concept of PPCB. (b) Side view of the schematic of PPCB.

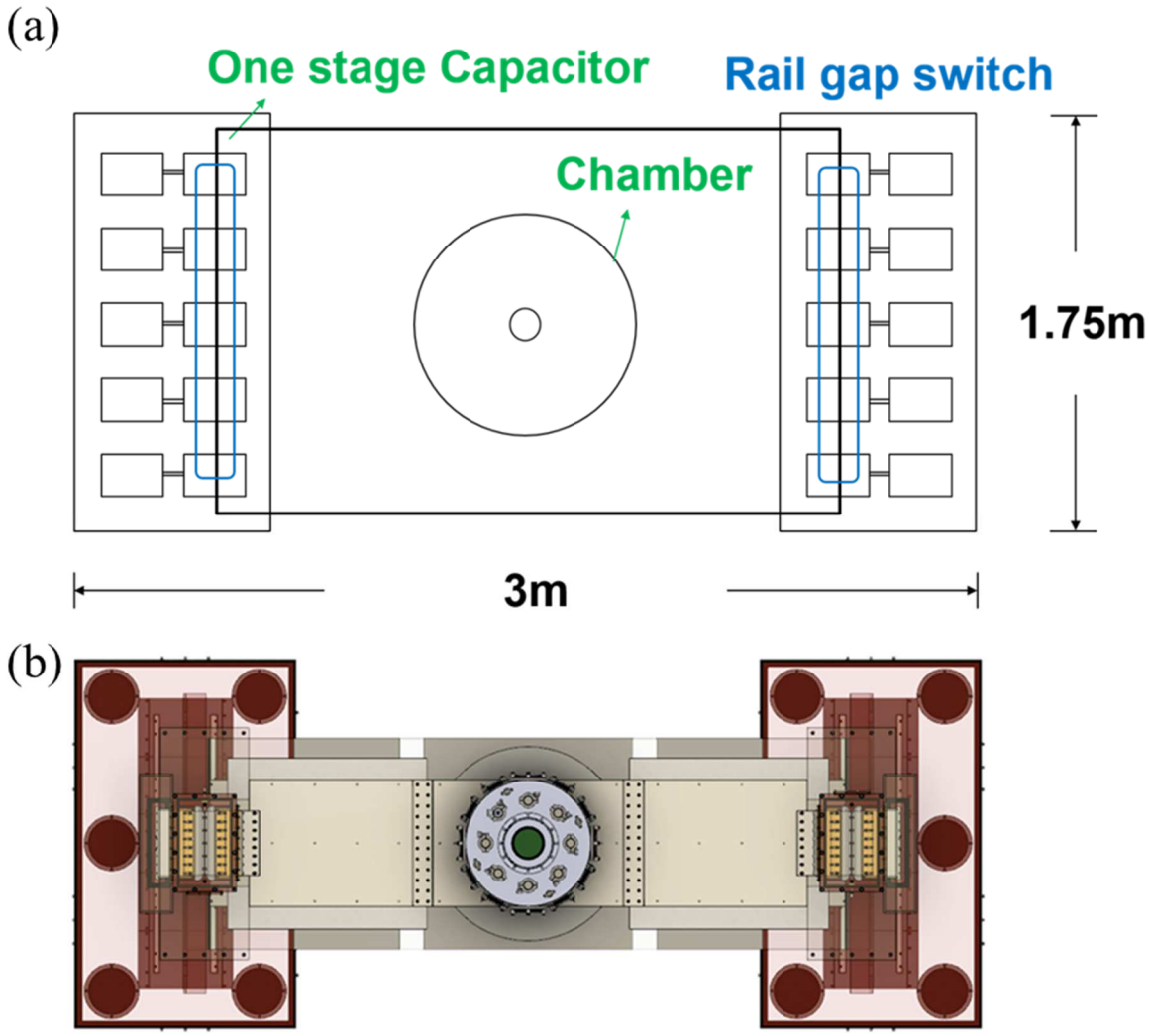

Figure 1-3 (a) Top view of the concept of PPCB. (b) Top view of the schematic of PPCB.

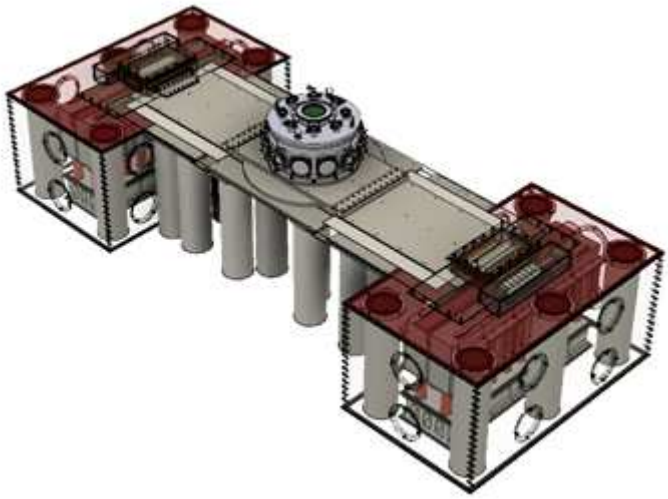

Figure 1-4 Schematic of PPCB.

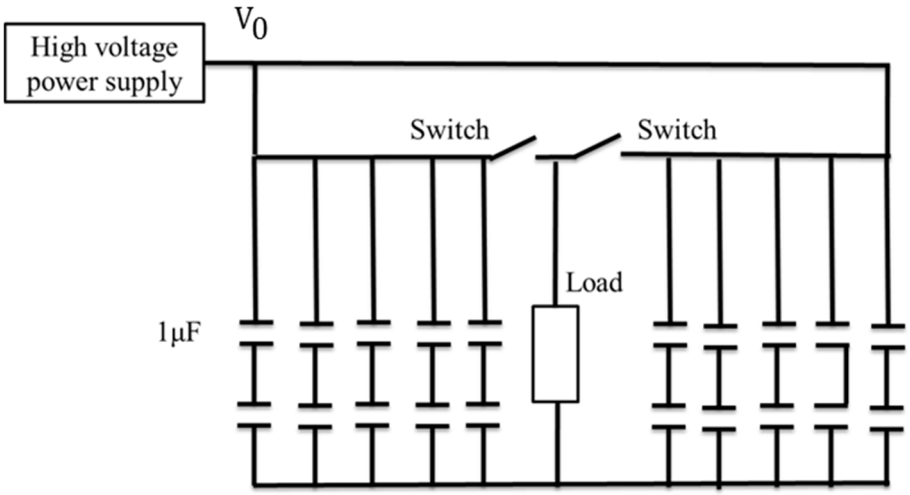

Figure 1-5 Circuit diagram of PPCB system.

Table 1-1 Parameters of PPCB system.

Capacitance	1 μF /each
# of capacitor	20
Total capacitance	5 μF
Voltage	80 kV

Total energy	16 kJ
Peak current	~800 kA
Rise time	~700 ns
Power	16 GW

1.2 Free-streaming electrons

Free-streaming electrons is studied in a uniform background plasma in this thesis. Free-streaming electrons can be generated by a strong electric field. A pulse electric field for accelerating electrons can be generated by the PPCB system in building by us. The pulsed-power system in our lab can provide a pulsed voltage up to 80kV, i.e., electrons can be accelerated to 80keV. Figure 1-1 is shown the potential experimental setup. The cathode is a disk while the anode is a ring electrode. When the system is discharged electrode, most electrons move from the cathode to the anode. Few electrons pass through the ring anode and become the same of the free-streaming electrons. Because of heavier weight of ions than electrons, electrons propagates much faster than ions when they have the same kinetic energy. Therefore, ions are treated as stationary. The distribution function of the experiment is shown in Figure 1-6. A Gaussian at v=0 represents the electrons of the background plasma. The Gaussian away from the center represents the free-streaming electrons. The plasma is in kinetic regime and is simulated by solving Vlasov equation.

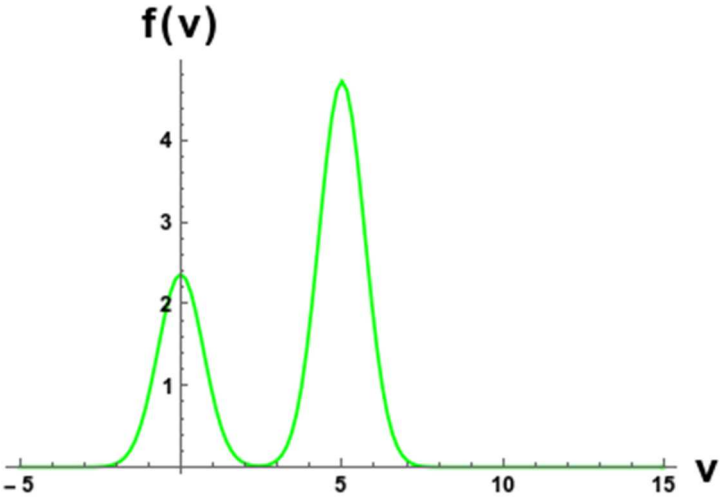

Figure 1-6 Distribution of free-streaming electrons.

1.3 Vlasov-Piosson system

Vlaosv equation describes how distribution functions evolve in kinetic regime without collisions. The main equations are called Vlasov-Poisson equations. They are given as following:

$$\partial_t f+\vec{v}\vec{\nabla}_x f+\frac{e\vec{E}}{m_e}\vec{\nabla}_v f=0, \text{ Vlasov equation,} \tag{1-1}$$

$$\vec{\nabla}_x^2\varphi=-\vec{\nabla}_x\vec{E}=-\frac{e}{\epsilon_0}(n_i-n_e), \text{ Poisson's equation.} \tag{1-2}$$

These two equations are called Vlasov-Poisson system. Vlasov equation is a partial differential equation describing time evolution of the distribution function of plasma consisting of charged particles interaction. Poisson's equation describes how the electric potential charges in the plasma. Numerical simulation methods and their benchmark of Vlasov solver are discussed in Chapter 2. Theory of two-stream instability is used to benchmark Vlasov solver. The simulation results are benchmark by compared with theory of two-stream instability. The simulation results of free-streaming electrons are discussed in Chapter 3. The conclusion and future work are shown in Chapter 4.

Chapter 2 Vlasov solver

Vlasov solver is used to solve Vlasov equation numerically to study plasma phenomena without collisions in kinetic regime. When simulating plasma in kinetic regime, there are two kinds of methods to simulate: Particle-in-Cell (PIC) method and Vlasov solver. Compared to PIC, Vlasov solver is harder for massively parallel computation, but has no noise problem in kinetic regime. One-dimensional (1-D) Vlasov-Poisson system is used in this thesis. Therefore, only one-dimensional electrostatic problems are simulated. To verify our Vlasov solver, two-stream instability is simulated. The instability occurs when two counter-streaming plasma beams interact with each others. In this chapter, all subroutines of Vlasov solver are introduced. In section 2.1, the basic equations in Vlasov solver are introduced first. These equations are called Vlasov-Poisson's system. In section 2.2, Vlasov-Poisson system is normalized. In section 2.3, the simulation sequence and subroutines are introduced. In section 2.4, the numerical grids and range of simulation are introduced. Furthermore in section 2.5, details of numerical methods in Vlasov solver to solve the equations in Vlasov-Poisson system are discussed. All subroutines are benchmarked. Finally in section 2.6, The two-stream instability is used to benchmark the whole Vlasov solver.

2.1 Basic equations

The basic equations of Vlasov solver in one dimension is shown in Eq.(2-1) to Eq.(2-5). Eq.(2-1) is Vlasov equation in one dimension, $f(x,v,t)$ is the distribution function of electrons in plasma, x and v are position and velocity of electrons respectively, and t is time. $a(x)$ is acceleration of electrons due to electric field, and the relation is shown in Eq.(2-5). Eq.(2-2) is the integration of distribution function $f(x,v,t)$ by velocity v, and $n(x)$ is the number density of electrons. Eq.(2-3) is a Poisson's equation, where $\varphi(x)$ is electric

potential, e is electric charge, ϵ_0 is electric permittivity of free space. Eq.(2-3) can be solved with number density n. Because the electrons are much lighter than ions, electrons move much faster than ions with the same energy. Therefore, ions are set as a static background and only motions of electrons are considered. As a result, the number density of ions n_i is set as a constant n_0 in our equations. On the other hand, the number density of electrons n_e is set as $n(x)$. Eq.(2-4) uses divergence relation between electric potential $\varphi(x)$ and electric field $E(x)$ to calculate the electric field. In Eq.(2-5), e is the same as Eq.(2-3), and m_e is matter of electrons.

$$\frac{\partial f(x,v,t)}{\partial t}+v\frac{\partial f(x,v,t)}{\partial x}+a(x)\frac{\partial f(x,v,t)}{\partial v}=0, \tag{2-1}$$

$$n_e=n(x)=\int f(x,v,t)dv, \tag{2-2}$$

$$\frac{d^2\varphi(x)}{dx^2}=-\frac{e}{\epsilon_0}(n_i-n_e)=-\frac{e}{\epsilon_0}[n_0-n(x)], \tag{2-3}$$

$$E(x)=-\frac{d\varphi(x)}{dx}, \tag{2-4}$$

$$a(x)=-\frac{eE(x)}{m_e}. \tag{2-5}$$

2.2 Normalization

The Vlasov-Poisson system equations have some complex constants. To simplify, these equations are normalized to dimensionless equations using some characteristic quantities. All variables in the Vlasov-Poisson equations are normalized in the following units where the variables with subscript “char” is their own characteristic quantities (characteristic time t_{char}, length x_{char}, velocity v_{char}, acceleration a_{char}, number density n_{char}, distribution function f_{char}, electric potential φ_{char}, and electric field E_{char}). There are seven characteristic quantities to be set as Eq.(2-6) to Eq.(2-13).

$$t_{char}=\omega_p^{-1} \text{ where } \omega_p=\sqrt{\frac{n_0 e^2}{\varepsilon_0 m_e}}, \tag{2-6}$$

$$x_{char}=\lambda_D \text{ where } \lambda_D=\sqrt{\frac{\varepsilon_0 k_B T_e}{n_0 e^2}}, \tag{2-7}$$

$$v_{char}=v_{th} \text{ where } v_{th}=\lambda_D \omega_p=\sqrt{\frac{k_B T_e}{m_e}}, \tag{2-8}$$

$$a_{char}=\lambda_D \omega_p^2=v_{th}\omega_p, \tag{2-9}$$

$$n_{char}=n_0, \tag{2-10}$$

$$f_{char}=\frac{n_0}{v_{th}}, \tag{2-11}$$

$$\varphi_{char}=\frac{e n_0 \lambda_D^2}{\varepsilon_0}=\frac{m_e v_{th}^2}{e}, \tag{2-12}$$

$$E_{char}=\frac{e n_0 \lambda_D}{\varepsilon_0}=\frac{m_e v_{th}^2}{e\lambda_D}. \tag{2-13}$$

The two main characteristic quantities are in time and in length. Time is normalized by one over plasma frequency ω_p^{-1}. Length is normalized by Debye length of the plasma λ_D. Velocity is normalized by thermal velocity v_{th}. Number density is normalized by number density of ions. In Eq.(2-7) and Eq.(2-8), k_B is Boltzmann constant and T_e is electron temperature. Derivation of these normalized variables are shown in Eq.(2-14) to Eq.(2-25), respectively, where variables with hats represents normalized variables (normalized time $\hat{t}$, position $\hat{x}$, velocity $\hat{v}$, acceleration $\hat{a}$, number density $\hat{n}$, distribution function $\hat{f}$., electric potential $\hat{\varphi}$, and electric field $\hat{E}$). Eq.(2-14) and Eq.(2-15) are shown the definition of normalized time and position. Eq.(2-16) and Eq.(2-17) are shown the derivation of velocity and acceleration by using $v=\frac{dx}{dt}$ and $a=\frac{d^2x}{dt^2}$ respectively. Normalized number density and distribution function are derived in Eq.(2-18) and Eq.(2-20) by using Eq.(2-2). Eq.(2-21) to Eq.(2-23) are the steps using Eq.(2-3) to normalize electric potential, and Eq.(2-24) and

Eq.(2-25) is the steps using Eq.(2-4) to normalize electric potential. Eq.(2-26) and Eq.(2-27) are normalized Eq.(2-5).

$$t=t_{char}\hat{t}=\frac{\hat{t}}{\omega_p}, \tag{2-14}$$

$$v=v_{char}\hat{v}=\frac{x_{char}d\hat{x}}{t_{char}d\hat{t}}=\lambda_D\omega_p\frac{d\hat{x}}{d\hat{t}}=v_{th}\frac{d\hat{x}}{d\hat{t}}, \tag{2-15}$$

$$x=x_{char}\hat{x}=\lambda_D\hat{x}. \tag{2-16}$$

$$a=a_{char}\hat{a}=\frac{x_{char}d^2\hat{x}}{{t_{char}}^2d\hat{t}^2}=\lambda_D{\omega_p}^2\frac{d^2\hat{x}}{d\hat{t}^2}=v_{th}\omega_p\frac{d^2\hat{x}}{d\hat{t}^2}, \tag{2-17}$$

$$n=n_{char}\hat{n}=n_0\hat{n}=f_{char}v_{char}\int\hat{f}d\hat{v}=f_{char}v_{th}\int\hat{f}d\hat{v}, \tag{2-18}$$

$$\Longrightarrow n=n_0=f_{char}v_{th}, \tag{2-19}$$

$$\Longrightarrow f=f_{char}=\frac{n_0}{v_{th}}, \tag{2-20}$$

$$\frac{\varphi_{char}d^2\hat{\varphi}}{{\lambda_D}^2d\hat{x}^2}=\frac{e}{\epsilon_0}n_0\hat{n}, \tag{2-21}$$

$$\Longrightarrow\varphi_{char}\frac{d^2\hat{\varphi}}{d\hat{x}^2}={n_0\lambda_D}^2\frac{e}{\epsilon_0}\hat{n}. \tag{2-22}$$

$$\Longrightarrow\varphi_{char}=\frac{en_0{\lambda_D}^2}{\varepsilon_0}=\frac{en_0{v_{th}}^2}{\varepsilon_0{\omega_p}^2}=\frac{en_0{v_{th}}^2}{\varepsilon_0}\frac{\varepsilon_0m_e}{n_0e^2}=\frac{m_e{v_{th}}^2}{e}. \tag{2-23}$$

$$E=E_{char}\hat{E}=-\frac{\varphi_{char}}{x_{char}}\frac{d\hat{\varphi}}{d\hat{x}}=-\frac{en_0{\lambda_D}^2}{\lambda_D\varepsilon_0}\frac{d}{d\hat{x}}\hat{n}d\hat{x}^2=-\frac{en_0\lambda_D}{\varepsilon_0}\hat{n}d\hat{x}. \tag{2-24}$$

$$\Longrightarrow E_{char}=-\frac{en_0{\lambda_D}^2}{\lambda_D\varepsilon_0}=-\frac{en_0{v_{th}}^2}{\varepsilon_0\lambda_D{\omega_p}^2}=-\frac{en_0{v_{th}}^2}{\varepsilon_0\lambda_D}\frac{\varepsilon_0m_e}{n_0e^2}=-\frac{m_e{v_{th}}^2}{e\lambda_D}. \tag{2-25}$$

$$a_{char}\hat{a}=-\frac{e}{m_e}E_{char}\hat{E} \tag{2-26}$$

$$\Longrightarrow a_{char}=\frac{e}{m_e}\frac{m_e{v_{th}}^2}{e\lambda_D}=\frac{{v_{th}}^2}{\lambda_D}=\lambda_D{\omega_p}^2 \tag{2-27}$$

Therefore, basic equations of Vlasov-Poisson system in Eq.(2-1) to Eq.(2-5) can be normalized as Eq.(2-28) to Eq.(2-32).

$$\frac{\partial\hat{f}(\hat{x},\hat{v},\hat{t})}{\partial\hat{t}}+\hat{v}\frac{\partial\hat{f}(\hat{x},\hat{v},\hat{t})}{\partial\hat{x}}+\hat{a}(\hat{x})\frac{\partial\hat{f}(\hat{x},\hat{v},\hat{t})}{\partial\hat{v}}=0, \tag{2-28}$$

$$\hat{n}(\hat{x})=\int_{-\infty}^{\infty}\hat{f}(\hat{x},\hat{v},\hat{t})d\hat{v}, \tag{2-29}$$

$$\frac{d^2\hat{\varphi}(\hat{x})}{d\hat{x}^2}=-[1-\hat{n}(\hat{x})], \tag{2-30}$$

$$\hat{E}(\hat{x})=-\frac{d\hat{\varphi}(\hat{x})}{d\hat{x}}, \tag{2-31}$$

$$\hat{a}(\hat{x})=-\hat{E}(\hat{x}). \tag{2-32}$$

To simply the notation, variables without hats in the rest of this thesis represents normalized quantities.

2.3 Simulation structure

The process of Vlasov simulation follows the equations in Vlasov-Poisson system. The Figure 2-1 is shown the flow chart of Vlasov simulation. A distribution function is given as an initial condition first. In each time step Δt, simulation does the following steps: (1) Calculate the number density of electrons n(x) by integrating the distribution function f(x,v,t) as Eq.(2-28) . (2) Calculate Poisson's equation to get electric potential $\varphi(x)$ as Eq.(2-30). (3) Calculate Gauss's Law in electric field to get electric field E(x) and its acceleration a(x) as Eq.(2-31) and Eq.(2-32). (4) Calculate Vlasov equation to get new distribution function f(x,v,t) as Eq.(2-28). Data are output at specific time steps. Finally, this simulation is stopped when time reaches the total simulation time.

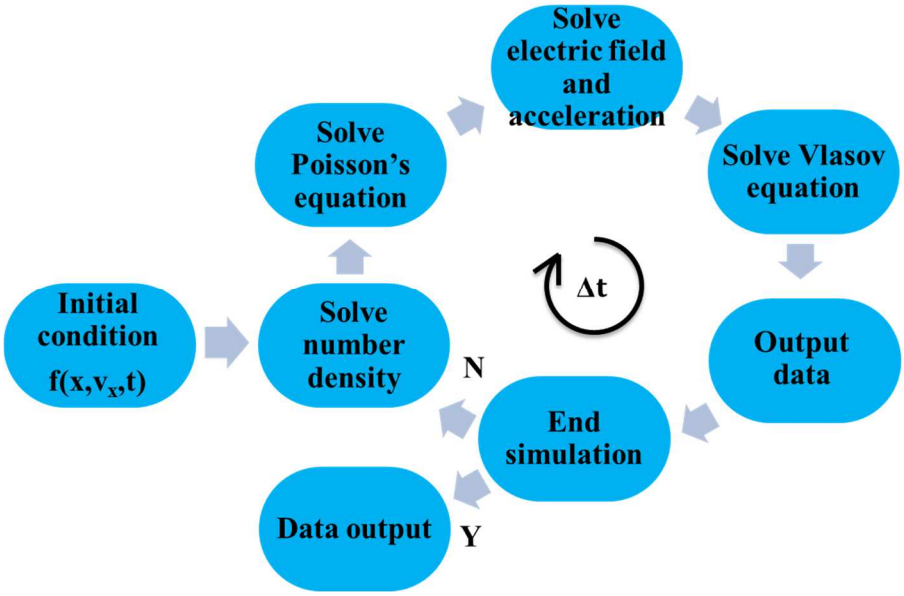

Figure 2-1 Flow chart of Vlasov solver.

Detail structure of the program is shown in Figure 2-2. The function of each subprogram is discussed below.

- Main – main program.
- Module – set numerical variables.
- Initial – set initial distribution function.
- Boundary – set boundary conditions of f(x,v).
- Vboundary – set boundary conditions of n(x), E(x), φ(x), a(x).
- Density – calculate number density.
- Poisson – calculate Poisson's equation.
- Electric – calculate electric field by using electric potential relation.
- Splitx – calculate divided advection equation in x.
- Splitv - calculate divided advection equation in v.

Main program
Main

- Module
- Initial
- Boundary
- Density
- Poisson
- Vboundary
- Electric
- Vboundary
- for time loop
  - Splitv
  - Boundary
  - Splitx
  - Boundary
  - Density
  - Poisson
  - Vboundary
  - Electric
  - Vboundary

Figure 2-2 Subprograms of the Vlasov solver.

2.4 Simulation grids

To calculate equations of Vlasov-Poisson system in simulation, numerical grids need to be defined so that they can be solved by using computers. In Vlasov solver. Vlasov solver sees a discrete phase space graph (x-v graph) in simulation. Therefore, the real space x is discretized as spatial grids “ix” in each position and velocity v is discretized as velocity space grids “iv” in each velocity space. Figure 2-3 shows the numerical grids of discrete phase space. In Figure 2-3, the simulation range in x from 0 to length L is discretized from 0 to nx and the simulation range in v from v_0 to v_{nv} is discretized from 0 to nv. The “0” and “nv” in subscript are the minimum and maximum values respectively in real space x and velocity space v. Therefore, length of one grid in spatial and velocity space are defined as Eq.(2-33)

and Eq.(2-34).

$$\Delta x=\frac{x_{nx}-x_0}{nx}=\frac{L-0}{nx}, \tag{2-33}$$

$$\Delta v=\frac{v_{nx}-v_0}{nv}. \tag{2-34}$$

Each grid is set as $x_{ix}=ix*\Delta x$ in spatial grids and $v_{iv}=iv*\Delta v$ in velocity space grids, where x_{ix} and v_{iv} are the real values at ix and iv grids. The real time in simulation is discretized from 0 to nt steps in "it" temporal grids. The total time is defined as $t=nt*\Delta t$ and time at each time step is $t_{it}=it*\Delta t$ where Δt is the length of one time step that is defined by using CFL condition in section 2.5.6. Because all physical quantities in Vlasov-Poisson system are normalized by one over plasma frequency ω_{pe}^{-1} and Debye length λ_D, all values in simulation are in normalized unit. If dealing with real physics, every physical quantities should be changed in real unit. The discretized parameters are shown in Table 2-1.

Table 2-1 Parameters for running Vlasov simulation.

Parameters	Definition
x	Real space
v	Real velocity space
ix	Number of grid in space
iv	Number of grid in velocity
nx	Total number of grid in space
nv	Total number of grid in velocity
L	Total length in space
t	Real time
it	Number of time step
t_{it}	Time at time step it
nt	Total number of time step

Δt	Size of each time step
x_{ix}	Position at grid ix
x_0	Maximum position in space
x_{nx}	Minimum position in space
Δx	Grid size in space
v_{iv}	Velocity of grid iv
v_0	Maximum velocity
v_{nv}	Minimum velocity
Δv	Grid size in velocity

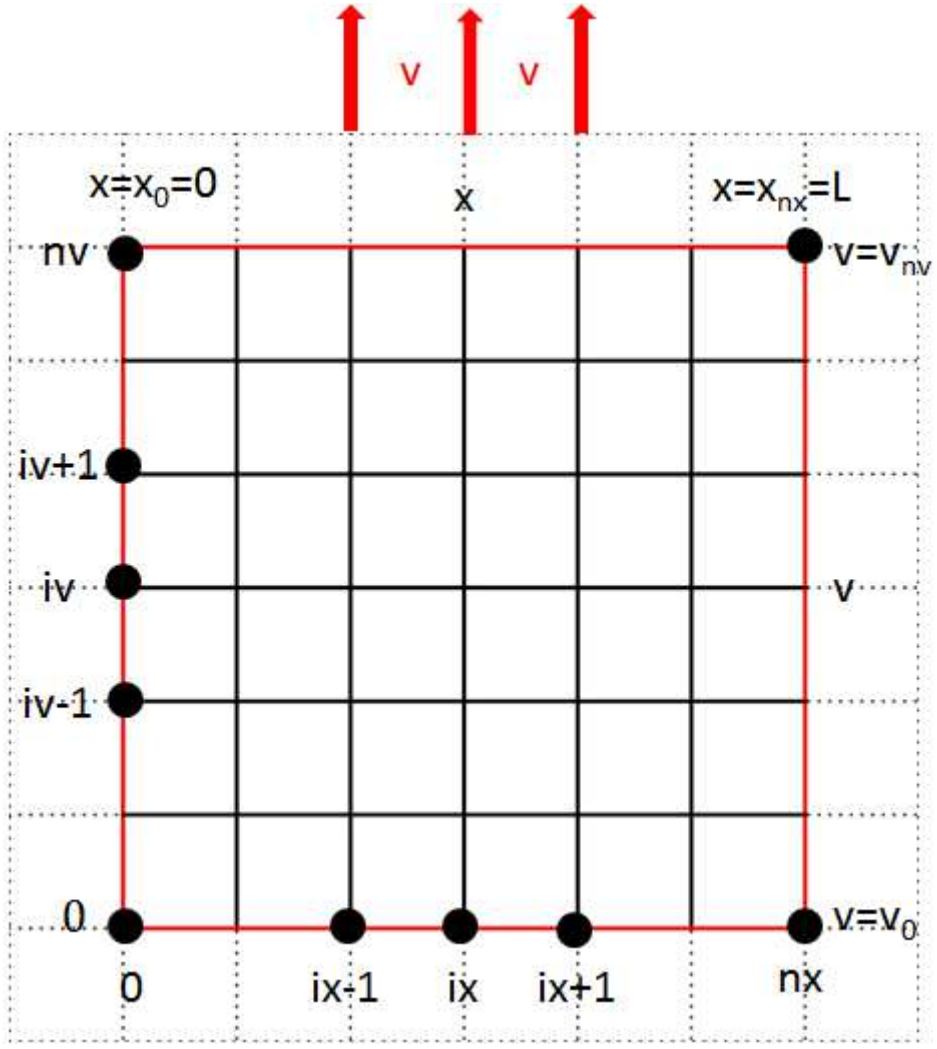

Figure 2-3 Grids in phase space in Vlasov solver.

2.5 Numerical methods and verification

Details of each subroutine and its benchmark is shown in this section. Following equations are solved in sequence: (1) initial condition, (2) boundary conditions, (3) integration of distribution function to obtain density of electrons, (4) Poisson's equation to obtain electric potential, (5) electric field and acceleration, (6) Vlasov equation.

2.5.1 Initial condition

This subroutine generate the initial condition for simulations. Comparison between the simulation result and the analytical equation is given in Figure 2-4. The green line represents the function given in Eq.(2-35) while the red dots are the simulation result from the code.

$$f(v,t=0)=e^{-\frac{(v-2\pi)^2}{2}}. \tag{2-35}$$

They are overlapped to each other. This shows that the subroutine for calculating initial condition is benchmarked.

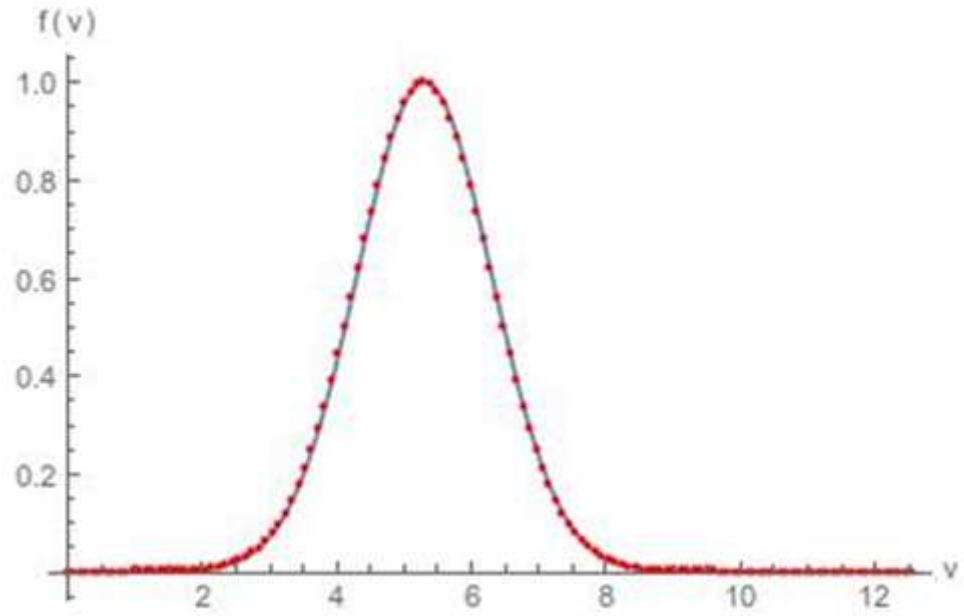

Figure 2-4 Initial condition given in Eq.(2-35).

2.5.2 Boundary conditions

Each variable in Vlasov-Poisson system has its own boundary condition. They are defined as below in sequence (distribution function f(x,v,t), number density n(x), electric potential φ(x), electric field E(x), acceleration a(x)).

2.5.2.1 Set of boundary conditions

1. Distribution function f(x,v,t)

Distribution function f(x,v,t) have two boundary conditions in x and v respectively. They are defined as below.

(1) Periodic boundary condition is used in spatial grids x:

In periodic boundary condition, particles leaving the simulation region from one boundary automatically coming back with the same velocity from the other boundary. This behavior ensure the particles are conserved in our simulation range. It can be defined as Eq.(2-36). In other words, two boundaries are connected with each other.

$$f(x_0,v) = f(x_{nx},v). \tag{2-36}$$

In numerical simulation, the periodic boundary condition is defined as Eq.(2-37).

$$\begin{aligned} &f_{-1}=f_{nx-1},\ f_{-2}=f_{nx-2},\ f_{-3}=f_{nx-3},\\ &f_{nx+1}=f_1,\ f_{nx+2}=f_2,\ f_{nx+3}=f_3. \end{aligned} \tag{2-37}$$

Points beyond boundaries are called virtual numerical grids or ghost cells. Numbers of virtual grids are used depends on the simulation algorithm. Figure 2-5 shows the settings of Eq.(2-37).

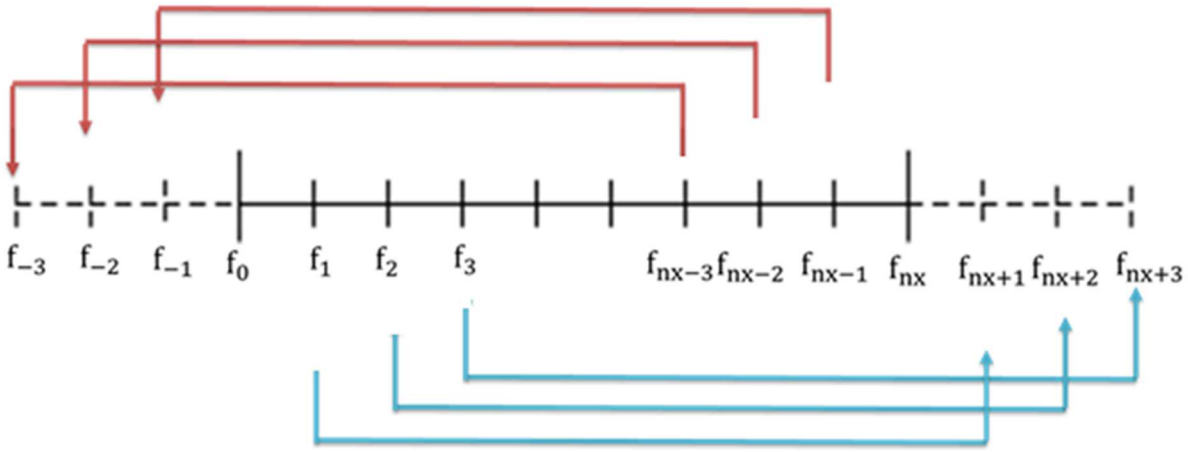

Figure 2-5 Periodic boundary condition in x for distribution function is used.

(2) Dirichlet boundary condition is used in velocity space grids v:

Dirichlet boundary condition is used and distribution function on the boundary in velocity is set as zero because the Gaussian distribution function goes zero with large number. It can be defined as Eq.(2-38).

$$f(x,v_0) = 0,\ \ f(x,v_{nv}) = 0. \tag{2-38}$$

As a result, in numerical simulation, Dirichlet boundary condition can be set as Eq.(2-39).

Figure 2-6 shows the settings in Eq.(2-39).

$$f_{-1}=0,\ f_{-2}=0,\ f_{-3}=0,$$
$$f_{nv+1}=0,\ f_{nv+2}=0,\ f_{nv+3}=0. \tag{2-39}$$

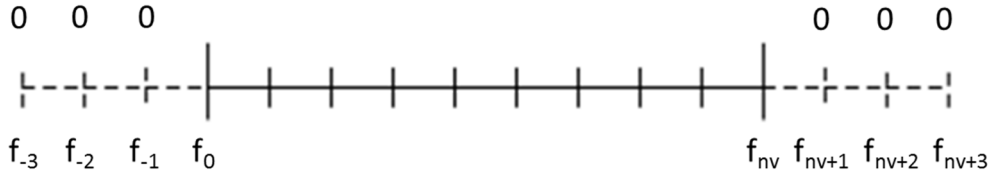

Figure 2-6 Dirichlet boundary condition in v for distribution function is used.

2. Number density n(x), electric potential φ(x), electric field E(x), acceleration a(x)

These four variables all depends on space x so their boundary conditions are also periodic. They are defined as Eq.(2-40).

$$n(x_0) = n(x_{nx}),\ \varphi(x_0) = \varphi(x_{nx}),\ E(x_0) = E(x_{nx}),\ a(x_0) = a(x_{nx}). \tag{2-40}$$

In numerical simulation, they are set as the same as the form in Eq.(2-37) and shown in Figure 2-7.

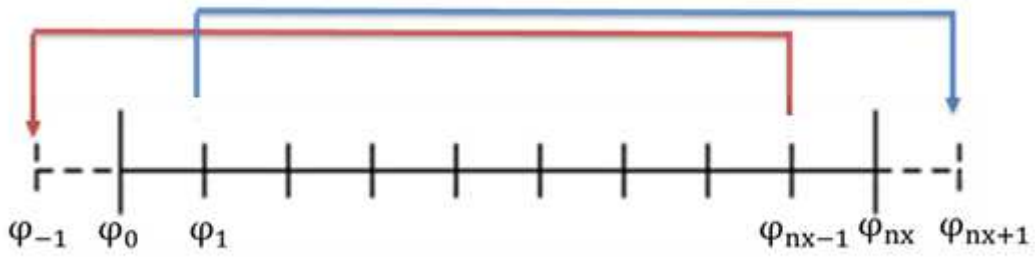

Figure 2-7 Periodic boundary condition in x for n(x), φ(x), E(x), a(x) is used.

2.5.2.2 Benchmark of boundary conditions

To benchmark the subroutine calculates boundary condition. The boundary condition $f(x,v_0)=f(x,v_{nv})=1$ is used. A given distribution function set as Eq.(2-41) and shown in Figure 2-8 is used.

$$f(x,v,t=0)=\frac{2}{7\sqrt{2\pi}}(1+5v^2)\,[1+0.01(\frac{\cos x+\cos 1.5x}{1.2}+\cos 0.5x)]e^{-\frac{v^2}{2}}. \quad (2\text{-}41)$$

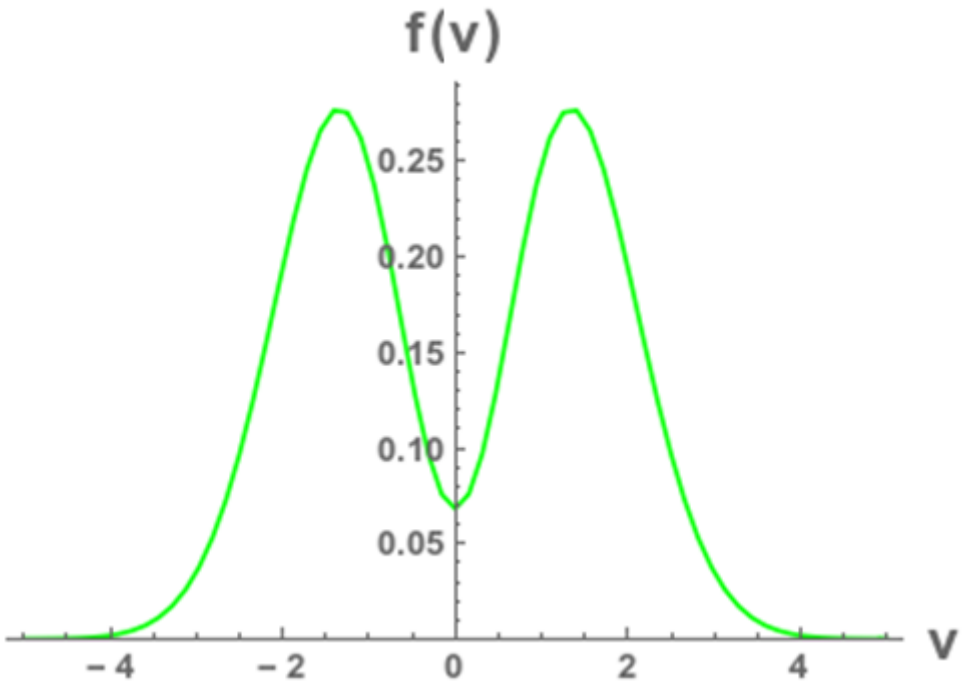

Figure 2-8 Distribution function given in Eq.(2-41).

The distribution function initially goes to zero at v_0 and v_{nv}. However, after applying boundary condition, points on the boundary become 1 showing in Figure 2-9. This shows that the subroutine for calculation boundary condition is benchmarked.

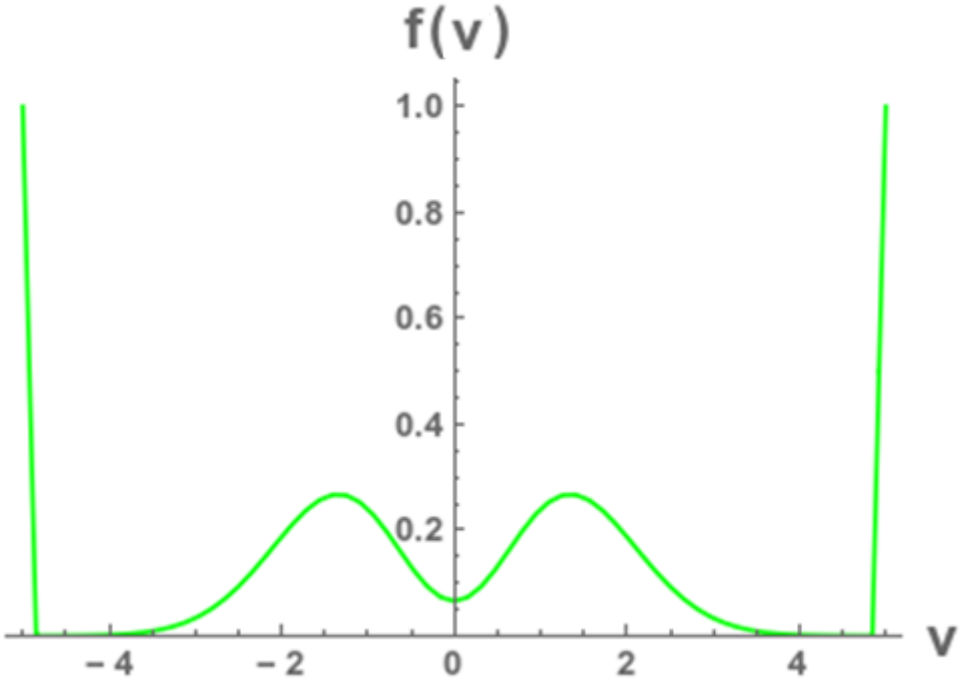

Figure 2-9 Distribution function after applying boundary conditions.

After the subroutine of the boundary condition is benchmarked, the boundary condition is changed back to what were described in 2.5.2.1.

2.5.3 Density of electrons

The density of electrons is calculated by integrating distribution function f in Eq.(2-29). It is rewritten in Eq.(2-42).

$$n(x)=\int_{v_0}^{v_{nv}} f(x,v,t)dv. \qquad (2\text{-}42)$$

Note that the integration region is changed from 0 to infinity (∞) to v_0 to v_{nv} since the distribution function is almost zero for $v < v_0$ and $v > v_{nv}$.

2.5.3.1 Using trapezoidal method to solve numerical integration

To do the integration numerically, trapezoidal method[2] is used. Figure 2-10 shows the

concept of trapezoidal method. Trapezoidal method approximates the area under the curve of the function as lots of trapezoids and calculates their area. The integral is approximated by a summation given in Eq.(2-43). This equation shows that it is the summation of many trapezoids, where Δv is the height and $f(v_{iv})$ is sides of trapezoids.

$$\begin{aligned} n \approx & \frac{\Delta v}{2}[f(v_0)+f(v_1)]+\frac{\Delta v}{2}[f(v_1)+f(v_2)]+\cdots+\frac{\Delta v}{2}[f(v_{iv-1})+f(v_{iv})] \\ & +\frac{\Delta v}{2}[f(v_{iv})+f(v_{iv+2})]+\cdots+\frac{\Delta v}{2}[f(v_{nv-1})+f(v_{nv})] \\ = & \frac{\Delta v}{2}[f(v_0)+2f(v_1)+\cdots+2f(v_{iv})+\cdots+2f(v_{nv-1})+f(v_{nv})] \end{aligned} \tag{2-43}$$

$$\text{where } \Delta v=\frac{V_{nv}-V_0}{nv}.$$

The Eq.(2-43) can be rewritten in Eq.(2-44).

$$n=\int_{v_0}^{v_{nv}} f dv = \Delta v\left\{\sum_{iv=1}^{nv-1} f(v_{iv})+\frac{1}{2}[f(v_0)+f(v_{nv})]\right\}. \tag{2-44}$$

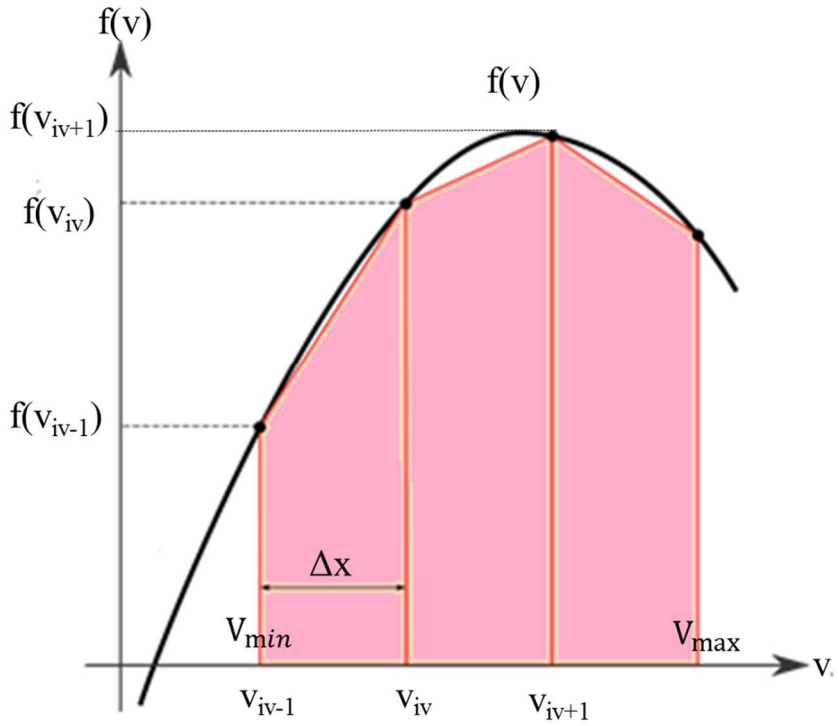

Figure 2-10 Trapezoidal method is used for integration.

2.5.3.2 Benchmark of number density

To benchmark numerical integration using trapezoidal method, a distribution function $f(v) = v^4$ is used. To test the integration subroutine, this distribution function is integrated from v = -5 t0 v = 5 as shown in Eq.(2-45).

$$n(x) = \int_{-5}^{5} v^4 dv = \frac{v^5}{5}\Big|_{-5}^{5} = 1250. \tag{2-45}$$

The numerical calculation is 1250.034 with an error of $2.72\times10^{-3}\%$. It shows the subroutine that calculates the integration is benchmarked.

2.5.4 Poisson's equation

The Poisson's equation from Eq.(2-30) is given again in Eq.(2-46).

$$\frac{d^2\varphi(x)}{dx^2} = n(x)\text{-}1. \tag{2-46}$$

The density(x) on the right hand side of Eq.(2-46) has already been calculated in section 2.5.3.

2.5.4.1 Numerical methods of solving Poisson's equation

To solve the Poisson's equation, finite difference method (FDM) is used. As a result, using finite difference method, the left hand side of Eq.(2-46) can be changed to a discrete form as Eq.(2-47).

$$\frac{d^2\varphi(x)}{dx^2} \approx \frac{\varphi_{ix-1}\text{-}2\varphi_{ix}+\varphi_{ix+1}}{\Delta x^2}. \tag{2-47}$$

Inserting Eq.(2-47) back to Eq.(2-46) so that Eq. (2-46) becomes Eq.(2-48) and Eq.(2-49).

$$\frac{\varphi_{ix-1}\text{-}2\varphi_{ix}+\varphi_{ix+1}}{\Delta x^2} = n_{ix}\text{-}1. \tag{2-48}$$

$$\varphi_{ix-1}-2\varphi_{ix}+\varphi_{ix+1}=(n_{ix}-1)\Delta x^2. \tag{2-49}$$

There are nx equations and nx unknowns of φ_{ix} where ix = 0 to nx. Periodic boundary condition with the definition $\varphi_{-1}=\varphi_{nx-1}$ and $\varphi_{nx+1}=\varphi_1$ are used. The series of equations are shown in Eq.(2-50).

$$\begin{cases} \varphi_{nx-1}-2\varphi_0+\varphi_1=(n_0-1)\Delta x^2 \\ \varphi_0-2\varphi_1+\varphi_2=(n_1-1)\Delta x^2 \\ \vdots \\ \varphi_{ix-1}-2\varphi_{ix}+\varphi_{ix+1}=(n_{ix}-1)\Delta x^2 \\ \vdots \\ \varphi_{nx-2}-2\varphi_{nx-1}+\varphi_{nx}=(n_{nx-1}-1)\Delta x^2 \\ \varphi_{nx-1}-2\varphi_{nx}+\varphi_1=(n_{nx}-1)\Delta x^2 \end{cases}. \tag{2-50}$$

To simplify, $(n_{ix}-1)\Delta x^2 \equiv g_{ix}$ is used. The series of equations is shown in Eq.(2-51).

$$\begin{cases} -2\varphi_0+\varphi_1+1\varphi_{nx-1}=g_0 \\ \varphi_0-2\varphi_1+\varphi_2=g_1 \\ \vdots \\ \varphi_{ix-1}-2\varphi_{ix}+\varphi_{ix+1}=g_{ix} \\ \vdots \\ \varphi_{nx-2}-2\varphi_{nx-1}+\varphi_{nx}=g_{nx-1} \\ \varphi_1+\varphi_{nx-1}-2\varphi_{nx}=g_{nx} \end{cases}. \tag{2-51}$$

Eq.(2-51) also can be written in matrix form as Eq.(2-53) for calculation.

$$\begin{bmatrix} -2 & 1 & 0 & \cdots & 0 & 1 & 0 \\ 1 & -2 & 1 & & & & \vdots \\ 0 & 1 & \ddots & \ddots & & & \vdots \\ \vdots & & \ddots & \ddots & \ddots & & \vdots \\ \vdots & & & \ddots & \ddots & 1 & 0 \\ \vdots & & & & 1 & -2 & 1 \\ 0 & 1 & 0 & \cdots & 0 & 1 & -2 \end{bmatrix} \begin{bmatrix} \varphi_0 \\ \vdots \\ \vdots \\ \vdots \\ \varphi_{nx} \end{bmatrix} = \begin{bmatrix} g_0 \\ \vdots \\ \vdots \\ \vdots \\ g_{nx} \end{bmatrix}. \tag{2-52}$$

To solve Eq.(2-51), these linear equations can be written in the matrix form as Eq.(2-53), where $\varphi_{ix}=\varphi_i$, and $g_{ix}=b_i$ and, $a_{i,j}$ represents elements in the matrix.

$$\begin{cases} a_{0,0}\varphi_0+a_{0,1}\varphi_{0_1}+\cdots+a_{0,nx-1}\varphi_{nx-1}+a_{0,nx}\varphi_{nx}=b_0 \\ a_{1,0}\varphi_0+a_{1,1}\varphi_1+\cdots+a_{1,nx-1}\varphi_{nx-1}+a_{1,nx}\varphi_{nx}=b_1 \\ \vdots \\ a_{nx,0}\varphi_0+a_{nx,1}\varphi_1+\cdots+a_{nx,nx-1}\varphi_{nx-1}+a_{nx,nx}\varphi_{nx}=b_{nx} \end{cases}. \tag{2-53}$$

Generally, there are two kinds of methods to solve the system of equations in the matrix form.

One is iteration method including Jacobi's method[2], Gauss-Seidel's method[2]. The other one is direct method including Gauss elimination[2] and LU decomposition method[2]. They are both introduced in the below

1. Iteration methods

Iteration methods solve each linear equation for φ_i sequentially from an initial guess. Equations are solved by iteration until the solution converges. Two methods of iteration methods, Jacobi's method and Gauss-Seidel's method are introduced.

(1) Jacobi's method

The equation is rewritten in the following form in Eq.(2-20).

$$\begin{aligned}
\varphi_0^{k+1} &= \frac{b_0 - a_{0,1}\varphi_1^k - a_{0,2}\varphi_2^k \cdots - a_{0,n-1}\varphi_{nx-1}^k - a_{0,nx}\varphi_{nx}^k}{a_{1,1}}, \\
\varphi_1^{k+1} &= \frac{b_1 - a_{1,0}\varphi_0^k - a_{1,2}\varphi_2^k \cdots - a_{1,n-1}\varphi_{nx-1}^k - a_{1,nx}\varphi_{nx}^k}{a_{2,2}}, \\
&\vdots \\
\varphi_{nx}^{k+1} &= \frac{b_{nx} - a_{nx,0}\varphi_0^k - a_{nx,1}\varphi_1^k \cdots - a_{nx,nx-1}\varphi_{nx-1}^k}{a_{nx,nx}}.
\end{aligned} \tag{2-54}$$

It is written into a summation form.

$$\varphi_i^{k+1} = \left(b_i - \sum_{j=0}^{i-1} a_{i,j}\varphi_j^k - \sum_{j=i+1}^{nx} a_{i,j}\varphi_j^k\right) \Big/ a_{i,i} \quad \text{where } i=0,\cdots,nx \text{ and } k=0,\cdots,nx. \tag{2-55}$$

The superscript k is the number of iteration temporary steps. A new φ_i^{k+1} are calculated based on the previous iteration φ_i^k. The iteration is stopped until φ_i^k in the equations are converged The convergent criteria will be given later in the part (3) in this section.

(2) Gauss-Seidel's method

Gauss-Seidel's method is an improved method from Jacobi's method. Eq.(2-54) is rewritten as following.

$$\varphi_0^{k+1}=\frac{b_0^k-a_{0,1}\varphi_1^k-a_{0,2}\varphi_2^k\cdots-a_{0,n-1}\varphi_{nx-1}^k-a_{0,nx}\varphi_{nx}^k}{a_{1,1}},$$
$$\varphi_1^{k+1}=\frac{b_1^k-a_{1,0}\varphi_0^{k+1}-a_{1,2}\varphi_2^k\cdots-a_{1,n-1}\varphi_{nx-1}^k-a_{1,nx}\varphi_{nx}^k}{a_{2,2}}, \qquad (2\text{-}56)$$
$$\vdots$$
$$\varphi_n^{k+1}=\frac{b_{nx}-a_{nx,0}\varphi_0^{k+1}-a_{nx,1}\varphi_1^{k+1}\cdots-a_{nx,nx-1}\varphi_{nx-1}^{k+1}}{a_{nx,nx}}.$$

Eq.(2-56) can also be rewritten in a summation form as Eq.(2-57).

$$\varphi_i^{k+1}=\left(b_i-\sum_{j=0}^{i-1}a_{i,j}\varphi_j^{k+1}-\sum_{j=i+1}^{nx}a_{i,j}\varphi_j^k\right)\Big/a_{i,i}\ ,\ i=0,\cdots,nx \text{ and } k=0,\cdots,nx. \qquad (2\text{-}57)$$

Comparing with Jacobi's method, the computation in Gauss-Seidel's method of φ_i^{k+1} uses the elements of φ_j^{k+1} where $j < i$ that have already been computed. Therefore, Gauss-Seidel's method converges faster than Jacobi's method.

(3) Convergent condition

To define the convergence of Jacobi's method and Gauss-Seidel's method, approximated errors need to be calculated. The approximated errors ε is defined as Eq.(2-58).

$$|\varepsilon|_i=\left|\frac{\varphi_i^{k+1}-\varphi_i^k}{\varphi_i^{k+1}+10^{-6}}\right|. \qquad (2\text{-}58)$$

The number 10^{-6} in the denominator is to ensure that the denominator isn't zero even when φ_i^{k+1} is very small. The iteration is stopped when the absolute value of approximated error being less than a pre-specified tolerance when the condition is met (10^{-6} in our simulation).

2. Direct solvers

Direct solvers solve linear equations directly to get the exact solutions. Two kinds of direct solvers are introduced in this part: Gauss elimination method and LU decomposition method. To solve linear equations of Poisson's equation directly,

The system of linear equations in the matrix form is rewritten again in the following.

$$\begin{bmatrix} a_{0,0} & \cdots & a_{0,nx} \\ \vdots & \ddots & \vdots \\ a_{nx,0} & \cdots & a_{nx,nx} \end{bmatrix} \begin{bmatrix} \varphi_0 \\ \vdots \\ \varphi_{nx} \end{bmatrix} = \begin{bmatrix} b_0 \\ \vdots \\ b_{nx} \end{bmatrix}. \tag{2-59}$$

To help us keep track on the steps of this process, we will denote the initial system with the superscript as Eq.(2-60).

$$\begin{bmatrix} a_{0,0}^{(0)} & \cdots & a_{0,nx}^{(0)} \\ \vdots & \ddots & \vdots \\ a_{nx,0}^{(0)} & \cdots & a_{nx,nx}^{(0)} \end{bmatrix} \begin{bmatrix} \varphi_0 \\ \vdots \\ \varphi_{nx} \end{bmatrix} = \begin{bmatrix} b_0^{(0)} \\ \vdots \\ b_{nx}^{(0)} \end{bmatrix}. \tag{2-60}$$

(1) Gauss elimination

First, elements in the first row $a_{0,j}^{(0)}$ and $b_0^{(0)}$ is divided by the leading elements of the row $a_{0,0}^{(0)}$. These steps are shown in Eq.(2-61) and Eq.(2-62).

$$a_{0,j}^{(1)} = \frac{a_{0,j}^{(0)}}{a_{0,0}^{(0)}} \text{ where } j=0,\cdots,nx, \tag{2-61}$$

$$b_0^{(1)} = \frac{b_0^{(0)}}{a_{0,0}^{(0)}}. \tag{2-62}$$

After this step, Eq.(2-60) can be shown as Eq.(2-63)

$$\begin{bmatrix} a_{0,0}^{(1)} & a_{0,1}^{(1)} & \cdots & a_{0,nx-1}^{(1)} & a_{0,nx}^{(1)} \\ a_{1,0}^{(0)} & \ddots a_{1,1}^{(0)} & \ddots & \ddots & a_{1,nx}^{(0)} \\ \vdots & \ddots & a_{i,j}^{(0)} & \ddots & \vdots \\ \vdots & \ddots & \ddots & \ddots & \vdots \\ a_{nx,0}^{(0)} & a_{nx,1}^{(0)} & \cdots & a_{nx,nx-1}^{(0)} & a_{nx,nx}^{(0)} \end{bmatrix} \begin{bmatrix} \varphi_0 \\ \vdots \\ \varphi_i \\ \vdots \\ \varphi_{nx} \end{bmatrix} = \begin{bmatrix} b_0^{(1)} \\ \vdots \\ b_i^{(0)} \\ \vdots \\ b_{nx}^{(0)} \end{bmatrix}. \tag{2-63}$$

Elements beside the leading element in the first column can be eliminated using the following equations. Then subtract the result from row i, this yields new matrix elements of $a_{i,j}$ as Eq.(2-32) and Eq.(2-33).

$$a_{i,j}^{(1)} = a_{i,j}^{(0)} - \frac{a_{i,0}^{(0)}}{a_{0,0}^{(0)}} a_{0j}^{(0)} = a_{i,j}^{(0)} - a_{i,0}^{(0)} a_{0,j}^{(1)} \text{ where } i=1,\cdots,nx \text{ and } j=0,\cdots,nx, \tag{2-64}$$

$$b_i^{(1)}=b_i^{(0)}-\frac{a_{i,0}^{(0)}}{a_{0,0}^{(0)}}b_i^{(0)}=b_i^{(0)}-b_i^{(0)}a_{0,j}^{(1)} \text{ where } i=1,\cdots,nx. \tag{2-65}$$

Note that elements in the first column are eliminated as following.

$$a_{i,0}^{(1)}=a_{i,0}^{(0)}-\frac{a_{i,0}^{(0)}}{a_{0,0}^{(0)}}a_{0,0}^{(0)}=0 \text{ where } i=1,\cdots,nx. \tag{2-66}$$

Therefore, Eq.(2-63) becomes

$$\begin{bmatrix} 1 & a_{0,1}^{(1)} & \cdots & a_{0,nx}^{(1)} \\ 0 & a_{1,1}^{(1)} & \cdots & a_{1,nx}^{(1)} \\ \vdots & \vdots & \ddots & \vdots \\ 0 & a_{nx,1}^{(1)} & \cdots & a_{nx,nx}^{(1)} \end{bmatrix} \begin{bmatrix} \varphi_0 \\ \vdots \\ \varphi_{nx} \end{bmatrix} = \begin{bmatrix} b_0^{(1)} \\ \vdots \\ b_{nx}^{(1)} \end{bmatrix}. \tag{2-67}$$

Similarly, the second column and sequentially of each column are eliminated as following.

$$a_{k,j}^{(k)}=\frac{a_{k,j}^{(k-1)}}{a_{k,k}^{(k-1)}} \text{ where } j=k,\cdots,nx \text{ and } k=1,\cdots,nx. \tag{2-68}$$

$$a_{i,j}^{(k)}=a_{i,j}^{(k-1)}-\frac{a_{i,k}^{(k-1)}}{a_{k,k}^{(k-1)}}a_{k,j}^{(k-1)} \text{ where } i=k+1,\cdots,nx,\ j=k,\cdots,nx, \text{ and } k=1,\cdots,nx, \tag{2-69}$$

$$b_k^{(k-1)}=\frac{b_k^{(k-1)}}{a_{k,k}^{(k-1)}} \text{ where } j=k,\cdots,nx \text{ and } k=1,\cdots,nx \text{ and } k=0,\cdots,nx, \tag{2-70}$$

$$b_k^{(k)}=b_k^{(k-1)}-\frac{a_{i,k}^{(k-1)}}{a_{k,k}^{(k-1)}}b_k^{(k-1)} \text{ where } i=k+1,\cdots,nx \text{ and } k=0,\cdots,nx. \tag{2-71}$$

The superscript k equals 1 to nx represents the steps of elimination. After applying the elimination, Eq.(2-59) becomes

$$\begin{bmatrix} 1 & a_{0,1}^{(1)} & \cdots & \cdots & a_{0,nx}^{(1)} \\ 0 & 1 & a_{1,2}^{(2)} & \cdots & a_{1,nx}^{(2)} \\ \vdots & 0 & \ddots & \ddots & \vdots \\ \vdots & \vdots & \ddots & \ddots & a_{nx-1,nx}^{(nx-1)} \\ 0 & 0 & \cdots & 0 & 1 \end{bmatrix} \begin{bmatrix} \varphi_0 \\ \vdots \\ \varphi_{nx} \end{bmatrix} = \begin{bmatrix} b_0^{(1)} \\ \vdots \\ b_{nx}^{(nx)} \end{bmatrix}. \tag{2-72}$$

Eq.(2-72) can be represented by using $a_{i,j}^{(k)}=a_{i,j}^{'}$ and $b_i^{(k)}=b_i^{'}$ in the following.

$$\begin{bmatrix} 1 & a'_{0,1} & \cdots & \cdots & a'_{0,nx} \\ 0 & 1 & a'_{1,2} & \cdots & a'_{1,nx} \\ \vdots & 0 & \ddots & \ddots & \vdots \\ \vdots & \vdots & \ddots & \ddots & a'_{nx-1,nx} \\ 0 & 0 & \cdots & 0 & 1 \end{bmatrix} \begin{bmatrix} \varphi_0 \\ \vdots \\ \varphi_{nx} \end{bmatrix} = \begin{bmatrix} b'_0 \\ \vdots \\ b'_{nx} \end{bmatrix}. \tag{2-73}$$

These steps are called forward elimination. Apparently, $\varphi_{nx}=b'_{nx}$. After substituting $\varphi_{nx}=b'_{nx}$ to the last second row of the matrix, and φ_{nx-1} can be obtained. This is called back substitution. It can be represented as Eq.(2-74).

$$\varphi_i=(b'_i-\sum_{j=i+1}^{nx} a'_{i,j}\varphi_j)\Big/a'_{ii} \text{ where } i=nx-1,\cdots,0. \tag{2-74}$$

As a result, all φ_i can be solved exactly.

(2) LU decomposition

To solve the matrix by using LU decomposition, Eq.(2-59) is written in Eq.(2-75) and Eq.(2-76). LU decomposition separates A into two separated triangular matrix. it is shown in Eq.(2-77).

$$A\Phi=B. \tag{2-75}$$

$$A=\begin{bmatrix} a_{0,0} & \cdots & a_{0,nx} \\ \vdots & \ddots & \vdots \\ a_{nx,0} & \cdots & a_{nx,nx} \end{bmatrix},\ \Phi=\begin{bmatrix} \varphi_0 \\ \vdots \\ \varphi_{nx} \end{bmatrix},\ B=\begin{bmatrix} b_0 \\ \vdots \\ b_{nx} \end{bmatrix}. \tag{2-76}$$

$$A=\begin{bmatrix} 1 & 0 & \cdots & 0 & 0 \\ l_{1,0} & 1 & \ddots & \vdots & \vdots \\ l_{2,0} & l_{2,1} & \ddots & 0 & \vdots \\ \vdots & \vdots & \ddots & 1 & 0 \\ l_{nx,0} & l_{nx,1} & \cdots & l_{nx,nx-1} & 1 \end{bmatrix} \begin{bmatrix} u_{0,0} & u_{0,1} & \cdots & \cdots & u_{0,nx} \\ 0 & u_{1,1} & \cdots & \cdots & u_{1,nx} \\ \vdots & 0 & \ddots & \ddots & \vdots \\ \vdots & \vdots & \ddots & \ddots & \vdots \\ 0 & 0 & \cdots & 0 & u_{nx,nx} \end{bmatrix}. \tag{2-77}$$

These two matrixes are called the upper matrix U and the lower matrix L shown in Eq.(2-78).

$$U=\begin{bmatrix} u_{0,0} & u_{0,1} & \cdots & \cdots & u_{0,nx} \\ 0 & u_{1,1} & \cdots & \cdots & u_{1,nx} \\ \vdots & 0 & \ddots & \ddots & \vdots \\ \vdots & \vdots & \ddots & \ddots & \vdots \\ 0 & 0 & \cdots & 0 & u_{nx,nx} \end{bmatrix} \text{ and } L=\begin{bmatrix} 1 & 0 & \cdots & 0 & 0 \\ l_{1,0} & 1 & \ddots & \vdots & \vdots \\ l_{2,0} & l_{2,1} & \ddots & 0 & \vdots \\ \vdots & \vdots & \ddots & 1 & 0 \\ l_{nx,0} & l_{nx,1} & \cdots & l_{nx,nx-1} & 1 \end{bmatrix}. \quad (2\text{-}78)$$

The lower matrix L and the upper matrix U are obtained by using Gauss elimination shown in part (1). Upper matrix U is obtained using the same way given in Eq.(2-69) and it is rewritten in Eq.(2-79).

$$\begin{cases} u_{i,j}=a_{0,j}^{(0)} \text{ where } j=0,\cdots,nx, \\ u_{i,j}=a_{i,j}^{(k)}=a_{i,j}^{(k-1)}-\dfrac{a_{i,k}^{(k-1)}}{a_{k,k}^{(k-1)}}a_{k,j}^{(k-1)} \text{ where } i=k+1,\cdots,nx,\ j=k+1,\cdots,nx, \text{ and } k=1,\cdots,nx, \\ u_{i,j}=0 \text{ where } i>j. \end{cases} \quad (2\text{-}79)$$

Finally, the matrix form of upper matrix U is shown as Eq.(2-80).

$$U=\begin{bmatrix} a_{0,0}^{(0)} & a_{0,1}^{(0)} & \cdots & \cdots & a_{0,nx}^{(0)} \\ 0 & a_{1,1}^{(1)} & \cdots & \cdots & a_{1,nx}^{(1)} \\ \vdots & 0 & \ddots & \ddots & \vdots \\ \vdots & \vdots & \ddots & \ddots & \vdots \\ 0 & 0 & \cdots & 0 & a_{nx,nx}^{(nx)} \end{bmatrix}=\begin{bmatrix} u_{0,0} & u_{0,1} & \cdots & \cdots & u_{0,nx} \\ 0 & u_{1,1} & \cdots & \cdots & u_{1,nx} \\ \vdots & 0 & \ddots & \ddots & \vdots \\ \vdots & \vdots & \ddots & \ddots & \vdots \\ 0 & 0 & \cdots & 0 & u_{nx,nx} \end{bmatrix} \quad (2\text{-}80)$$

Lower matrix L is obtained from origin matrix A as following.

$$\begin{cases} l_{i,j}=\dfrac{a_{i,j}^{(i)}}{a_{j,j}^{(i)}} \text{ where } i=1,\cdots,nx \text{ and } j=0,\cdots,i-1,\ i>j, \\ l_{i,j}=1 \text{ where } i=j, \\ l_{i,j}=0 \text{ where } i<j. \end{cases} \quad (2\text{-}81)$$

After doing these steps, the matrix form of lower matrix L is shown in Eq.(2-82).

$$L=\begin{bmatrix} 1 & 0 & \cdots & 0 & 0 \\ l_{1,0} & 1 & \ddots & \vdots & \vdots \\ l_{2,0} & l_{2,1} & \ddots & 0 & \vdots \\ \vdots & \vdots & \ddots & 1 & 0 \\ l_{nx,0} & l_{nx,1} & \cdots & l_{nx,nx-1} & 1 \end{bmatrix}. \quad (2\text{-}82)$$

To ensure Eq.(2-82) is correct, LU=A should be verified. Let a matrix be

$$M^{(0)}=\begin{bmatrix} 1 & 0 & \cdots & 0 & 0 \\ -l_{1,0} & 1 & \ddots & \vdots & \vdots \\ -l_{2,0} & 0 & \ddots & 0 & \vdots \\ \vdots & \vdots & \ddots & 1 & 0 \\ -l_{nx,0} & 0 & \cdots & 0 & 1 \end{bmatrix}. \tag{2-83}$$

The origin matrix is defined as $A=A^{(0)}$, and multiply the matrix $M^{(0)}A^{(0)}$.

$$A^{(1)}=M^{(0)}A^{(0)}$$

$$=\begin{bmatrix} 1 & 0 & \cdots & 0 & 0 \\ -l_{1,0} & 1 & \ddots & \vdots & \vdots \\ -l_{2,0} & 0 & \ddots & 0 & \vdots \\ \vdots & \vdots & \ddots & 1 & 0 \\ -l_{nx,0} & 0 & \cdots & 0 & 1 \end{bmatrix}\begin{bmatrix} a_{0,0}^{(0)} & \cdots & a_{0,nx}^{(0)} \\ \vdots & \ddots & \vdots \\ a_{nx,0}^{(0)} & \cdots & a_{nx,nx}^{(0)} \end{bmatrix}=\begin{bmatrix} a_{0,0}^{(0)} & a_{0,1}^{(0)} & \cdots & a_{0,nx}^{(0)} \\ 0 & a_{1,1}^{(1)} & \cdots & a_{1,nx}^{(1)} \\ \vdots & \vdots & \ddots & \vdots \\ 0 & a_{nx,1}^{(1)} & \cdots & a_{nx,nx}^{(1)} \end{bmatrix}. \tag{2-84}$$

The relationship can be found in Eq.(2-84) which is shown in the following.

$$a_{i,j}^{(1)}=a_{i,j}^{(0)}-\frac{a_{i,0}^{(0)}}{a_{0,0}^{(0)}}a_{0,j}^{(0)}=a_{i,j}^{(0)}-l_{i,0}a_{0,j}^{(0)} \text{ where } i=1,\cdots,nx \text{ and } j=1,\cdots,nx. \tag{2-85}$$

Therefore, in next step, $A^{(2)}$ is calculated as Eq.(2-86).

$$A^{(2)}=M^{(1)}A^{(1)}=M^{(1)}M^{(0)}A^{(0)} \text{ where } M^{(1)}=\begin{bmatrix} 1 & 0 & \cdots & \cdots & \cdots & 0 \\ 0 & 1 & \ddots & & & \vdots \\ \vdots & -l_{2,1} & \ddots & \ddots & & \vdots \\ \vdots & -l_{2,2} & 0 & \ddots & \ddots & \vdots \\ \vdots & \vdots & \vdots & \ddots & \ddots & 0 \\ 0 & -l_{nx,1} & 0 & \cdots & 0 & 1 \end{bmatrix}. \tag{2-86}$$

Generally, after k steps, the matrix A becomes

$$A^{(k)}=M^{(k)}M^{(k-1)}A^{(k-1)}=M^{(k)}\cdots M^{(0)}A^{(0)} \tag{2-87}$$

$M^{(k)}$ is defined as Eq.(2-88).

$$M^{(k)}=\begin{bmatrix} 1 & 0 & \cdots & \cdots & \cdots & \cdots & \cdots & 0 \\ 0 & \ddots & \ddots & & & & & \vdots \\ \vdots & \ddots & \ddots & \ddots & & & & \vdots \\ \vdots & & 0 & \ddots & \ddots & & & \vdots \\ \vdots & & \vdots & -l_{k+1,k} & \ddots & \ddots & & \vdots \\ \vdots & & \vdots & \vdots & 0 & \ddots & \ddots & \vdots \\ \vdots & & \vdots & \vdots & \vdots & \ddots & \ddots & 0 \\ 0 & \cdots & 0 & -l_{n,k} & 0 & \cdots & 0 & 1 \end{bmatrix} \tag{2-88}$$

From Eq.(2-85), at k step, $A^{(k)}$ can be calculated by Eq.(2-89).

$$a_{i,j}^{(k)}=a_{i,j}^{(k)}-\frac{a_{i,k}^{(k-1)}}{a_{k,k}^{(k-1)}}a_{k,j}^{(k-1)}=a_{i,j}^{(k-1)}-l_{i,k}a_{k,j}^{(k-1)} \text{ where } i=k,\cdots,nx \text{ and } j=k,\cdots,nx. \tag{2-89}$$

Apparently, $A^{(k)}$ has the form in following.

$$A^{(k)}=A^{(nx)}=\begin{bmatrix} a_{0,0}^{(0)} & a_{0,1}^{(0)} & \cdots & \cdots & a_{0,nx}^{(0)} \\ 0 & a_{1,1}^{(1)} & \cdots & \cdots & a_{1,nx}^{(1)} \\ \vdots & 0 & \ddots & \ddots & \vdots \\ \vdots & \vdots & \ddots & \ddots & \vdots \\ 0 & 0 & \cdots & 0 & a_{nx,nx}^{(nx)} \end{bmatrix}=U \tag{2-90}$$

From above, the upper matrix U have and origin matrix A have the relation as following equations.

$$\begin{aligned} U=A^{(nx)}&=M^{(nx-1)}\cdots M^{(1)}M^{(0)}A^{(0)}, \\ A=A^{(0)}&=\left[M^{(0)}\right]^{-1}\left[M^{(1)}\right]^{-1}\cdots[M^{(nx-1)}]^{-1}U \end{aligned} \tag{2-91}$$

Because $[M^{(k)}]^{-1}$ has a relationship can be found as Eq.(2-92).

$$[M^{(k)}]^{-1}=\begin{bmatrix} 1 & 0 & \cdots & \cdots & \cdots & \cdots & \cdots & 0 \\ 0 & \ddots & \ddots & & & & & \vdots \\ \vdots & \ddots & \ddots & \ddots & & & & \vdots \\ \vdots & & 0 & \ddots & \ddots & & & \vdots \\ \vdots & & \vdots & l_{k+1,k} & \ddots & \ddots & & \vdots \\ \vdots & & \vdots & \vdots & 0 & \ddots & \ddots & \vdots \\ \vdots & & \vdots & \vdots & \vdots & \ddots & \ddots & 0 \\ 0 & \cdots & 0 & l_{n,k} & 0 & \cdots & 0 & 1 \end{bmatrix}=L^{(k)} \tag{2-92}$$

These show that $M^{(k)}$ and $L^{(k)}$ are inverse matrix as $M^{(k)}\,L^{(k)}=I$, where I is identity matrix. L is the product of $L^{(k)}$ as Eq.(2-93).

$$L=L^{(0)}L^{(1)}\cdots L^{(nx-1)}=\left[M^{(0)}\right]^{-1}[M^{(1)}]^{-1}\cdots[M^{(k)}]^{-1} \tag{2-93}$$

As a result, A=LU has been proofed.

$$A=\left[M^{(0)}\right]^{-1}\left[M^{(1)}\right]^{-1}\cdots\left[M^{(nx-1)}\right]^{-1}U=L^{(0)}L^{(1)}L^{(nx-1)}U=LU \tag{2-94}$$

After decomposition of lower matrix L and upper matrix U, Eq.(2-75) can be represented as Eq.(2-95).

$$A\Phi=(LU)\Phi=L(U\Phi)=B. \tag{2-95}$$

The solution to the original matrix is founded by two steps of triangular solve process:

$$U\Phi=Y,\ LY=B. \tag{2-96}$$

They are solved in sequence to get matrix Φ. The matrix form of LY=B is shown in Eq.(2-97).

$$\begin{bmatrix} 1 & 0 & \cdots & 0 & 0 \\ l_{1,0} & 1 & \ddots & \vdots & \vdots \\ l_{2,0} & l_{2,1} & \ddots & 0 & \vdots \\ \vdots & \vdots & \ddots & 1 & 0 \\ l_{nx,0} & l_{nx,1} & \cdots & l_{nx,nx-1} & 1 \end{bmatrix} \begin{bmatrix} y_0 \\ \vdots \\ y_{nx} \end{bmatrix} = \begin{bmatrix} b_0 \\ \vdots \\ b_{nx} \end{bmatrix}. \tag{2-97}$$

This matrix is solved by Eq.(2-98) as following.

$$y_i=b_i-\sum_{j=1}^{i-1} l_{ij}y_j \quad \text{where } i=1,\cdots,nx. \tag{2-98}$$

The matrix form of UΦ=Y is shown in Eq.(2-99).

$$\begin{bmatrix} u_{0,0} & u_{0,1} & \cdots & \cdots & u_{0,nx} \\ 0 & u_{1,1} & \cdots & \cdots & u_{1,nx} \\ \vdots & 0 & \ddots & \ddots & \vdots \\ \vdots & \vdots & \ddots & \ddots & \vdots \\ 0 & 0 & \cdots & 0 & u_{nx,nx} \end{bmatrix} \begin{bmatrix} \varphi_0 \\ \vdots \\ \varphi_{nx} \end{bmatrix} = \begin{bmatrix} y_0 \\ \vdots \\ y_{nx} \end{bmatrix}. \tag{2-99}$$

The matrix in Eq.(2-99) can also be solved in the same way as Eq.(2-100).

$$\varphi_i=(y_i-\sum_{j=i+1}^{nx} u_{ij}\varphi_j)\Big/u_{ii} \quad \text{where } i=1,\cdots,nx. \tag{2-100}$$

2.5.4.2 Benchmark of Poisson's equation

To benchmark the simulation for calculating Poisson's equation, there is a given function $g(x)=\sin(\frac{3x}{4\pi})$ is used. The equation becomes the following.

$$\frac{d^2\varphi}{dx^2}=\sin\left(\frac{3x}{4\pi}\right). \tag{2-101}$$

The boundary conditions are set as $\varphi(0)=0$ and $\varphi(4\pi)=0$. The exact solution of Eq.(2-101) is

$$\varphi(x)=\frac{4}{9}\left[\pi x\sin(3)-4\pi^2\sin\left(\frac{3x}{4\pi}\right)\right]. \tag{2-102}$$

The exact solution is compared with the numerical one solved by the iterative and direct methods respectively They are shown in Figure 2-11 and Figure 2-12. Figure 2-11 is solved by using Gauss-Seidel's method, and Figure 2-12 is solved by using LU decomposition. In these two graphs, the black dashed points are simulation results, and the green solid lines are analytical results. As a result, the subroutine calculate the Poisson's equation is benchmarked. Gauss-Seidel method is used in our code since it solves the Poisson's equation faster.

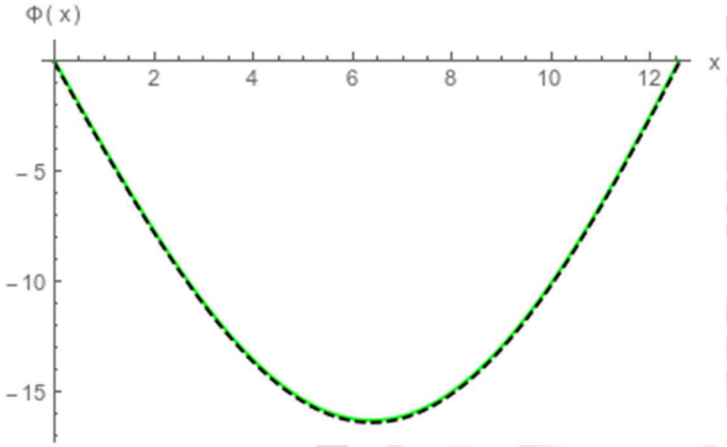

Figure 2-11 Result of calculating electric potential for Poisson's equation using Gauss-Seidel's method. The black dashed points are simulation results, and the green solid lines are analytical results.

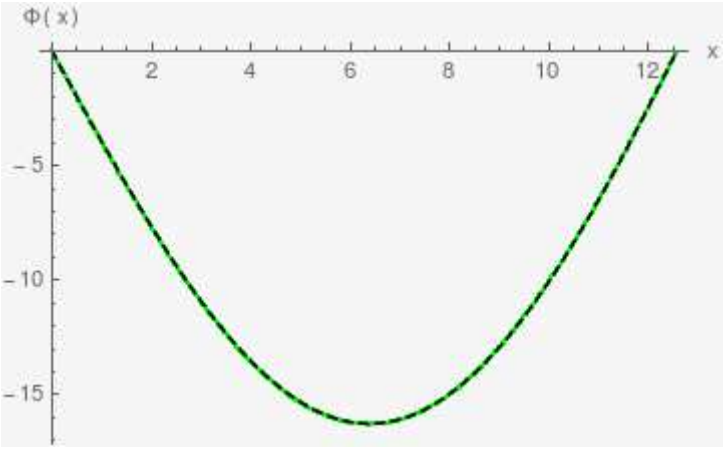

Figure 2-12 Result of calculating electric potential for Poisson's equation using LU decomposition. The black dashed points are simulation results, and the green solid lines are analytical results.

2.5.5 Electric field and acceleration

The subroutine of electric field and acceleration are discussed in the section. Acceleration a(x) is obtained by electric field E(x) using Eq.(2-32). Electric field E(x) are calculated from electric potential φ(x) using Eq.(2-31). Electric potential φ(x) is obtained from the result of Poisson's equation.

2.5.5.1 Method of numerical differentiation

To solve the differentiation in Eq.(2-31), it needs to be discretized using finite difference method (FDM)[2]. From Taylor's series, φ(x) can be represented as Eq.(2-103).

$$\begin{aligned}\varphi(x+\Delta x)&=\varphi(x)+\varphi'(x)\Delta x+\frac{\varphi''(x)}{2!}\Delta x^2+\cdots\\ \varphi(x-\Delta x)&=\varphi(x)-\varphi'(x)\Delta x+\frac{\varphi''(x)}{2!}\Delta x^2-\cdots\end{aligned}. \tag{2-103}$$

Adding two equations:

$$\varphi'(x)=\frac{\varphi(x+\Delta x)+\varphi(x-\Delta x)}{2\Delta x} \tag{2-104}$$

Therefore, the electric field is

$$E_{ix}=-\frac{\varphi_{ix+1}-\varphi_{ix-1}}{2\Delta x}. \quad (2\text{-}105)$$

The acceleration is

$$a_{ix}=-E_{ix}. \quad (2\text{-}106)$$

2.5.5.2 Benchmark of the subroutine calculating electric field and acceleration

To benchmark the subroutine, the result in Eq.(2-102) from section 2.5.4 is used. The analytical solution of the electric field is

$$E=\frac{4}{3}\left[\pi\cos\left(\frac{3x}{4\pi}\right)-\frac{1}{3}\pi\mathrm{Sin}(3)\right] \quad (2\text{-}107)$$

The analytical solution of acceleration is

$$a=-\frac{4}{3}\left[\pi\cos\left(\frac{3x}{4\pi}\right)-\frac{1}{3}\pi\mathrm{Sin}(3)\right] \quad (2\text{-}108)$$

The simulation result of Eq.(2-105) is shown in Figure 2-13 and compared with the exact solution in Eq.(2-107). The black dashed points are the simulation result and the green solid line is the analytical result.

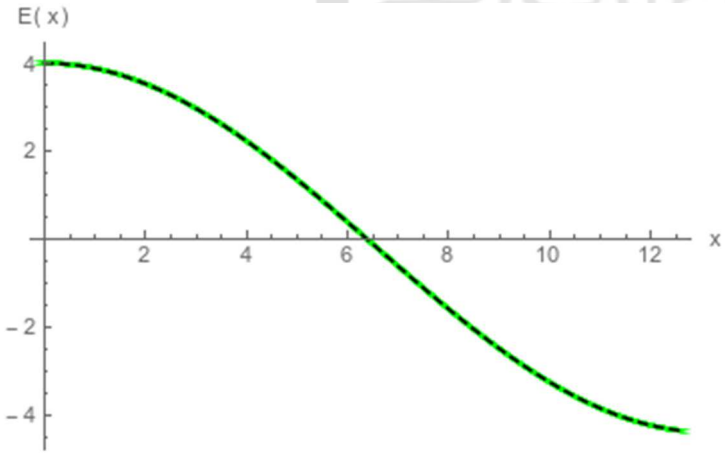

Figure 2-13 Comparison of the analytical solution in green solid line and the simulated result in black dashed line.

The simulation result of Eq.(2-106) is shown in Figure 2-14 and compared with the exact

solution in Eq.(2-108). The black dashed points are the simulation result and the green solid line is the analytical result. Therefore, the subroutine calculate the differentiation and acceleration is benchmarked.

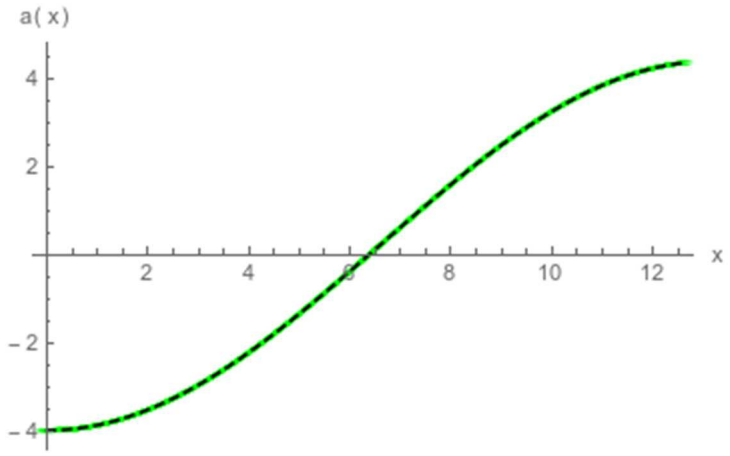

Figure 2-14 Comparison of the analytical solution in green solid line and the simulated result in black dashed line.

2.5.6 Advection equations and Vlasov equation

To calculate Vlasov equation or advection equation, there are many ways to discretized Vlasov equation. Finite volume method (FVM)[1][2][8] is used in this thesis. For a discretized equation, operator splitting scheme[3][6] can be used to separate a single equation to several equations. Therefore, Vlasov equation can be split into two advection equations in space and velocity space, respectively. This method makes our solver easier to solve Vlasov equation numerically. The two advection equations are solved by either piecewise linear method (PLM)[1][8][10] or by piecewise parabolic method (PPM)[1][4][5][9]. These two methods can be combined together. Piecewise linear method and piecewise parabolic method are both based on Godunov's scheme, which is also a method using finite volume method. Both piecewise linear method and Piecewise parabolic method are benchmarked. The advection equation solvers are benchmarked in space x and velocity v separately.

2.5.6.1 Finite volume method

Consider a one-dimensional advection equation as Eq.(2-109).

$$\frac{\partial f}{\partial t}+v\frac{\partial f}{\partial x}=0. \tag{2-109}$$

To discretize Eq.(2-109), this advection equation is integrated over a zone from $x_{i-\frac{1}{2}}$ to $x_{i+\frac{1}{2}}$ and averaged by the zone length $\Delta x=x_{i+\frac{1}{2}}-x_{i-\frac{1}{2}}$. Then Eq.(2-109) becomes Eq.(2-110).

$$\frac{1}{\Delta x}\int_{x_{i=\frac{1}{2}}}^{x_{i+\frac{1}{2}}}\frac{\partial f}{\partial t}dx=-\frac{v}{\Delta x}\int_{x_{i=\frac{1}{2}}}^{x_{i+\frac{1}{2}}}\frac{\partial f}{\partial x}dx. \tag{2-110}$$

Let $\bar{f}_i^n$ represent the average of distribution function f(x,t) over the interval Δx and f_i^n is defined as $f(x_i,t^n)=f_i^n$. f_i^n is the distribution function f(x,t) value on position i and time n. $\bar{f}_i^n$ is defined as Eq.(2-111).

$$\bar{f}_i^n=\frac{\int_{x_{i-\frac{1}{2}}}^{x_{i+\frac{1}{2}}}f(x)dx}{x_{i+\frac{1}{2}}-x_{i-\frac{1}{2}}}=\frac{\int_{x_{i-\frac{1}{2}}}^{x_{i+\frac{1}{2}}}f_i^n dx}{\Delta x}. \tag{2-111}$$

Substituting $\bar{f}_i$ in Eq. (2-111) to Eq.(2-110), and doing the integration, Eq.(2-112) is given.

$$\frac{\partial}{\partial t}\bar{f}_i^n=-\frac{v}{\Delta x}\int_{x_{i=\frac{1}{2}}}^{x_{i+\frac{1}{2}}}\frac{\partial f_i^n}{\partial x}dx=-\frac{v}{\Delta x}(f_{i+\frac{1}{2}}^n-f_{i-\frac{1}{2}}^n). \tag{2-112}$$

Similarly, Eq. (2-112) can be integrated over the interval $\Delta t=t^{n+1}-t^n$ and becomes Eq.(2-113).

$$\int_{t^n}^{t^{n+1}}\frac{\partial \bar{f}_i^n}{\partial t}dt=(\bar{f}_i^{n+1}-\bar{f}_i^n)=-\frac{v}{\Delta x}\int_{t^n}^{t^{n+1}}(f_{i+\frac{1}{2}}-f_{i-\frac{1}{2}})dt. \tag{2-113}$$

So Eq.(2-113) can be rewritten to Eq.(2-114).

$$\bar{f}_i^{n+1}-\bar{f}_i^n=\frac{v}{\Delta x}\int_{t^n}^{t^{n+1}}(f_{i+\frac{1}{2}}-f_{i-\frac{1}{2}})dt. \tag{2-114}$$

Eq.(2-114) also can be written as Eq.(2-115) , and this is the general form of finite volume

equation.

$$\bar{f}_i^{n+1}=\bar{f}_i^{n}-\frac{v}{\Delta x}\int_{t^n}^{t^{n+1}}(f_{i+\frac{1}{2}}-f_{i-\frac{1}{2}})dt. \tag{2-115}$$

Dividing Eq.(2-115) with Δt, it becomes

$$\frac{\bar{f}_i^{n+1}}{\Delta t}=\frac{\bar{f}_i^{n}}{\Delta t}-\frac{v}{\Delta x\Delta t}\int_{t^n}^{t^{n+1}}(f_{i+\frac{1}{2}}-f_{i-\frac{1}{2}})dt. \tag{2-116}$$

If there is an average value $\bar{f}_{i\pm\frac{1}{2}}$ is defined as a average value between temporal time n and n+1 as Eq.(2-117).

$$\bar{f}_{i\pm\frac{1}{2}}=\frac{\int_{t^n}^{t^{n+1}} f_{i\pm\frac{1}{2}}dt}{\Delta t} \tag{2-117}$$

Bring Eq.(2-117) back to Eq.(2-116).

$$\bar{f}_i^{n+1}=\bar{f}_i^{n}-\frac{v\Delta t}{\Delta x}(\bar{f}_{i+\frac{1}{2}}-\bar{f}_{i-\frac{1}{2}}) \tag{2-118}$$

This is also the general form of finite volume equation.

Courant–Friedrichs–Lewy condition (CFL condition)[2] is a necessary condition for convergence while solving advection partial differential equations. It is defined as Eq.(2-119)

$$\frac{v\Delta t}{\Delta x}\le 1. \tag{2-119}$$

$$\Delta t\le\frac{\Delta x}{v}. \tag{2-120}$$

2.5.6.2 Operator splitting scheme

Consider the advection equation above from Eq.(2-28). Take the integration of time from t^n to t^{n+1}, Eq.(2-121) is given.

$$\int_{t^n}^{t^{n+1}}\frac{\partial f}{\partial t}dt+\int_{t^n}^{t^{n+1}}v\frac{\partial f}{\partial x}dt+\int_{t^n}^{t^{n+1}}a\frac{\partial f}{\partial v}dt=0. \tag{2-121}$$

$$f^{n+1}-f^{n}+\int_{t^n}^{t^{n+1}}v\frac{\partial f}{\partial x}dt+\int_{t^n}^{t^{n+1}}a\frac{\partial f}{\partial v}dt=0. \tag{2-122}$$

Take the integration in x and v from $x_{ix-\frac{1}{2}}$ to $x_{ix+\frac{1}{2}}$ and $v_{iv-\frac{1}{2}}$ to $v_{iv+\frac{1}{2}}$. Eq. is given.

$$\int_{x_{ix-\frac{1}{2}}}^{x_{ix+\frac{1}{2}}}\int_{v_{iv-\frac{1}{2}}}^{v_{iv+\frac{1}{2}}}(f^{n+1}-f^{n})dxdv+$$
$$\int_{t^n}^{t^{n+1}}\int_{x_{ix-\frac{1}{2}}}^{x_{ix+\frac{1}{2}}}\int_{v_{iv-\frac{1}{2}}}^{v_{iv+\frac{1}{2}}}v\frac{\partial f}{\partial x}dtdxdv+\int_{t^n}^{t^{n+1}}\int_{x_{ix-\frac{1}{2}}}^{x_{ix+\frac{1}{2}}}\int_{v_{iv-\frac{1}{2}}}^{v_{iv+\frac{1}{2}}}a\frac{\partial f}{\partial v}dtdxdv=0. \quad (2\text{-}123)$$

$$\int_{x_{ix-\frac{1}{2}}}^{x_{ix+\frac{1}{2}}}\int_{v_{iv-\frac{1}{2}}}^{v_{iv+\frac{1}{2}}}(f^{n+1}-f^{n})dxdv+$$
$$\int_{t^n}^{t^{n+1}}\int_{v_{iv-\frac{1}{2}}}^{v_{iv+\frac{1}{2}}}v(f_{ix+\frac{1}{2}}-f_{ix-\frac{1}{2}})dtdv+\int_{t^n}^{t^{n+1}}\int_{x_{ix-\frac{1}{2}}}^{x_{ix+\frac{1}{2}}}a(f_{iv+\frac{1}{2}}-f_{iv-\frac{1}{2}})dtdx=0. \quad (2\text{-}124)$$

In operator splitting method, adding a temporary time step f^{*} between f^{n+1} and f^{n}, and Eq.(2-125) is given.

$$\int_{x_{ix-\frac{1}{2}}}^{x_{ix+\frac{1}{2}}}\int_{v_{iv-\frac{1}{2}}}^{v_{iv+\frac{1}{2}}}(f^{n+1}-f^{*})dxdv+\int_{x_{ix-\frac{1}{2}}}^{x_{ix+\frac{1}{2}}}\int_{v_{iv-\frac{1}{2}}}^{v_{iv+\frac{1}{2}}}(f^{*}-f^{n})dxdv+$$
$$\int_{t^n}^{t^{n+1}}\int_{v_{iv-\frac{1}{2}}}^{v_{iv+\frac{1}{2}}}v(f_{ix+\frac{1}{2}}-f_{ix-\frac{1}{2}})dtdv+\int_{t^n}^{t^{n+1}}\int_{x_{ix-\frac{1}{2}}}^{x_{ix+\frac{1}{2}}}a(f_{iv+\frac{1}{2}}-f_{iv-\frac{1}{2}})dtdx=0. \quad (2\text{-}125)$$

Therefore, Eq.(2-125) can be separated into two equations.

$$\int_{x_{ix-\frac{1}{2}}}^{x_{ix+\frac{1}{2}}}\int_{v_{iv-\frac{1}{2}}}^{v_{iv+\frac{1}{2}}}(f^{*}-f^{n})dxdv+\int_{t^n}^{t^{n+1}}\int_{x_{ix-\frac{1}{2}}}^{x_{ix+\frac{1}{2}}}a(f_{iv+\frac{1}{2}}-f_{iv-\frac{1}{2}})dtdx=0. \quad (2\text{-}126)$$

$$\int_{x_{ix-\frac{1}{2}}}^{x_{ix+\frac{1}{2}}}\int_{v_{iv-\frac{1}{2}}}^{v_{iv+\frac{1}{2}}}(f^{n+1}-f^{*})dxdv+\int_{t^n}^{t^{n+1}}\int_{v_{iv-\frac{1}{2}}}^{v_{iv+\frac{1}{2}}}v(f_{ix+\frac{1}{2}}-f_{ix-\frac{1}{2}})dtdv=0. \quad (2\text{-}127)$$

For Eq.(2-126) and Eq.(2-127) and chose arbitrary integral region of x and v respectively. They becomes

$$\int_{v_{iv-\frac{1}{2}}}^{v_{iv+\frac{1}{2}}}(f^{*}-f^{n})dv+\int_{t^n}^{t^{n+1}}a(f_{iv+\frac{1}{2}}-f_{iv-\frac{1}{2}})dt=0, \quad (2\text{-}128)$$

$$\int_{x_{ix-\frac{1}{2}}}^{x_{ix+\frac{1}{2}}} (f^{n+1}-f^{*})dx + \int_{t^n}^{t^{n+1}} v(f_{ix+\frac{1}{2}}-f_{ix-\frac{1}{2}})dt = 0. \tag{2-129}$$

These two equations can also be written in the form as Eq.(2-115).

$$\bar{f}_{iv}^{*} = \bar{f}_{iv}^{n} - \frac{a}{\Delta v}\int_{t^n}^{t^{n+1}} (f_{iv+\frac{1}{2}}-f_{iv-\frac{1}{2}})dt\,. \tag{2-130}$$

$$\bar{f}_{ix}^{n+1} = \bar{f}_{ix}^{*} - \frac{v}{\Delta x}\int_{t^n}^{t^{n+1}} (f_{ix+\frac{1}{2}}-f_{ix-\frac{1}{2}})dt\,. \tag{2-131}$$

After using operator splitting method, Vlasov equation can be separated to two advection equations Eq.(2-130) and Eq.(2-131). These two equations are solved in the section below. After applying the CFL condition in Eq.(2-119), our simulation CFL condition is defined by using the following equation.

$$\Delta t \le \min\left(\frac{\Delta x}{v}, \frac{\Delta v}{a}\right). \tag{2-132}$$

2.5.6.3 Piecewise linear method

The distribution function f(x,t) are shown in Eq.(2-133) and Eq.(2-134) with different direction of velocity. In time-space graph of advection equation, we can plot the characteristic curves for the advection equation. It is shown in Figure 2-15 and Figure 2-16. The integration in time from t^n to t^{n+1} can be transferred to the integration into I cell using the characteristic curves.

$$f\left(x_{i+\frac{1}{2}},t\right) = \begin{cases} f\left(x_{i+\frac{1}{2}}+v\Delta t,t_n\right) & \text{for } v < 0, \\ f\left(x_{i+\frac{1}{2}}-v\Delta t,t_n\right) & \text{for } v \ge 0. \end{cases} \tag{2-133}$$

$$f\left(x_{i+\frac{1}{2}},t\right) = \begin{cases} f\left(x_{i-\frac{1}{2}}+v\Delta t,t_n\right) & \text{for } v < 0, \\ f\left(x_{i-\frac{1}{2}}-v\Delta t,t_n\right) & \text{for } v \ge 0. \end{cases} \tag{2-134}$$

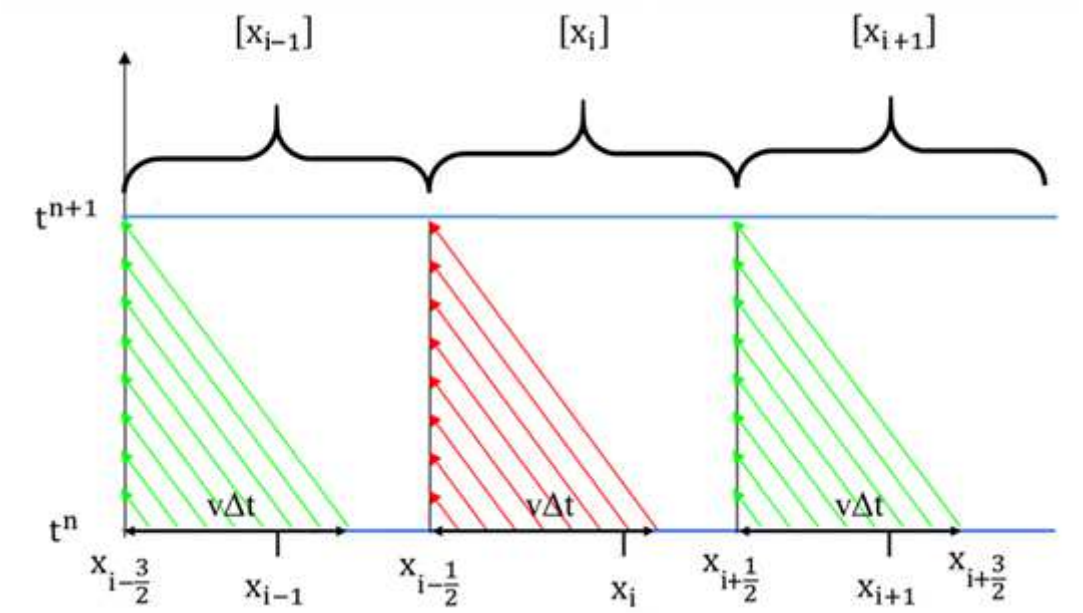

Figure 2-15 Space-time plane from t^n~ t^{n+1} to $x_{i\pm\frac{1}{2}} + v\Delta t$ ~ $x_{i\pm\frac{1}{2}}$ for $v < 0$.

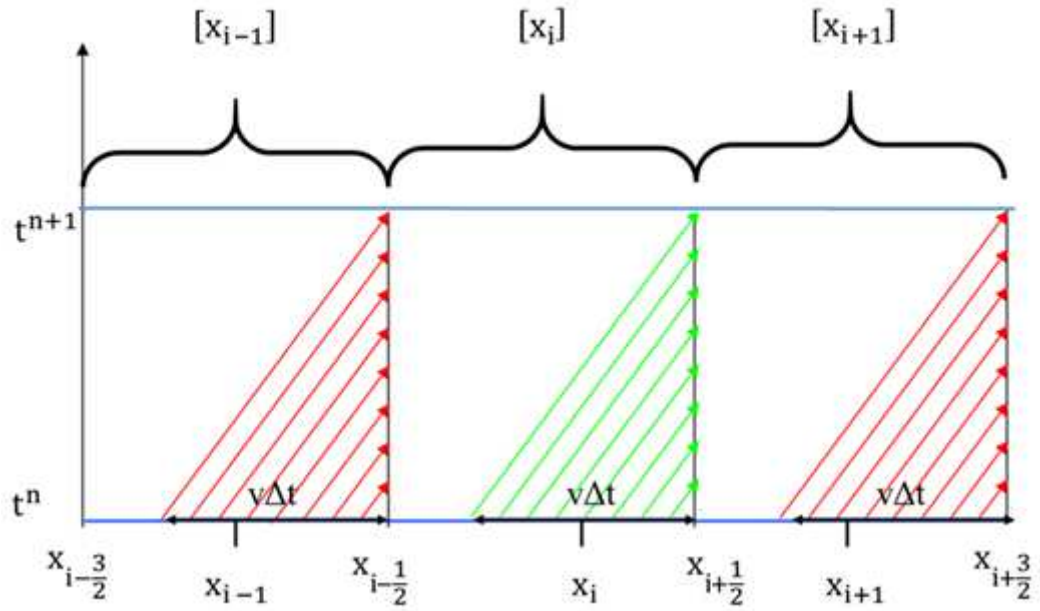

Figure 2-16 Space-time plane from t^n~ t^{n+1} to $x_{i\pm\frac{1}{2}}$ ~ $x_{i\pm\frac{1}{2}} - v\Delta t$ for $v \geq 0$.

As a result, Eq.(2-118) can be rewritten in Eq.(2-135) and Eq.(2-136).

$$\bar{f}_{i+\frac{1}{2}}=\frac{\int_{t^n}^{t^{n+1}} f_{i+\frac{1}{2}}dt}{\Delta t}=\frac{1}{v\Delta t}\int_{x_{i+\frac{1}{2}}}^{x_{i+\frac{1}{2}}+v\Delta t} f(x_{i+1})dx=\frac{1}{v\Delta t}\int_{x_{i+\frac{1}{2}}-v\Delta t}^{x_{i+\frac{1}{2}}} f(x_i)dx \tag{2-135}$$

$$\bar{f}_{i-\frac{1}{2}}=\frac{\int_{t^n}^{t^{n+1}} f_{i-\frac{1}{2}}dt}{\Delta t}=\frac{1}{v\Delta t}\int_{x_{i+\frac{1}{2}}}^{x_{i+\frac{1}{2}}+v\Delta t} f(x_i)dx=\frac{1}{v\Delta t}\int_{x_{i+\frac{1}{2}}-v\Delta t}^{x_{i+\frac{1}{2}}} f(x_{i-1})dx \tag{2-136}$$

The right hand side of Eq.(2-135) and Eq.(2-136) are redefined in the following.

$$\bar{f}^n_{i+1}=\frac{1}{v\Delta t}\int_{x_{i+\frac{1}{2}}}^{x_{i+\frac{1}{2}}+v\Delta t} f(x_{i+1})dx \tag{2-137}$$

$$\bar{f}^n_{i}=\frac{1}{v\Delta t}\int_{x_{i-\frac{1}{2}}}^{x_{i-\frac{1}{2}}+v\Delta t} f(x_i)dx=\frac{1}{v\Delta t}\int_{x_{i+\frac{1}{2}}-v\Delta t}^{x_{i+\frac{1}{2}}} f(x_i)dx \tag{2-138}$$

$$\bar{f}^n_{i-1}=\frac{1}{v\Delta t}\int_{x_{i-\frac{1}{2}}-v\Delta t}^{x_{i-\frac{1}{2}}} f(x_{i-1})dx \tag{2-139}$$

There is an interface between two conjunctive grids. Value on the interface can be calculate from the value in the grid on either side of the interface. The choice of which grid to use depends on the advection equation propagates direction. One is using the left of interface of i (which have + subscript as $\bar{f}^n_{i,+}$), and the other one is using the right of the interface of i (which have - subscript as $\bar{f}^n_{i,-}$).

$$\bar{f}^n_{i+\frac{1}{2}}=\begin{cases}\bar{f}^n_{i,+}=\dfrac{1}{v\Delta t}\displaystyle\int_{x_{i+\frac{1}{2}}-v\Delta t}^{x_{i+\frac{1}{2}}} f(x_i)dx\ ,v\geq 0\\ \bar{f}^n_{i+1,-}=\dfrac{1}{v\Delta t}\displaystyle\int_{x_{i+\frac{1}{2}}}^{x_{i+\frac{1}{2}}+v\Delta t} f(x_{i+1})dx\ ,v<0\end{cases},$$

$$\bar{f}^n_{i-\frac{1}{2}}=\begin{cases}\bar{f}^n_{i-1,+}=\dfrac{1}{v\Delta t}\displaystyle\int_{x_{i-\frac{1}{2}}-v\Delta t}^{x_{i-\frac{1}{2}}} f(x_{i-1})dx\ ,v\geq 0\\ \bar{f}^n_{i,-}=\dfrac{1}{v\Delta t}\displaystyle\int_{x_{i-\frac{1}{2}}}^{x_{i-\frac{1}{2}}+v\Delta t} f(x_i)dx\ ,v<0\end{cases}. \tag{2-140}$$

Before understanding piecewise linear method (PLM), we first look at the piecewise constant method (PCoM)[7][8] and Godunov's method[7][8]. To solve Eq.(2-118), Godunov's

method is a finite volume method which treats the solution as piecewise function. The piecewise constant method is the basic Godunov's method, it uses piecewise constant function to approximate the mean cell averages

$$f(x)=\bar{f}_i^n. \tag{2-141}$$

By using Eq.(2-141), we know that $\bar{f}_i^n = \bar{f}_{i,+} = \bar{f}_{i,-}$ so Eq.(2-140) becomes

$$\begin{aligned} \bar{f}_{i+\frac{1}{2}}^n &= \begin{cases} \bar{f}_i^n, v \geq 0 \\ \bar{f}_{i+1}^n, v < 0 \end{cases}, \\ \bar{f}_{i-\frac{1}{2}}^n &= \begin{cases} \bar{f}_{i-1}^n, v \geq 0 \\ \bar{f}_i^n, v < 0 \end{cases}. \end{aligned} \tag{2-142}$$

This is shown in Figure 2-17. In Figure 2-17, $\bar{f}_{i,+}^n$ term represents $\bar{f}_i^n$ term when v > 0, and the, and $\bar{f}_{i,-}^n$ term represents $\bar{f}_i^n$ term when v < 0. These are consistent with Eq.(2-142).

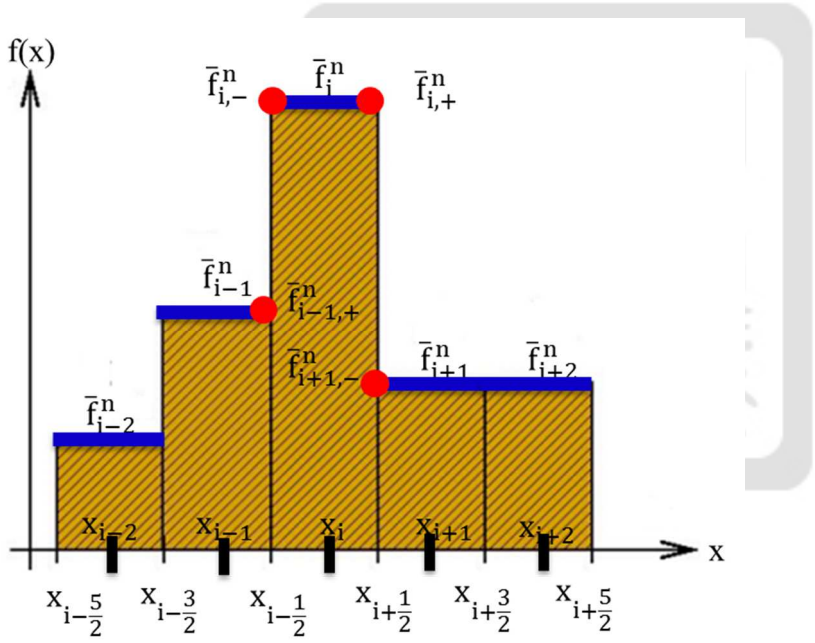

Figure 2-17 Approximation line of piecewise constant method (PCoM).

As a result, Eq.(2-118) also can be written as following in using piecewise constant method (PCoM).

$$\begin{cases} \bar{f}_i^{n+1} = \bar{f}_i^n - \dfrac{v\Delta t}{\Delta x}\left(\bar{f}_i^n - \bar{f}_{i-1}^n\right) \text{ for } v \geq 0, \\ \bar{f}_i^{n+1} = \bar{f}_i^n - \dfrac{v\Delta t}{\Delta x}\left(\bar{f}_{i+1}^n - \bar{f}_i^n\right) \text{ for } v < 0. \end{cases} \tag{2-143}$$

Piecewise linear method (PLM) is also a Godunov's type finite volume method, this method uses function $f(x_i)$ reconstructed by a linear function in each cell. The $f(x_i)$ can be written in Eq.(2-144).

$$f(x)=c_0+c_1(x-x_i). \tag{2-144}$$

The left and right boundary of grids are shown in Eq.(2-145) and Eq.(2-146) respectively.

$$f\left(x_{i-\frac{1}{2}}\right)=c_0+c_1\left(x_{i-\frac{1}{2}}-x_i\right)=c_0-c_1\frac{\Delta x}{2}=f_{i,-}, \tag{2-145}$$

$$f\left(x_{i+\frac{1}{2}}\right)=c_0+c_1\left(x_{i+\frac{1}{2}}-x_i\right)=c_0+c_1\frac{\Delta x}{2}=f_{i,+}. \tag{2-146}$$

The integration of Eq.(2-144) is

$$\bar{f}_i^n=\int_{x_{i-\frac{1}{2}}}^{x_{i+\frac{1}{2}}}f(x_i)dx=\int_{x_{i-\frac{1}{2}}}^{x_{i+\frac{1}{2}}}[c_0+c_1(x-x_i)]dx=c_0. \tag{2-147}$$

Therefore, c_0 and c_1 are shown in the following.

$$c_0.=\bar{f}_i^n, \tag{2-148}$$

$$c_1=\frac{f_{i,+}-f_{i,-}}{\Delta x}=\frac{\Delta f_i}{\Delta x}. \tag{2-149}$$

By brining Eq.(2-148) and Eq.(2-149) back to Eq.(2-144), $f(x_i)$ becomes

$$f(x)=\bar{f}_i^n+(x-x_i)\Delta\bar{f}_i^n \text{ where } \Delta\bar{f}_i^n=\frac{\Delta f_i}{\Delta x}. \tag{2-150}$$

Figure 2-18 is shown that the piecewise linear function is used to approximate function f(x). The $\bar{f}_{i,+}^n$ term represents $\bar{f}_i^n$ term when v > 0, and the, and the $\bar{f}_{i,-}^n$ term represents $\bar{f}_i^n$ term when v < 0.

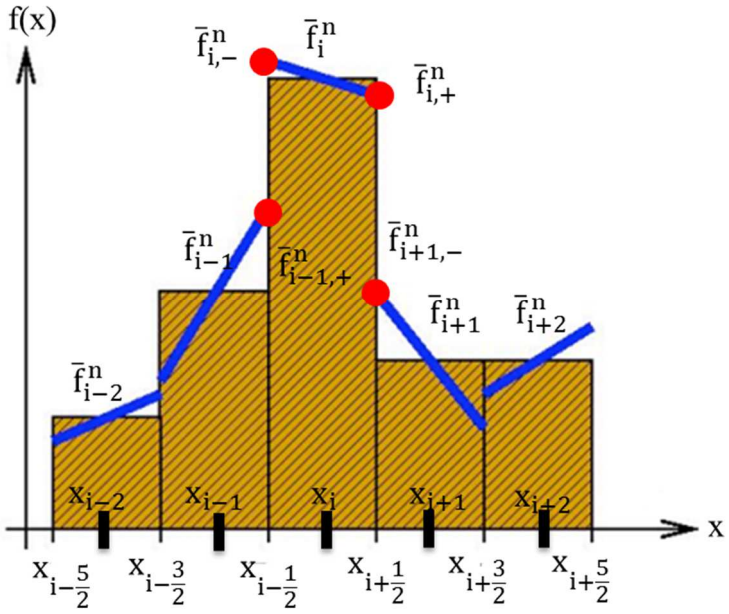

Figure 2-18 Approximation line of piecewise linear method (PLM).

Eq.(2-150) can be integrated by using Eq.(2-140) and shown in Eq.(2-151).

$$\bar{f}_{i+\frac{1}{2}} = \begin{cases} \bar{f}_i^n + \frac{1}{2}\left(1-v\frac{\Delta t}{\Delta x}\right)\Delta\bar{f}_i^n, v \geq 0, \\ \bar{f}_{i+1}^n - \frac{1}{2}\left(1+v\frac{\Delta t}{\Delta x}\right)\Delta\bar{f}_{i+1}^n, v < 0. \end{cases}$$

$$\bar{f}_{i-\frac{1}{2}} = \begin{cases} \bar{f}_{i-1}^n + \frac{1}{2}\left(1-v\frac{\Delta t}{\Delta x}\right)\Delta\bar{f}_{i-1}^n, v \geq 0, \\ \bar{f}_i^n - \frac{1}{2}\left(1+v\frac{\Delta t}{\Delta x}\right)\Delta\bar{f}_i^n, v < 0. \end{cases} \quad (2\text{-}151)$$

Finally, $\bar{f}_{i+\frac{1}{2}}$ and $\bar{f}_{i-\frac{1}{2}}$ terms can be substituted into the finite volume form as Eq.(2-152).

$$\begin{cases} \bar{f}_i^{n+1} = \bar{f}_i^n - v\frac{\Delta t}{\Delta x}\left[(\bar{f}_i^n - \bar{f}_{i-1}^n) + \frac{1}{2}(\Delta\bar{f}_i^n - \Delta\bar{f}_{i-1}^n)\left(1-v\frac{\Delta t}{\Delta x}\right)\right], v \geq 0, \\ \bar{f}_i^{n+1} = \bar{f}_i^n - v\frac{\Delta t}{\Delta x}\left[(\bar{f}_{i+1}^n - \bar{f}_i^n) - \frac{1}{2}(\Delta\bar{f}_{i+1}^n - \Delta\bar{f}_i^n)\left(1+v\frac{\Delta t}{\Delta x}\right)\right], v < 0. \end{cases} \quad (2\text{-}152)$$

There are lots of different definitions of slope $\Delta\bar{f}_i^n$. If $\Delta\bar{f}_i^n=0$, Eq.(2-152) is back to piecewise constant method (PCoM) as Eq.(2-143). However, choice of slope is very important in piecewise linear method for its accuracy. To reduce the numerical oscillation of numerical simulation, $\Delta\bar{f}_i^n$ should be set carefully. Therefore, $\Delta\bar{f}_i^n$ is also called slope-

limiter[1][8][10]. The vanLeer slope-limiter is used and is given in the following. This slope-limiter uses the harmonic mean of two slopes in each averaged cells to limit the reconstruction range in piecewise linear equation. This slope is shown in Eq.(2-153).

$$\Delta\bar{f}_i^n=\text{vanLeer}(a,b)=\text{vanLeer}\left(\frac{f_i^n-f_{i-1}^n}{\Delta x},\frac{f_{i+1}^n-f_i^n}{\Delta x}\right),$$
$$\text{vanLeer}(a,b)=\begin{cases}\frac{2ab}{a+b}, ab>0\\ 0, ab\le 0\end{cases}. \tag{2-153}$$

2.5.6.4 Piecewise parabolic method

Piecewise parabolic method (PPM) is also a Godunov's type finite volume method but with higher-order approximation to solve Eq. (2-118). The $\bar{f}_{i,+}^n$ term represents $\bar{f}_i^n$ term when v > 0, and the, and the $\bar{f}_{i,-}^n$ term represents $\bar{f}_i^n$ term when v < 0.

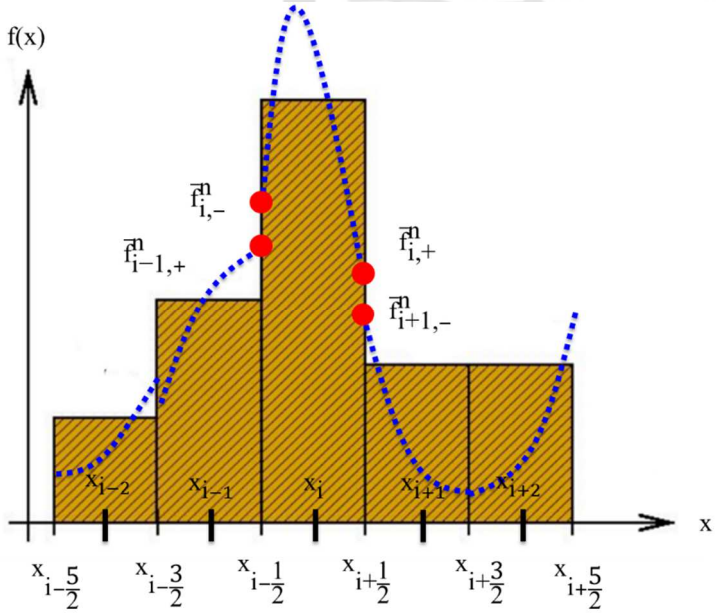

Figure 2-19 Approximation line of piecewise parabolic method (PPM).

PPM is assumed that the function f_i^n can be approximated by a parabola inside every grid cell, and it is shown in Eq.(2-154). Figure 2-19 is shown how the piecewise parabolic method

works on reconstructing the function f(x).

$$f(x)=c_0+c_1(x-x_i)+c_2(x-x_i)^2. \tag{2-154}$$

This equation can be solved as following.

$$f\left(x_{i-\frac{1}{2}}\right)=c_0+c_1\left(x_{i-\frac{1}{2}}-x_i\right)+c_2\left(x_{i-\frac{1}{2}}-x_i\right)^2=f_{i,-}, \tag{2-155}$$

$$f\left(x_{i+\frac{1}{2}}\right)=c_0+c_1\left(x_{i+\frac{1}{2}}-x_i\right)+c_2\left(x_{i+\frac{1}{2}}-x_i\right)^2=f_{i,+}. \tag{2-156}$$

These two equations are rewritten in the following.

$$f\left(x_{i-\frac{1}{2}}\right)=c_0-c_1\frac{\Delta x}{2}+c_2\frac{\Delta x^2}{4}=f_{i,-}, \tag{2-157}$$

$$f\left(x_{i+\frac{1}{2}}\right)=c_0+c_1\frac{\Delta x}{2}+c_2\frac{\Delta x^2}{4}=f_{i,+}. \tag{2-158}$$

These two equations result in Eq.(2-159) and Eq.(2-160).

$$f_{i,+}+f_{i,-}=2c_0+c_2\frac{\Delta x^2}{2}, \tag{2-159}$$

$$f_{i,+}-f_{i,-}=c_1\Delta x. \tag{2-160}$$

These two equations can help to do the integration of f(x) between Δx.

$$\bar{f}_i^n=\int_{x_{i-\frac{1}{2}}}^{x_{i+\frac{1}{2}}}f(x)dx=\int_{x_{i-\frac{1}{2}}}^{x_{i+\frac{1}{2}}}[c_0+c_1(x-x_i)+c_2(x-x_i)^2]dx=c_0+\frac{c_2}{12}\Delta x^2. \tag{2-161}$$

As a result, c_0, c_1, c_2 can be given in the following.

$$c_0=\bar{f}_i^n-\frac{c_2}{12}\Delta x^2 \tag{2-162}$$

$$c_1=\frac{1}{\Delta x}\left(f_{i,+}-f_{i,-}\right). \tag{2-163}$$

$$c_2=3\left(f_{i,+}+f_{i,-}\right)-6\bar{f}_i^n\equiv c_{2,i}. \tag{2-164}$$

Therefore, Eq.(2-154) can be rewritten in Eq.(2-165), and $\Delta f_i \equiv f_{i,+}-f_{i,-}$.

$$f(x)=\bar{f}_i^n-\frac{c_{2,i}}{12}\Delta x^2+\Delta\bar{f}_i^n(x-x_i)+\frac{c_{2,i}}{\Delta x^2}(x-x_i)^2 \text{ where } \Delta\bar{f}_i^n\equiv\frac{\Delta f_i}{\Delta x} \tag{2-165}$$

Eq.(2-140) can be calculated by using the integration of f(x) in Eq.(2-165).

$$\bar{f}_{i+\frac{1}{2}}=\begin{cases}\bar{f}^{n}_{i,+}=f_{i,+}-\dfrac{v\Delta t}{2\Delta x}\left[\Delta\bar{f}^{n}_{i}-\left(1-\dfrac{2v\Delta t}{3\Delta x}\right)c_{2,i}\right], v\geq 0,\\ \bar{f}^{n}_{i+1,-}=f_{i+1,-}+\dfrac{v\Delta t}{2\Delta x}\left[\Delta\bar{f}^{n}_{i+1}+\left(1-\dfrac{2v\Delta t}{3\Delta x}\right)c_{2,i+1}\right], v<0.\end{cases}$$

$$\bar{f}_{i-\frac{1}{2}}=\begin{cases}\bar{f}^{n}_{i-1,+}=f_{i-1,+}-\dfrac{v\Delta t}{2\Delta x}\left[\Delta\bar{f}^{n}_{i-1}-\left(1-\dfrac{2v\Delta t}{3\Delta x}\right)c_{2,i-1}\right], v\geq 0,\\ \bar{f}^{n}_{i,-}=f_{i,-}+\dfrac{v\Delta t}{2\Delta x}\left[\Delta\bar{f}^{n}_{i}+\left(1-\dfrac{2v\Delta t}{3\Delta x}\right)c_{2,i}\right], v<0.\end{cases}\qquad (2\text{-}166)$$

Bring Eq.(2-166) into Eq.(2-118).

$$\begin{cases}\bar{f}^{n+1}_{i}=\bar{f}^{n}_{i}-v\dfrac{\Delta t}{\Delta x}\left\{\left(f_{i,+}-f_{i-1,+}\right)-\dfrac{v\Delta t}{2\Delta x}\left[\left(\Delta\bar{f}^{n}_{i}-\Delta\bar{f}^{n}_{i-1}\right)-\left(1-\dfrac{2v\Delta t}{3\Delta x}\right)\left(c_{2,i}-c_{2,i-1}\right)\right]\right\}, v\geq 0,\\ \bar{f}^{n+1}_{i}=\bar{f}^{n}_{i}-v\dfrac{\Delta t}{\Delta x}\left\{\left(f_{i+1,-}-f_{i,-}\right)+\dfrac{v\Delta t}{2\Delta x}\left[\left(\Delta\bar{f}^{n}_{i+1}-\Delta\bar{f}^{n}_{i}\right)+\left(1-\dfrac{2v\Delta t}{3\Delta x}\right)\left(c_{2,i+1}-c_{2,i}\right)\right]\right\}, v<0.\end{cases}\qquad (2\text{-}167)$$

Let us focus on the process of obtaining $f_{i,+}$ and $f_{i,-}$. $f_{i,+}$ and $f_{i,-}$ can be obtained by specifying these values with cubic accuracy. Thus it defines a cubic polynomial equation $f(x)=a_0+a_1(x-x_{i\pm\frac{1}{2}})+a_2(x-x_{i\pm\frac{1}{2}})^2+a_3(x-x_{i\pm\frac{1}{2}})^3$, and do the integration in Eq.(2-168).

$$\bar{f}^{n}_{i-1}=\frac{1}{\Delta x}\int_{i-\frac{3}{2}}^{i-\frac{1}{2}}f(x)dx,\ \bar{f}^{n}_{i}=\frac{1}{\Delta x}\int_{i-\frac{1}{2}}^{i+\frac{1}{2}}f(x)dx,\ \bar{f}^{n}_{i+1}=\frac{1}{\Delta x}\int_{i+\frac{1}{2}}^{i+\frac{3}{2}}f(x)dx,$$

$$\bar{f}^{n}_{i-2}=\frac{1}{\Delta x}\int_{i-\frac{5}{2}}^{i-\frac{3}{2}}f(x)dx,\ \bar{f}^{n}_{i+2}=\frac{1}{\Delta x}\int_{i+\frac{3}{2}}^{i+\frac{5}{2}}f(x)dx.\qquad (2\text{-}168)$$

$$\bar{f}^{n}_{i-3}=\frac{1}{\Delta x}\int_{i-\frac{7}{2}}^{i-\frac{5}{2}}f(x)dx,\ \bar{f}^{n}_{i+3}=\frac{1}{\Delta x}\int_{i+\frac{5}{2}}^{i+\frac{7}{2}}f(x)dx.$$

f_i terms can become Eq.(2-169) to Eq.(2-172). The calculation are shown in Appendix A.

$$f_{i,+}=f_{i+1,-}=\left[\frac{7}{12}\left(\bar{f}^{n}_{i}+\bar{f}^{n}_{i+1}\right)-\frac{1}{12}\left(\bar{f}^{n}_{i+2}+\bar{f}^{n}_{i-1}\right)\right].\qquad (2\text{-}169)$$

$$f_{i+1,+}=f_{i+2,-}=\left[\frac{7}{12}\left(\bar{f}^{n}_{i+1}+\bar{f}^{n}_{i+2}\right)-\frac{1}{12}\left(\bar{f}^{n}_{i+3}+\bar{f}^{n}_{i}\right)\right],\qquad (2\text{-}170)$$

$$f_{i-1,+}=f_{i,-}=\left[\frac{7}{12}\left(\bar{f}^{n}_{i-1}+\bar{f}^{n}_{i}\right)-\frac{1}{12}\left(\bar{f}^{n}_{i+1}+\bar{f}^{n}_{i-2}\right)\right],\qquad (2\text{-}171)$$

$$f_{i-2,+}=f_{i-1,-}=\left[\frac{7}{12}\left(\bar{f}^{n}_{i-2}+\bar{f}^{n}_{i-1}\right)-\frac{1}{12}\left(\bar{f}^{n}_{i}+\bar{f}^{n}_{i-3}\right)\right].\qquad (2\text{-}172)$$

Eq.(2-169) to Eq.(2-172) are used in Eq.(2-167).

2.5.6.5 Benchmark of solving advection equation by using Godunov's scheme

Piecewise linear method and piecewise parabolic method are both used in split advection equations in velocity and space from Vlasov equation. In fact in each advection equation, both PLM and PPM are used at the same time. It is because using PPM gives a more accurate solution than using PLM but with numerical oscillation. PLM is less accurate than PPM but is more diffusive. Therefore, combing PPM and PLM can be beneficial since PPM gives an accurate solution and PLM can smear out the numerical solution. Thus, the split equations Eq.(2-128) and Eq.(2-129) are split again.

$$\int_{v_{iv-\frac{1}{2}}}^{v_{iv+\frac{1}{2}}}(f^{**}-f^{*})dv+\int_{v_{iv-\frac{1}{2}}}^{v_{iv+\frac{1}{2}}}(f^{*}-f^{n})dv$$
$$+\beta_1\int_{t^n}^{t^{n+1}}a(f_{iv+\frac{1}{2}-}-f_{iv-\frac{1}{2}})dt+(1-\beta_1)\int_{t^n}^{t^{n+1}}a(f_{iv+\frac{1}{2}-}-f_{iv-\frac{1}{2}})dt=0, \quad (2\text{-}173)$$

$$\int_{x_{ix-\frac{1}{2}}}^{x_{ix+\frac{1}{2}}}(f^{n+1}-f^{***})dx+\int_{x_{ix-\frac{1}{2}}}^{x_{ix+\frac{1}{2}}}(f^{***}-f^{**})dx$$
$$+\beta_2\int_{t^n}^{t^{n+1}}v(f_{ix+\frac{1}{2}-}-f_{ix-\frac{1}{2}})dt+(1-\beta_2)\int_{t^n}^{t^{n+1}}v(f_{ix+\frac{1}{2}-}-f_{ix-\frac{1}{2}})dt=0. \quad (2\text{-}174)$$

These two equations can be separated to the following four equations.

$$\int_{v_{iv-\frac{1}{2}}}^{v_{iv+\frac{1}{2}}}(f^{*}-f^{n})dv+\beta_1\int_{t^n}^{t^{n+1}}a(f_{iv+\frac{1}{2}-}-f_{iv-\frac{1}{2}})dt=0.$$
$$\int_{v_{iv-\frac{1}{2}}}^{v_{iv+\frac{1}{2}}}(f^{**}-f^{*})dv+(1-\beta_1)\int_{t^n}^{t^{n+1}}a(f_{iv+\frac{1}{2}-}-f_{iv-\frac{1}{2}})dt=0, \quad (2\text{-}175)$$

$$\int_{x_{ix-\frac{1}{2}}}^{x_{ix+\frac{1}{2}}}(f^{***}-f^{**})dx+\beta_2\int_{t^n}^{t^{n+1}}v(f_{ix+\frac{1}{2}-}-f_{ix-\frac{1}{2}})dt=0. \quad (2\text{-}176)$$

$$\int_{x_{ix-\frac{1}{2}}}^{x_{ix+\frac{1}{2}}} (f^{n+1}-f^{***})dx + (1-\beta_2)\int_{t^n}^{t^{n+1}} v(f_{ix+\frac{1}{2}}-f_{ix-\frac{1}{2}})dt = 0,$$

They become

$$\begin{aligned} \bar{f}_i^{*} &= f_i^n - \frac{a}{dv}\beta_1 \int_{t^n}^{t^{n+1}} (f_{iv+\frac{1}{2}}-f_{iv-\frac{1}{2}})dt . \\ \bar{f}_i^{**} &= f_i^{*} - \frac{a}{dv}(1-\beta_1)\int_{t^n}^{t^{n+1}} (f_{iv+\frac{1}{2}}-f_{iv-\frac{1}{2}})dt , \end{aligned} \qquad (2\text{-}177)$$

$$\begin{aligned} f^{***} &= f^{**} - \frac{v}{dx}\beta_2 \int_{t^n}^{t^{n+1}} (f_{ix+\frac{1}{2}}-f_{ix-\frac{1}{2}})dt . \\ f^{n+1} &= f^{***} - \frac{v}{dx}(1-\beta_2)\int_{t^n}^{t^{n+1}} (f_{ix+\frac{1}{2}}-f_{ix-\frac{1}{2}})dt , \end{aligned} \qquad (2\text{-}178)$$

In the method of combing PLM and PPM, the first equations in both Eq.(2-177) and Eq.(2-178) are solved by PPM. The second equation is solved by PLM. β_1 and β_2 are parameters smaller than 1 that can adjust the percentage of using PLM and PPM. The benchmark of piecewise linear method with van Leer slope-limiter and piecewise parabolic method in solving advection equation is shown in this section, the result is compared with an exact solution one.

First, the advection in velocity as Eq.(2-130) is benchmarked. The initial distribution function is set as $f(x,v,t=0)=e^{-\frac{(v-5)^2}{2}}$. The analytical solution is $f(x,v,t)=e^{-\frac{(v-5-at)^2}{2}}$ where a = 0 to 4π. The analytical solution is used to benchmark the numerical solution. The boundary condition is a periodic boundary condition in velocity space grids during the benchmark. The range of v is set from v = 0 v_{th} to v = 10 v_{th}. Total time t is set as 1 ω_p^{-1}, and Δt is set as 0.00125, total time steps are set as 800. Figure 2-20 shows the Eq.(2-130) solved by using PLM with vanLeer slope-limiter. Figure 2-21 shows the Eq.(2-130) solved by using PPM. Obviously that PPM has higher accuracy than PLM. PLM is diffusive after some time.

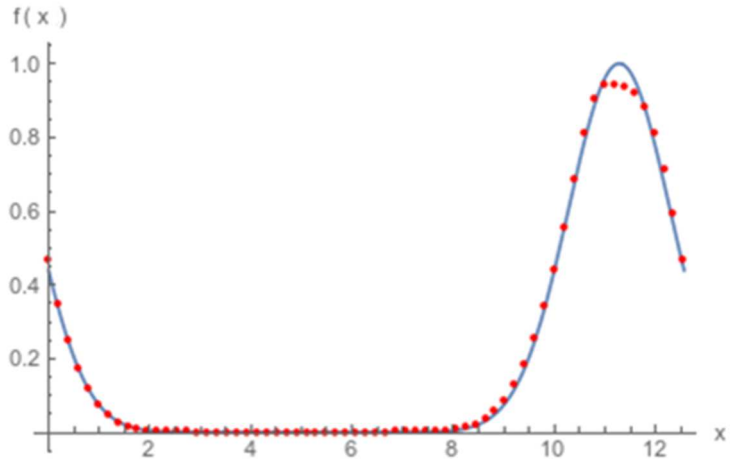

Figure 2-20 Advection equation in x by PLM with vanLeer slope-limiter. The red dashed points are simulation results, and the blue solid lines are analytical results.

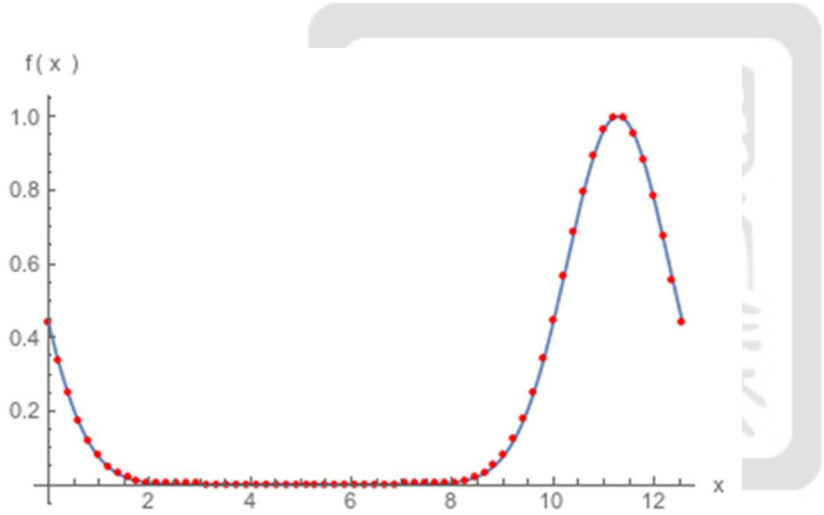

Figure 2-21 Advection equation in x by PPM. The red dashed points are simulation results, and the blue solid lines are analytical results.

Then, the advection in space as Eq.(2-131) is benchmarked. The initial distribution function is set as $f(x,v,t=0) = e^{-\frac{(x-2\pi)^2}{2}}$. The analytical solution is $f(x,v,t) = e^{-\frac{(x-2\pi-vt)^2}{2}}$ where v = -5 to 5. The analytical solution is used to benchmark the numerical solution. The boundary condition is a periodic boundary condition the same as section 2.5.2. The range of x is set as $L=4\pi\,\lambda_D$. The quantities of t, Δt, and it are set the same for solving Eq.(2-130). Figure 2-22 shows the

Eq.(2-131) solved by using PLM with vanLeer slope-limiter. Figure 2-23 shows the Eq.(2-131) solved by using PPM. Figure 2-24 shows the Eq.(2-131) solved by using the combination of PPM and PLM with vanLeer slope-limiter with β_2=0.5. The combination of two methods shows that a less diffusive than only using PLM.

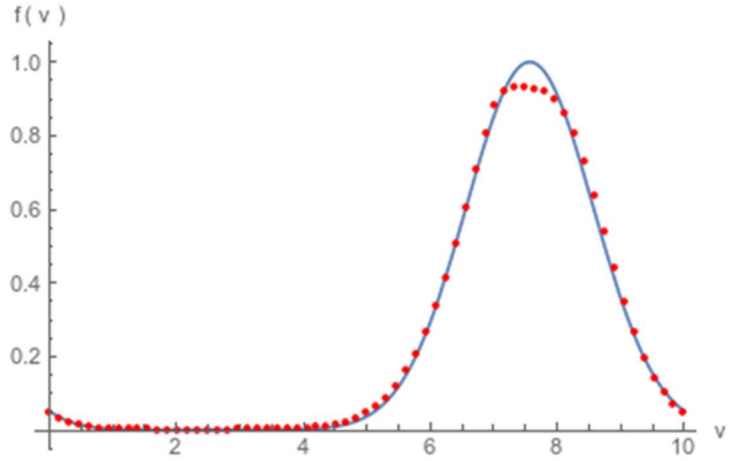

Figure 2-22 Advection equation in v by PLM with slope-limiter. The red dashed points are simulation results, and the blue solid lines are analytical results.

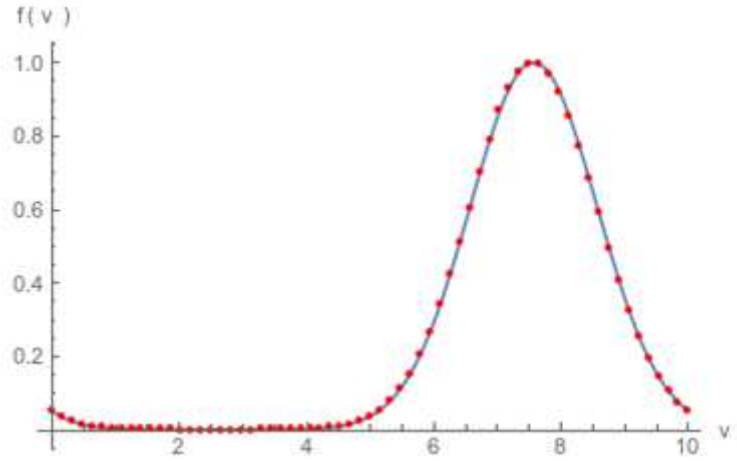

Figure 2-23 Advection equation in v by PPM. The red dashed points are simulation results, and the blue solid lines are analytical results.

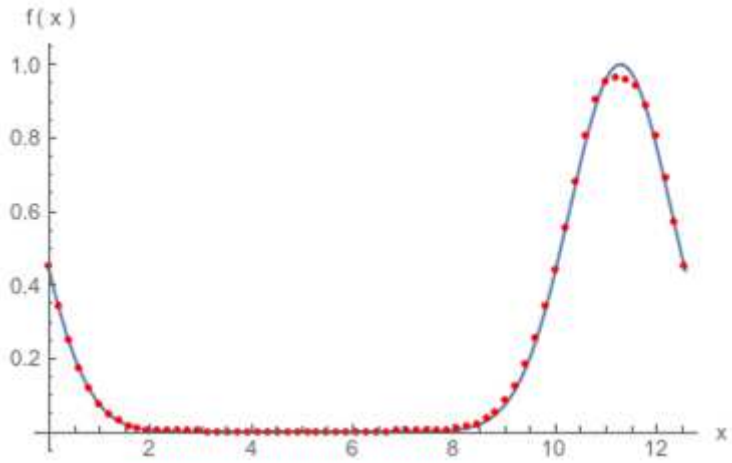

Figure 2-24 Advection equation in x by combination of PLM with vanLeer slope-limiter and PPM with β=0.5. The red dashed points are simulation results, and the blue solid lines are analytical results.

2.6 Benchmark by simulating two-stream instability

Two-stream instability is a kind of plasma phenomena It occurs when two counter-streaming plasma flow against each other. It is a suitable phenomenon to verify Vlasov code. The linearization of Vlasov-Poisson system and theory analysis of two-stream instability are derived from Vlasov-Poisson system in kinetic regime. The two-stream instability in code plasma are used to compare with the simulation results using Vlasov code.

2.6.1 Theory of two-stream instability

Vlasov-Poisson system are used to solve two-stream instability. Since two-stream instability is an electrostatic phenomena, only Vlasov equation and Poisson's equation are used to calculate. The Vlasov-Poisson system can be linearized by substituting $f=f_0+f_1$, $\varphi=\varphi_0+\varphi_1$, and $E=E_0+E_1$ into normalized Vlasov equation and Poisson's equation Eq.(2-28) to Eq.(2-32), they are shown in Eq.(2-179) to Eq.(2-181) respectively. Variables with

subscript 0 represents a steady, zeroth order solution while those with subscript 1 represent the first order perturbation.

$$\frac{\partial(f_0+f_1)}{\partial t}+v\frac{\partial(f_0+f_1)}{\partial x}-(E_0+E_1)\frac{\partial(f_0+f_1)}{\partial v}=0, \tag{2-179}$$

$$E_0+E_1=-\frac{\partial(\varphi_0+\varphi_1)}{\partial x}, \tag{2-180}$$

$$\frac{d^2(\varphi_0+\varphi_1)}{dx^2}=n_e-n_0=\int(f_0+f_1)dv-n_0. \tag{2-181}$$

Eq.(2-179) and Eq.(2-181) can be separated to zeroth order and first order equations as Eq.(2-182) to Eq. (2-183) and Eq.(2-184) to Eq.(2-185), respectively.

$$\frac{\partial f_0}{\partial t}+v\frac{\partial f_0}{\partial x}+\frac{\partial\varphi_0}{\partial x}\frac{\partial f_0}{\partial v}=0, \tag{2-182}$$

$$\frac{\partial f_1}{\partial t}+v\frac{\partial f_1}{\partial x}+\frac{\partial\varphi_1}{\partial x}\frac{\partial f_0}{\partial v}+\frac{\partial\varphi_1}{\partial x}\frac{\partial f_1}{\partial v}=0, \tag{2-183}$$

$$\frac{d^2\varphi_0}{dx^2}=\int f_0dv-n_0=n_0-n_0=0, \tag{2-184}$$

$$\frac{d^2\varphi_1}{dx^2}=\int f_1dv. \tag{2-185}$$

Because of $\varphi_0=0$ and $E_0=0$, the zeroth order solution is shown in Eq.(2-186) as initial state.

$$\frac{\partial f_0}{\partial t}+v\frac{\partial f_0}{\partial x}=0 \tag{2-186}$$

Because $\frac{\partial\varphi_1}{\partial x}\frac{\partial f_1}{\partial v}$ term is a second order term, it is neglected in Eq.(2-183) in the linearized equaiton and it is shown in Eq.(2-187).

$$\frac{\partial f_1}{\partial t}+v\frac{\partial f_1}{\partial x}+\frac{\partial\varphi_1}{\partial x}\frac{\partial f_0}{\partial v}=0 \tag{2-187}$$

Therefore, after doing linearization, only leading order terms are kept. Then this equation can be simplified in the following equations.

$$\frac{\partial f_1}{\partial t}+v\frac{\partial f_1}{\partial x}+\frac{\partial\varphi_1}{\partial x}\frac{\partial f_0}{\partial v}=0, \tag{2-188}$$

$$\frac{\partial^2 \varphi_1}{\partial x^2} = \int f_1 dv. \tag{2-189}$$

These two equations can be solved by Fourier transform. The Fourier transform of distribution function f and electric potential φ in time and space are shown in Eq.(2-190) and Eq.(2-191).

$$f_1(x,v,t) = \iint \tilde{f_1}(k,v,\omega) e^{-i(kx-\omega t)} dk d\omega, \tag{2-190}$$

$$\varphi_1(x) = \iint \tilde{\varphi}_1(k) e^{-i(kx-\omega t)} dk d\omega. \tag{2-191}$$

After substituting Eq.(2-190) and Eq.(2-191) into Eq.(2-188), the Vlasov equation becomes Eq.(2-192).

$$\iint \left[i(kv-\omega)\tilde{f_1} + ik\tilde{\varphi}_1 \frac{\partial f_0}{\partial v} \right] e^{-i(kx-\omega t)} dk d\omega = 0. \tag{2-192}$$

Apparently, there is a relation shown as below.

$$i(kv-\omega)\tilde{f_1} + ik\tilde{\varphi}_1 \frac{\partial f_0}{\partial v} = 0. \tag{2-193}$$

Fourier transform of distribution function f is shown in Eq.(2-194).

$$\tilde{f_1} = \frac{k\tilde{\varphi}_1}{(\omega-kv)} \frac{\partial f_0}{\partial v} = 0. \tag{2-194}$$

Inserting $\tilde{f_1}$ into Fourier-transformed Poisson's equation, and Poisson equation becomes

$$-k^2 \tilde{\varphi}_1 = \tilde{\varphi}_1 \int \frac{k}{(\omega-kv)} \frac{\partial f_0}{\partial v} dv, \tag{2-195}$$

$$\tilde{\varphi}_1 k^2 \left(1 + \frac{1}{k} \int \frac{1}{(\omega-kv)} \frac{\partial f_0}{\partial v} dv \right) = 0. \tag{2-196}$$

The equation inside bracket of Eq.(2-196) is called dispersion relation D. for a non-zero solution of $\tilde{\varphi}_1$, $D(\omega,k)=0$. Therefore, the dispersion relation is shown in Eq.(2-197).

$$D(\omega,k) = 1 + \frac{1}{k} \int \frac{1}{(\omega-kv)} \frac{\partial f_0}{\partial v} dv = 0 \tag{2-197}$$

For two stream instability of cold plasma, there are two counter-streaming beams as initial condition $f_0(v)$ in the following.

$$f_0(v)=\frac{1}{2}[\delta(v-v_0)+\delta(v-v_0)]. \tag{2-198}$$

Substituting Eq.(2-198) into dispersion relation in Eq.(2-197) and solving the integration, the dispersion relation becomes

$$D(\omega,k)=1-\frac{1}{2}\left[\frac{1}{(\omega-kv_0)^2}+\frac{1}{(\omega+kv_0)^2}\right]=0. \tag{2-199}$$

After moving the terms and sorting it out, it can be written in Eq.(2-200).

$$\omega^4-\left(1+2k^2v_0^2\right)\omega^2+\left(k^4v_0^4-k^2v_0^2\right)=0. \tag{2-200}$$

The $1+2k^2v_0^2$ is apparently positive, but the sign of $k^4v_0^4-k^2v_0^2$ depends on whether $k^2v_0^2>1$ or $k^2v_0^2<1$ respectively. The polynomial equation in Eq.(2-200) has two roots for ω^2 and it is shown in the following.

$$\omega_{\pm}^2=\frac{1}{2}\left(1+2k^2v_0^2\right)\pm\sqrt{\frac{1}{4}(1+2k^2v_0^2)^2-(k^4v_0^4-k^2v_0^2)}, \tag{2-201}$$

$$\Longrightarrow \omega_{\pm}^2=k^2v_0^2+\frac{1}{2}\left(1\pm\sqrt{1+8k^2v_0^2}\right). \tag{2-202}$$

When $k^2v_0^2>1$, i.e., $k^4v_0^4-k^2v_0^2>0$, $\omega_{\pm}^2$ are both positive and real values. Thus, there is no temporal growth or decay of the wave amplitude. On the other hand, for $k^2v_0^2<1$, $k^4v_0^4-k^2v_0^2<0$, ω_+^2 is positive so that ω_+ are real values but ω_-^2 is negative. Therefore, ω_- has two imaginary values with one positive and one negative. The positive and imaginary value of ω_- means the unstable situation, and it can be redefined as $\omega_-=i\omega_{(-)i}$. The solution of ω_- can be written as Eq.(2-203). This is where the growth rate of two-stream instability.

$$\omega_{(-)i}=\sqrt{-k^2v_0{}^2-\frac{1}{2}\left(1-\sqrt{1+8k^2v_0{}^2}\right)}, \tag{2-203}$$

The unstable condition occurs under the situation shown in Eq.(2-204).

$$0<k<\frac{1}{v_0} \tag{2-204}$$

The maximum growth rate is calculated by setting $\frac{d\omega^2}{dk}=0$ and $\omega_{(-)i}^2=-\omega_-^2$. To get their extreme values, the derivation of ω_-^2 is defined in Eq.(2-205).

$$\frac{d}{dk}\omega_-^2=2kv_0{}^2\left(1-\frac{2}{\sqrt{1+8k^2v_0{}^2}}\right)=0. \tag{2-205}$$

The minimum value of ω_-^2 occurs when $k=\frac{\sqrt{3}}{2\sqrt{2}v_0}$ and the maximum of $\omega_-^2=\frac{1}{8}$. The maximum growth rate of $\omega_{(-)i}$ is

$$\omega_{(-)i}=\frac{1}{2\sqrt{2}} \tag{2-206}$$

From above, v_0 can be defined as $v_0=\frac{\sqrt{3}}{2\sqrt{2}k}=\sqrt{\frac{3}{2}}$, $k=0.5$ and it is the condition to benchmark our simulation.

2.6.2 Benchmark of Vlasov solver using two-stream instability

To benchmark Vlasov simulation using two-stream instability, the Dirac delta function is used. It can be defined as Eq.(2-207).

$$\delta(v-v_0)=\lim_{v_{th}\to 0}\frac{1}{v_{th}\sqrt{\pi}}e^{-\frac{(v-v_0)^2}{v_{th}{}^2}}. \tag{2-207}$$

Eq.(2-198) can be rewritten as Eq.(2-208).

$$f_0(v)=\frac{1}{2}[\delta(v-v_0)+\delta(v+v_0)]=\frac{1}{2v_{th}\sqrt{\pi}}(e^{-\frac{(v-v_0)^2}{v_{th}^2}}+e^{-\frac{(v+v_0)^2}{v_{th}^2}}). \quad (2\text{-}208)$$

Therefore, the initial distribution function is set as Eq.(2-209) with a small quantity of v_{th}=0.3, $v_0=\sqrt{\frac{3}{2}}$, and k=0.5. The initial condition is shown in Eq.(2-209) and Figure 2-25. The distribution of f(x,v) in v and x are also shown in Figure 2-25. It is shown that the spatial distribution is a cosine function, and there are two Gaussian function in velocity space v.

$$f(x,v,0)=\frac{1}{2v_{th}\sqrt{\pi}}\left(e^{-\frac{(v-v_0)^2}{v_{th}^2}}+e^{-\frac{(v+v_0)^2}{v_{th}^2}}\right)[1+0.01\cos(kx)]. \quad (2\text{-}209)$$

This initial condition can be considered as a uniform plasma in which the ions are stationary and the electrons have a velocity v_0 relative to origin plasma. The dual Gaussian peaks centered at ±v0 in velocity space as the initial distribution function is used to study two-stream instability. The simulation range in x is set as $L=4\pi\lambda_D$, and v is set between -5 v_{th} to 5 v_{th}. Each time steps is defined as $\frac{1}{64}\Delta t$ where Δt is defined in Eq.(2-120). There are 128 grids in both x and v direction. The boundary condition is periodic in x and set as zero (Dirichlet boundary condition) in v. the simulation was first done only using PPM. The result iss shown in Figure 2-26. In Figure 2-26, it shows that there are a lot of numerical oscillations after running 30 ω_p^{-1}. That is because the stability of PPM isn't enough. After solving the advection equation, there are some values becoming negative. Figure 2-27 shows the simulation result by using PLM in both x and v direction. This graph shows a stable solution with oscillation but diffuse quickly compared to the combination method shown in Figure 2-28. As a result, the two advection equations split from Vlasov equation are solved by using combining PPM and PLM in velocity space grids v and only by using PLM in spatial grids x. The result of this combination method till 100 ω_p^{-1} is shown in Figure 2-28. For v_{th}=1, and $v_0=\sqrt{\frac{3}{2}}$ as the initial state using only PPM shown in Figure 2-29. The same problem was

simulated by using PLM and the combination of PPM and PLM. The result is shown in Figure 2-30 and Figure 2-31. The two figures shows that there are no much difference in using these two methods when v_{th}=1. Figure 2-32 shows the result of only using PPM in both split Vlasov equations. Few numerical oscillation occurs again. PPM have better details in simulation. The result combination of using PPM and PLM is more diffusive in the center of instabilities but with reasonable details. Therefore, PPM can only be used to do larger v_{th} problems, The numerical oscillation grows up as v_{th} decreases.

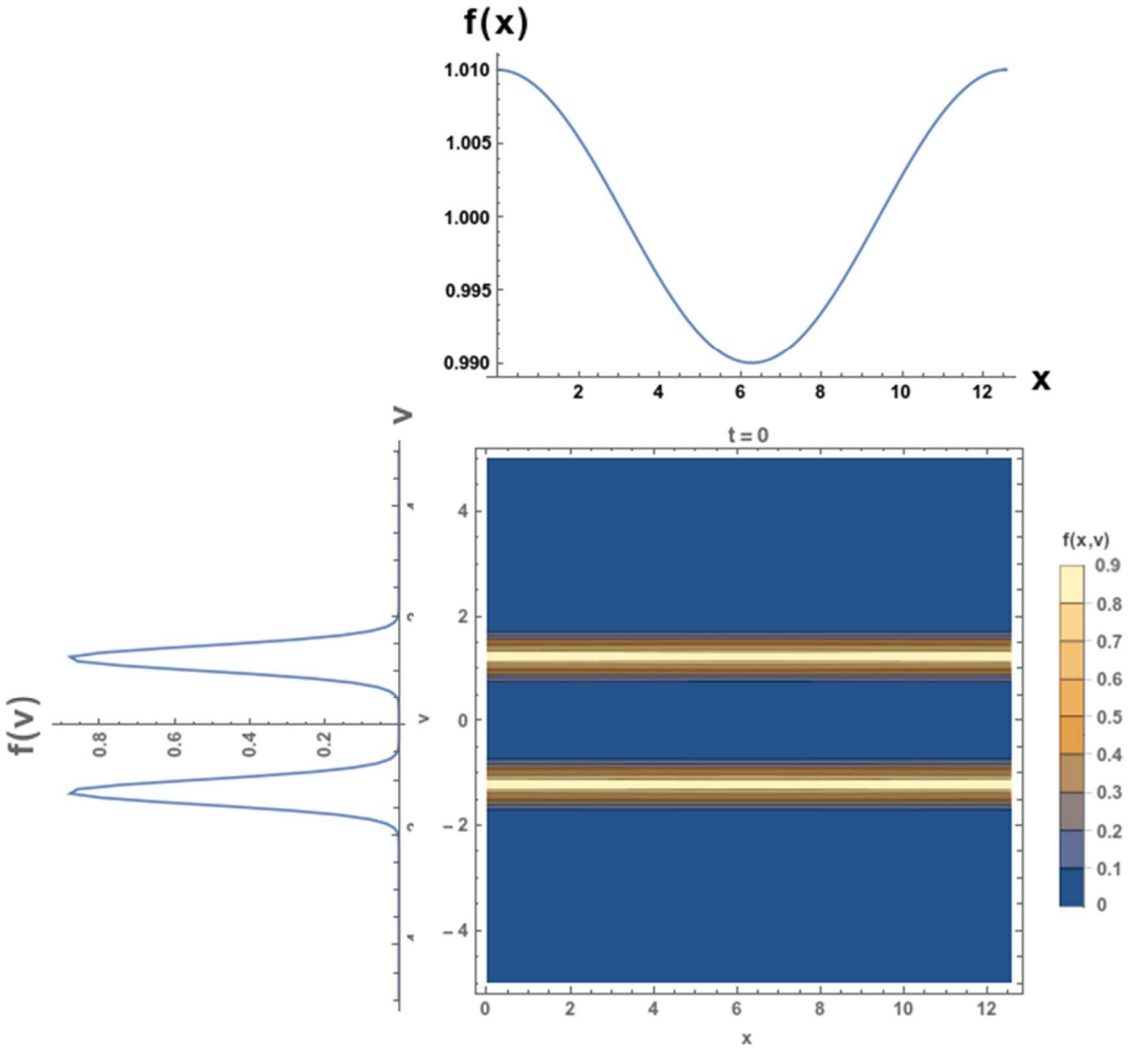

Figure 2-25 Initial state with v_{tth} = 0.3 and $v_0 = \sqrt{\frac{3}{2}}$.

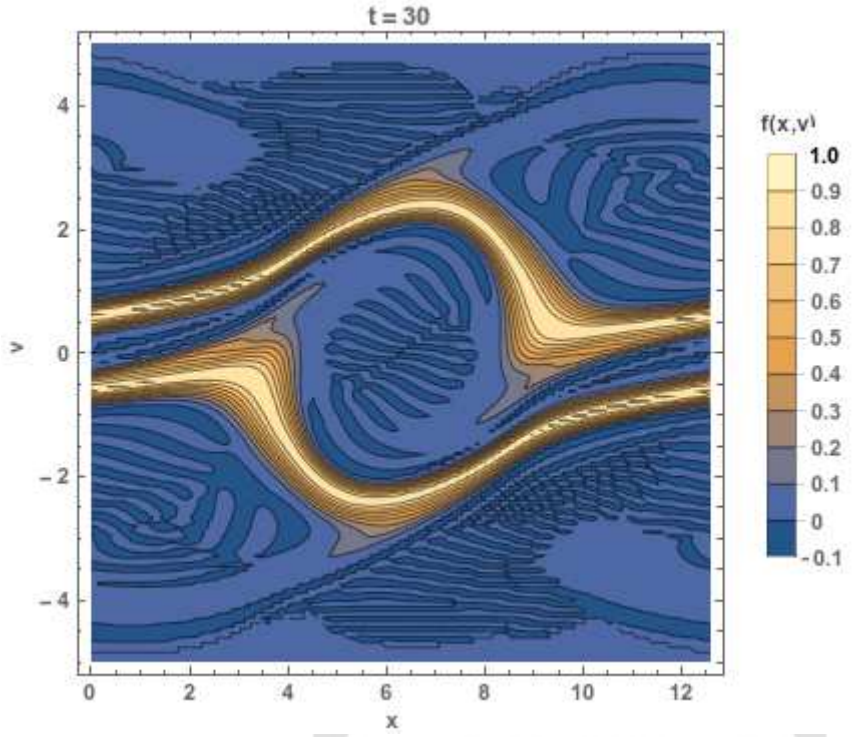

Figure 2-26 Simulation result after t = 30 ω_p^{-1} using PPM in both x and v direction.

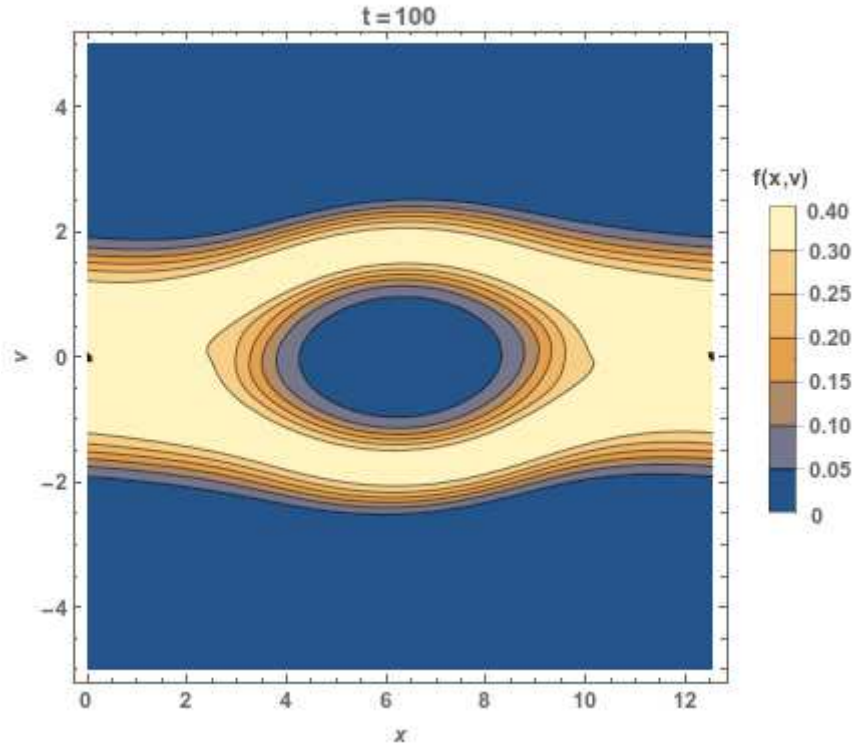

Figure 2-27 Simulation result after t = 100 ω_p^{-1} using PLM in both x and v direction.

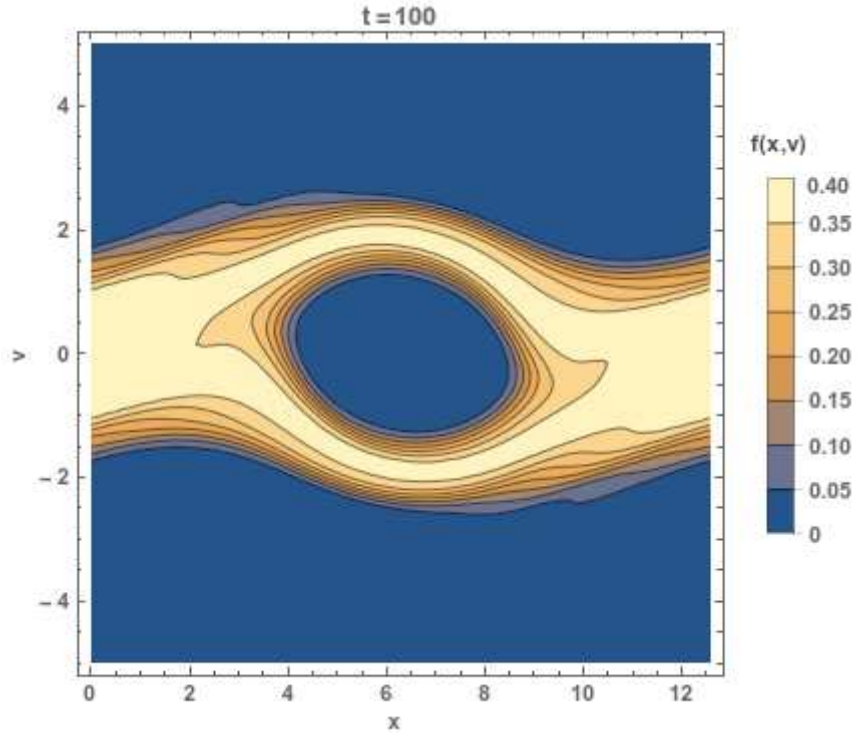

Figure 2-28 Simulation result after t = 100 ω_p^{-1} using PLM + PPM in x direction and PLM in v direction.

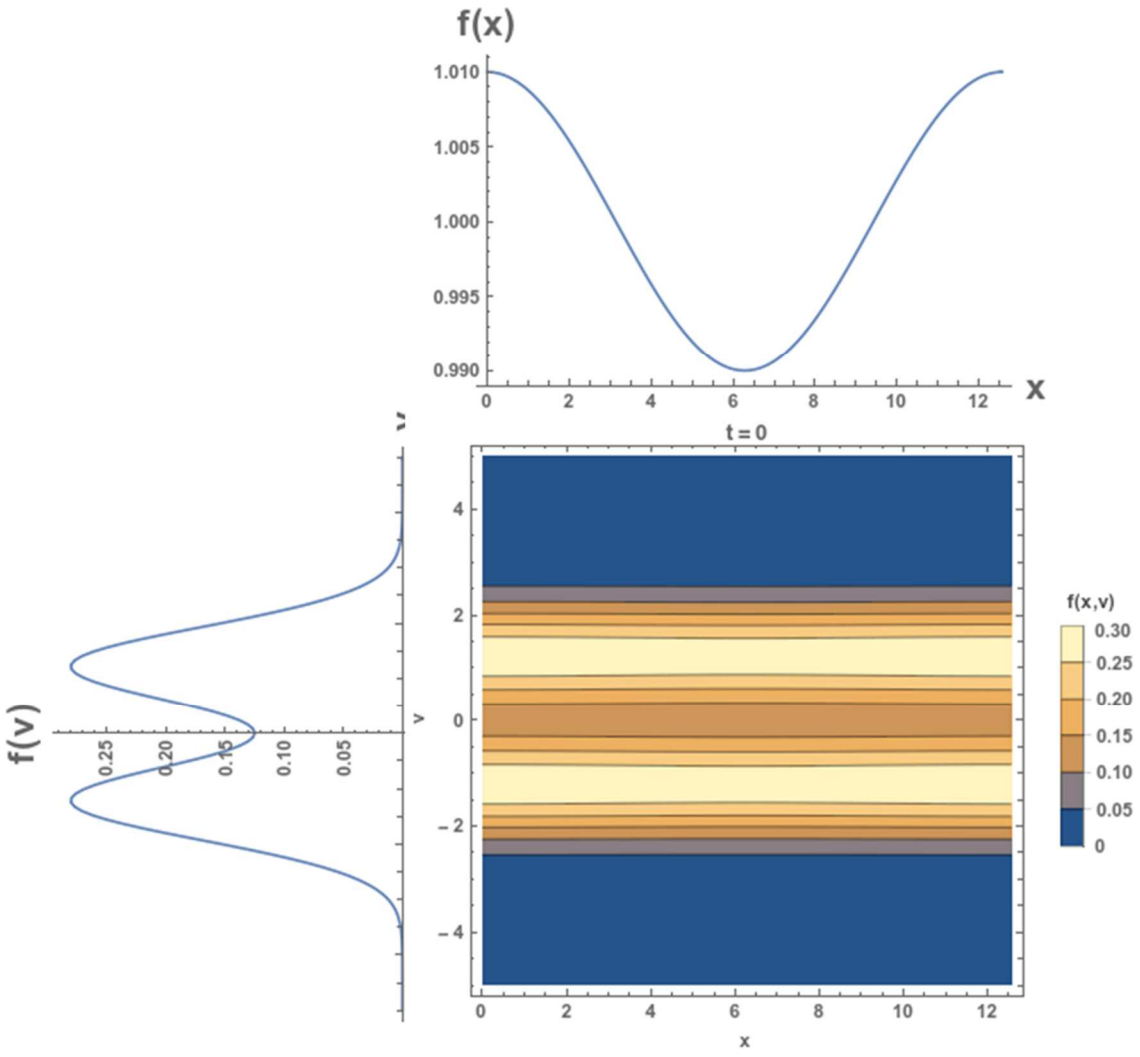

Figure 2-29 Initial state with $v_{tth} = 1$ and $v_0 = \sqrt{\frac{3}{2}}$.

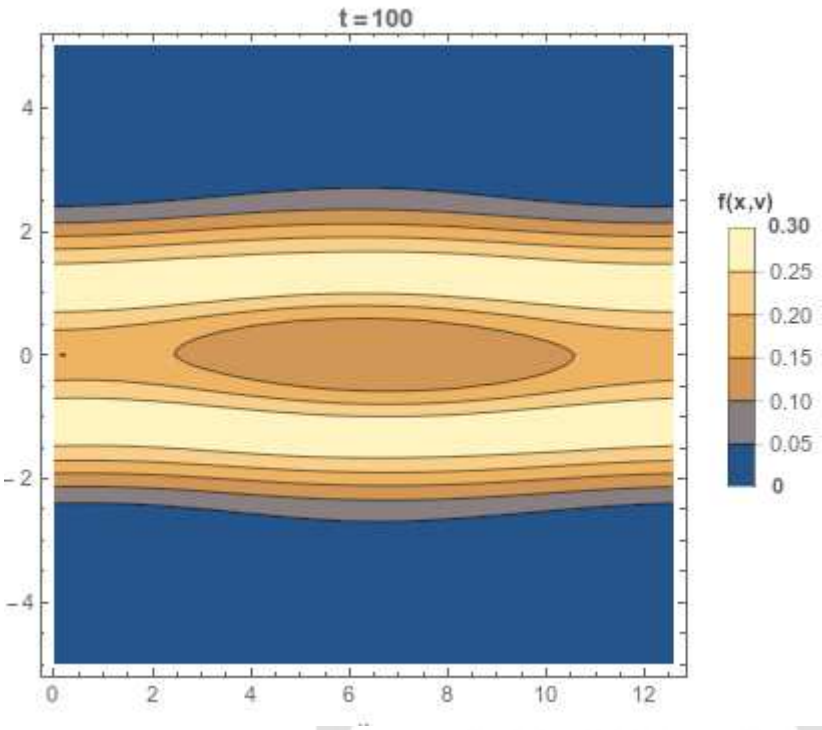

Figure 2-30 Simulation result after t = 100 ω_p^{-1} using PLM in both x and v direction.

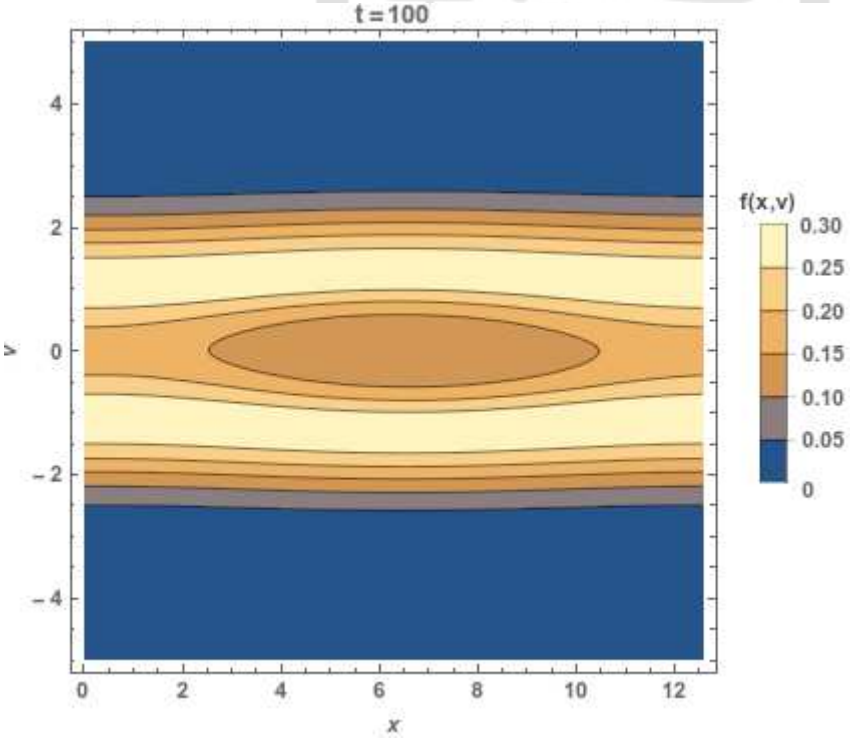

Figure 2-31 Simulation result after t = 100 ω_p^{-1} using PLM + PPM in x direction and PLM in v direction.

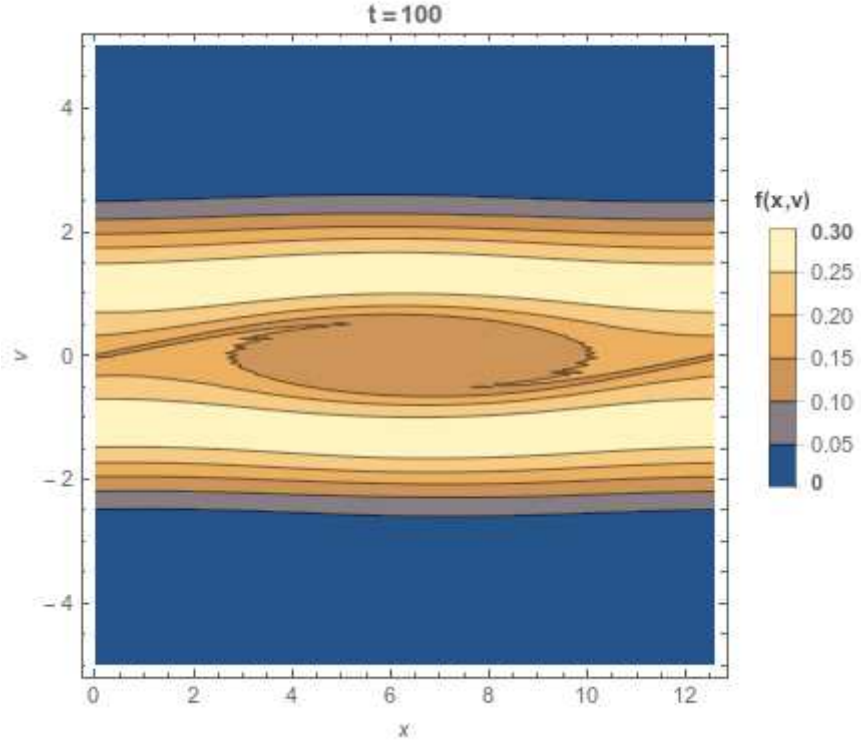

Figure 2-32 Simulation result after t = 100 ω_p^{-1} using PPM in both x and v direction.

The energy conservation should be checked in simulation. The total energy En_t in Vlasov solver are summation of electric energy En_e and kinetic energy En_k of electrons, and they are shown in Eq.(2-210) to Eq.(2-212).

$$En_t=En_k+En_e, \tag{2-210}$$

$$En_k=\iint \frac{1}{2} m_e v^2 f(x,v)dxdv, \tag{2-211}$$

$$En_e=\int \frac{1}{2} \varepsilon_0 E(x)^2 dx. \tag{2-212}$$

There are some constants in these equations, they can be normalized as shown in section 2.2. The normalized energy are shown in Eq.(2-213) and Eq.(2-214).

$$En_k=En_{k,char}\widehat{En}_k=\frac{1}{2} m_e v_{char}{}^3 f_{char} x_{char} \iint \hat{v}^2 \hat{f} d\hat{x} d\hat{v}, \tag{2-213}$$

$$En_e=En_{e,char}\widehat{En}_e=\frac{1}{2} \varepsilon_0 E_{char}{}^2 x_{char} \int \hat{E}^2 d\hat{x}. \tag{2-214}$$

Then the normalization constants should have the relation as Eq.(2-215).

$$m_e v_{char}{}^3 f_{char} x_{char} = \varepsilon_0 E_{char}{}^2 x_{char}. \quad (2\text{-}215)$$

?

The steps to verify of equality in Eq.(2-215) is shown in Eq.(2-216) to Eq.(2-219).

$$m_e v_{th}{}^2 n_0 \lambda_D = \varepsilon_0 \frac{e^2 n_0{}^2 \lambda_D{}^2}{\varepsilon_0{}^2} \lambda_D, \quad (2\text{-}216)$$

$$\Longrightarrow m_e v_{th}{}^2 = \frac{e^2 n_0 \lambda_D{}^2}{\varepsilon_0}, \quad (2\text{-}217)$$

$$\Longrightarrow \frac{v_{th}{}^2}{\lambda_D{}^2} = \frac{n_0 e^2}{\varepsilon_0 m_e}, \quad (2\text{-}218)$$

$$\Longrightarrow \omega_p{}^2 = \frac{n_0 e^2}{\varepsilon_0 m_e}. \quad (2\text{-}219)$$

So the normalized energy equations is shown in the following.

$$\widehat{En}_t = \widehat{En}_k + \widehat{En}_e, \quad (2\text{-}220)$$

$$\widehat{En}_k = \iint \frac{1}{2} \hat{v}^2 \hat{f} d\hat{x} d\hat{v}, \quad (2\text{-}221)$$

$$\widehat{En}_e = \int \frac{1}{2} \hat{E}^2 d\hat{x}. \quad (2\text{-}222)$$

To calculate Eq.(2-220) to Eq.(2-222), the trapezoidal method of numerical integration in section 2.5.3 is used. The kinetic energy equation in Eq.(2-221) can be written in Eq.(2-223).

$$En_k = \frac{1}{2} \int_{x_0}^{x_{nx}} \int_{v_0}^{v_{nv}} f v^2 dx dv. \quad (2\text{-}223)$$

First, do the integration of v, Eq.(2-223) becomes

$$En_k = \frac{1}{2} \int_{x_0}^{x_{nx}} \Delta v \left\{ \sum_{iv=1}^{nv-1} [f(x,v_{iv}) v_{iv}^2] + \frac{1}{2} \left[f(x,v_0) v_0^2 + f(x,v_{nv}) v_{nv}^2 \right] \right\} dx, \quad (2\text{-}224)$$

$$En_k = \int_{x_0}^{x_{nx}} \eta(x) dx. \quad (2\text{-}225)$$

$$\text{where } \eta(x)=\frac{1}{2}\Delta v\left\{\sum_{iv=1}^{nv-1}[f(x,v_{iv})v_{iv}^2]+\frac{1}{2}[f(x,v_0)v_0^2+f(x,v_{nv})v_{nv}^2]\right\}$$

Second, do the integration of x, and the kinetic energy is given.

$$En_k=\frac{1}{2}\Delta x\left\{\sum_{ix=1}^{nx-1}[\eta(x_{ix})]+\frac{1}{2}[\eta(x_0)+\eta(x_{nx})]\right\}. \tag{2-226}$$

In the same way, Eq.(2-222) can be integrated by using Eq.(2-227).

$$En_e=\frac{1}{2}\Delta x\left\{\sum_{ix=1}^{nx-1}[En^2(x_{ix})]+\frac{1}{2}[En^2(x_0)+En^2(x_{nx})]\right\}. \tag{2-227}$$

The total energy of simulation of two-stream instability are shown in Figure 2-33. The total energy variation is less than 0.3% meaning the system energy is conserved in simulation.

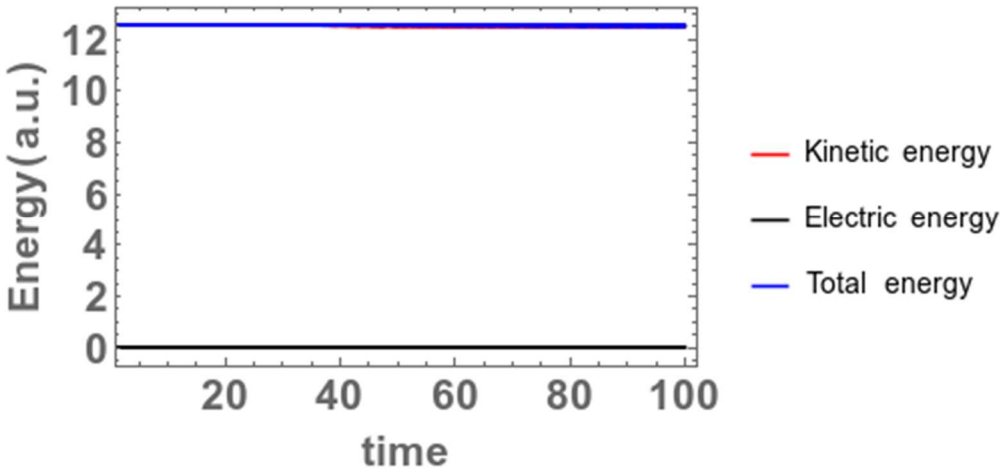

Figure 2-33 Checking of energy conservation of two-stream instability.

From Eq.(2-204), the limitation of two-stream instability to happen is $v_0 < \frac{1}{k} = 2$. Therefore, if for $v_0 > \frac{1}{k} = 2$, the two-stream instability should not occurred. Figure 2-34 and Figure 2-35 are the initial conditions of $v_0 = 1.9$ and $v_0 = 2.1$ respectively. The total simulation time is $t = 100\ \omega_p^{-1}$ for all cases. Figure 2-36 shows that there is an apparently two-stream

instability while $v_0 < 2.0$. Figure 2-37 shows that the perturbation doesn't grow with time proving that two-stream instability can't occur for $v_0 > 2.0$.

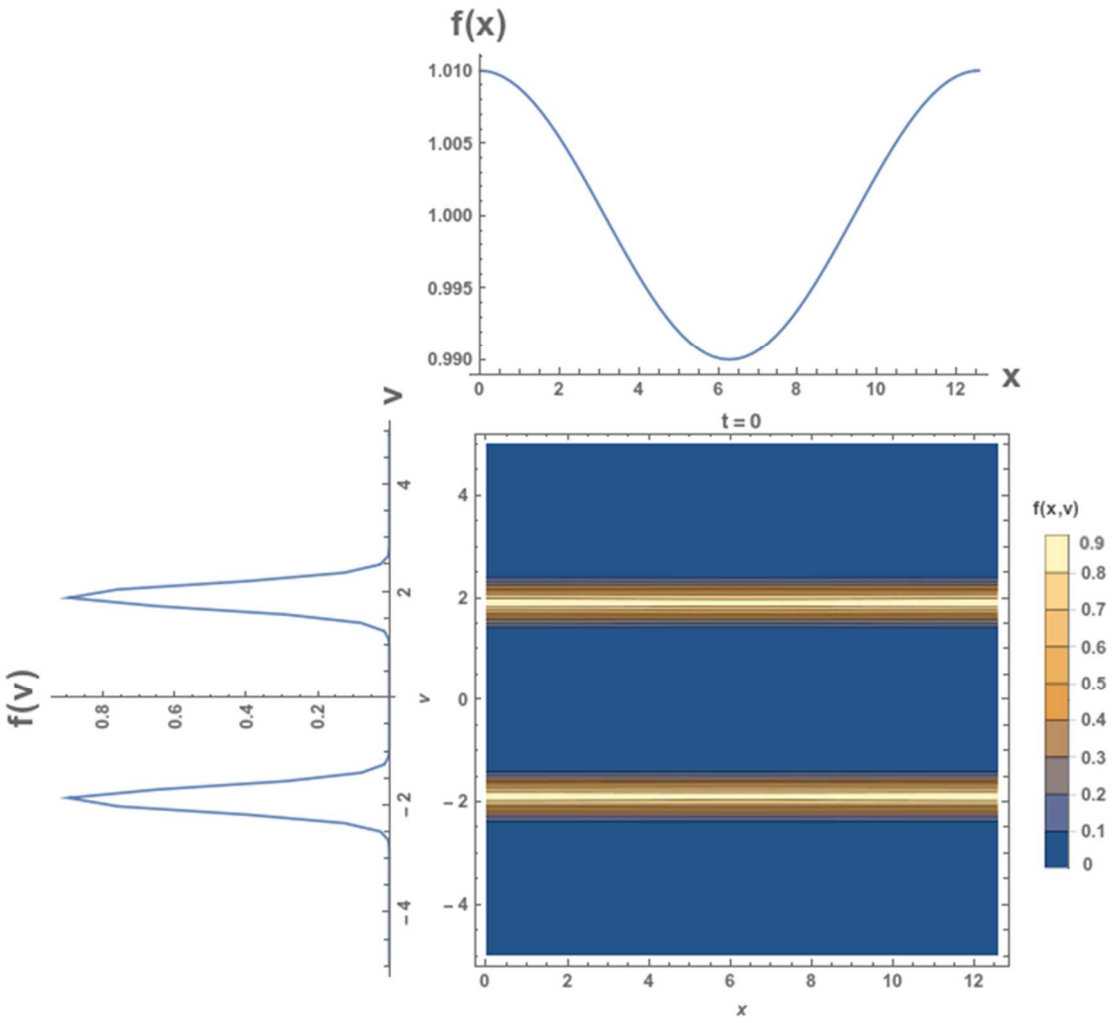

Figure 2-34 Initial state of $v_0 = 1.9$.

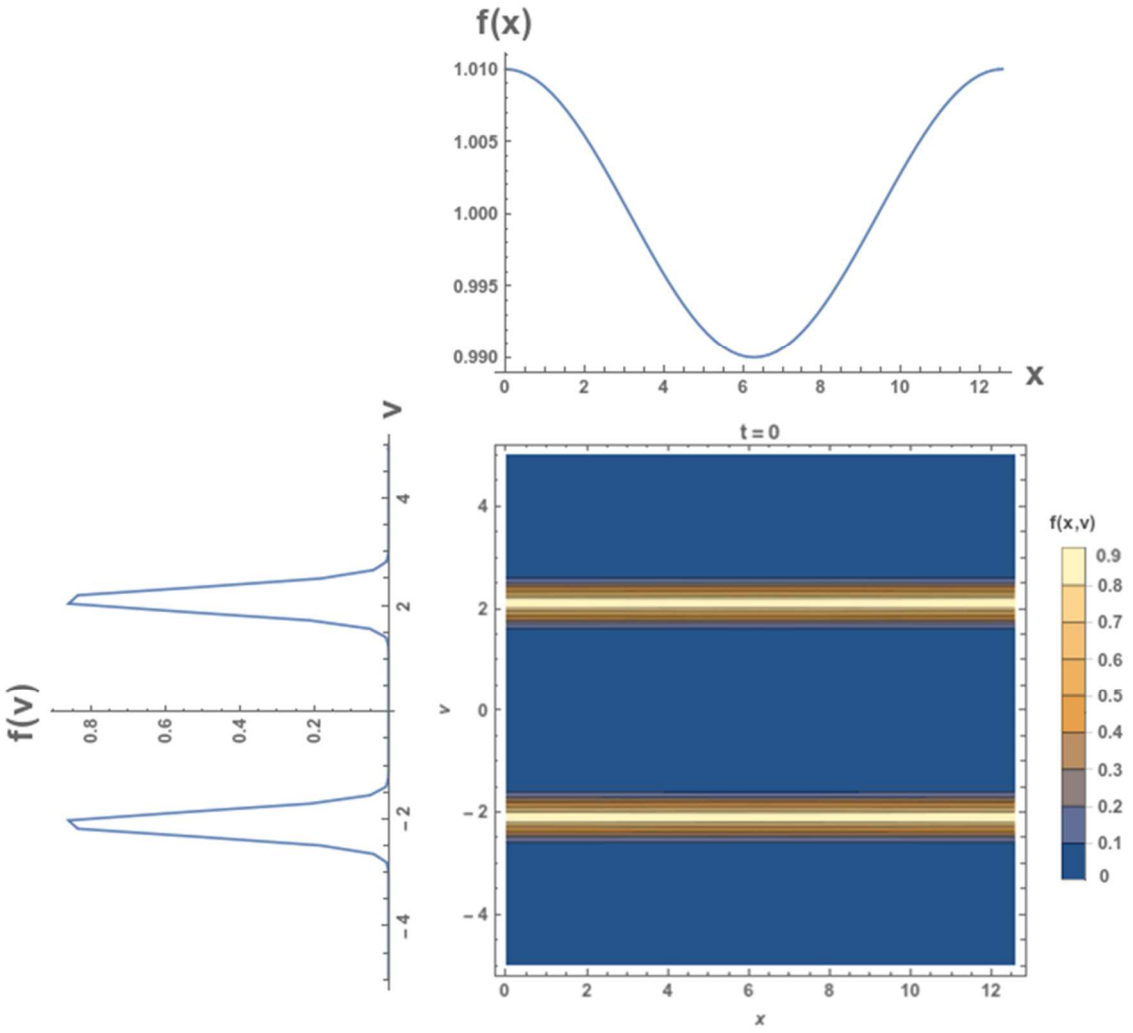

Figure 2-35 Initial state of $v_0 = 2.1$.

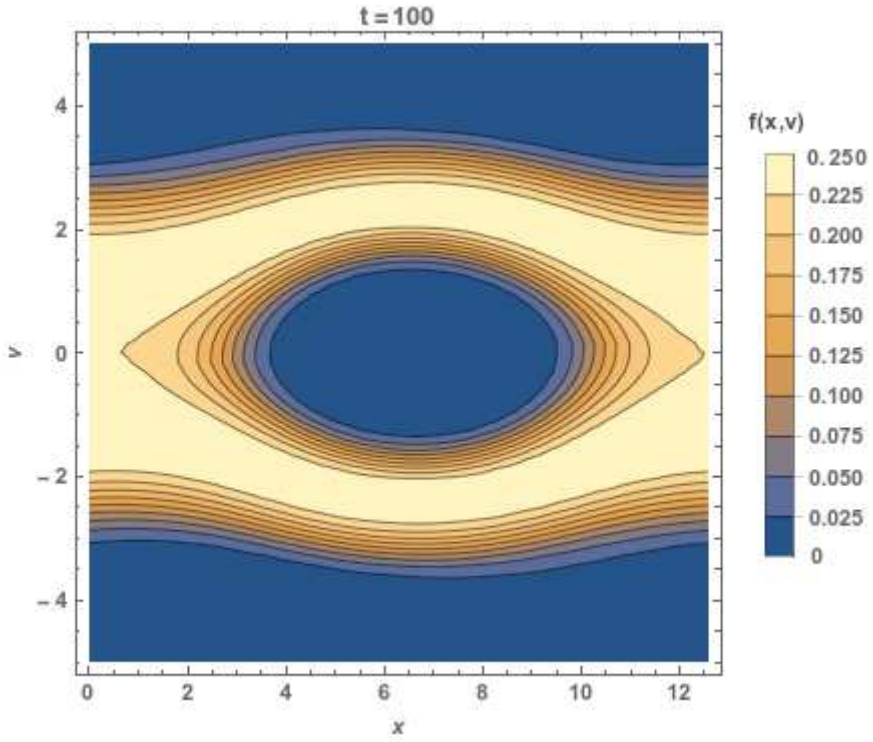

Figure 2-36 The simulation result after $t = 100\omega_p^{-1}$ with $v_{tth} = 1$ and $v_0 = 1.9$. Instability occurs.

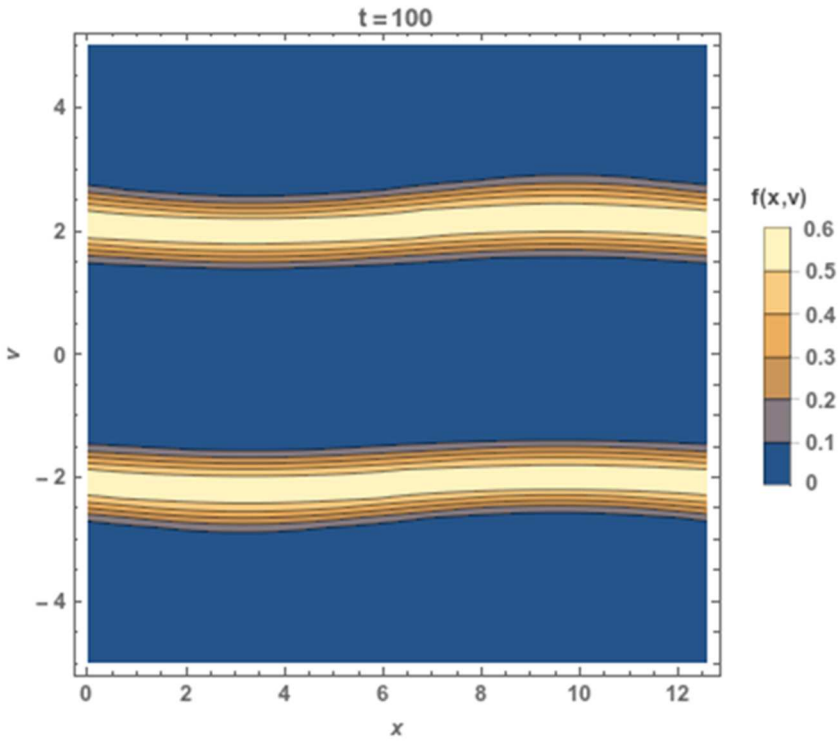

Figure 2-37 The simulation result after $t = 100\omega_p^{-1}$ with $v_{tth} = 1$ and $v_0 = 2.1$. No instability occurs.

Simulation results show that the initial double-peak Gaussian velocity distribution will gradually merge due to the instability. Figure 2-38 shows the growth rate for $v_0 = \sqrt{\frac{3}{2}}$.

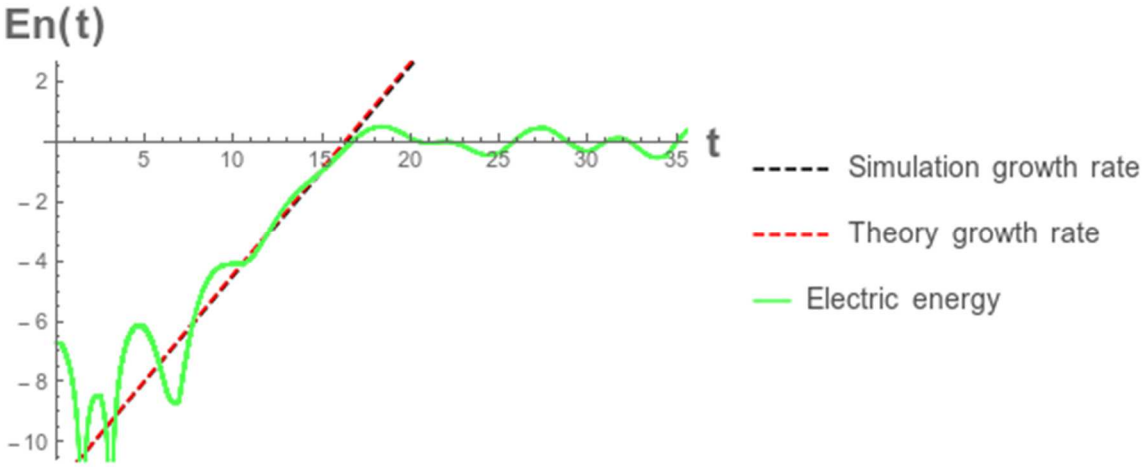

Figure 2-38 Growth rate of two-stream instability at $v_0 = \sqrt{\frac{3}{2}}$.

The growth rate from simulation is 0.701 is shown as the blue dashed line in Figure 2-38. To

compare, the analytical growth rate from Eq.(2-206) is $\frac{1}{2\sqrt{2}} \approx 0.35$. The logarithm of electric energy is logEn = $\log E^2$ = 2logE, so the analytical growth rate should be 2*0.35 = 0.7. In Figure 2-38, the black dashed line in the same figure is theory growth rate. Theory growth rate is 0.3% smaller than the simulation one. They are slightly different since our simulation is warm plasma and the theory is cold plasma theory.

Chapter 3 Free-streaming electrons

Free-streaming electrons is a beam-plasma phenomena. The instability arises when a single electron beam with number density n_0 and plasma frequency ω_p flows with speed v_b through a stationary plasma. Vlasov solver uses combination method of PPM and PLM with vanLeer slope-limiter to solve advection equation in x direction and PLM with vanLeer slope-limiter to solve advection equation in v direction and Poisson's equation uses Gauss-Seidel method to solve.

3.1 Initial condition of free-streaming electrons

To study this phenomena, the initial distribution function $f(x, v, 0)$ is used. It is shown in Eq.(3-1).

$$f(x,v,0)=\frac{1}{(1+\gamma)v_{th}\sqrt{\pi}}\left(e^{-\frac{v^2}{v_{th}^2}}+\gamma e^{-\frac{(v-v_0)^2}{v_{th}^2}}\right)[1+0.01\cos(kx)]. \quad (3\text{-}1)$$

The first exponential term represents the stationary plasma distribution and the second exponential term represents the electron beam. v_{th} is the thermal velocity, and v_b is the beam velocity between the background plasma and electron distributions. γ is a parameter so that the number density of the electron beam can be adjusted by us to simulate different beam intensities compared with the stationary plasma. The $1 + \gamma$ term in the denominator is to ensure the total electron number density is 1 as normalization in section 2.2. The initial number density and initial velocity distribution of electrons with γ set as 0.5, 1, 2 are shown in Figure 3-1, Figure 3-2, and Figure 3-3 respectively, their average number density are all 1 as normalized. The cos(kx) term is a perturbation term in x with k=0.5 and their distribution are also shown in Eq.(3-1) to Eq.(3-3) with $\gamma = 0.5$, $\gamma = 1$, $\gamma = 2$ respectively. The simulation range in real space x is between 0 to L, $L = 4\pi \lambda_D$, and from -5 v_{th} to 10 v_{th} in velocity space

v. The final time is set as t = 100 ω_p^{-1}. The boundary condition is periodic in spatial grids x and set as zero (Dirichlet boundary condition) in velocity space grids v. The size of each time step is defined as $\frac{1}{64}\Delta t$ where Δt is defined in Eq.(2-120). The number of grids are 128 in both x and v direction. To calculate free-streaming electrons, the simulation methods are combined with half-PPM and half-PLM with vanLeer slope-limiter in solving advection equation in x direction, and PLM with vanLeer slope-limiter in solving advection equation in v direction.

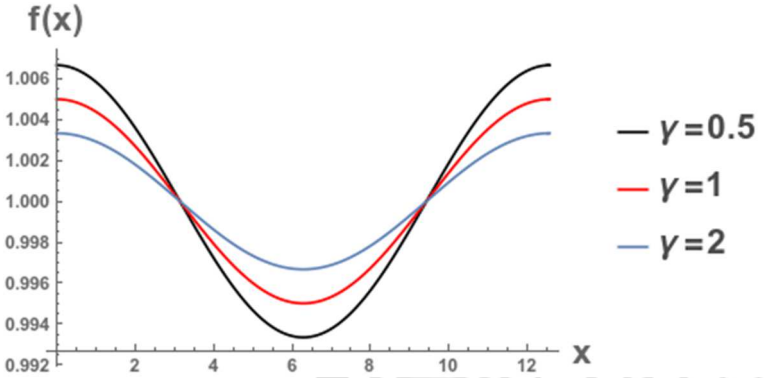

Figure 3-1 Initial number density with different γ.

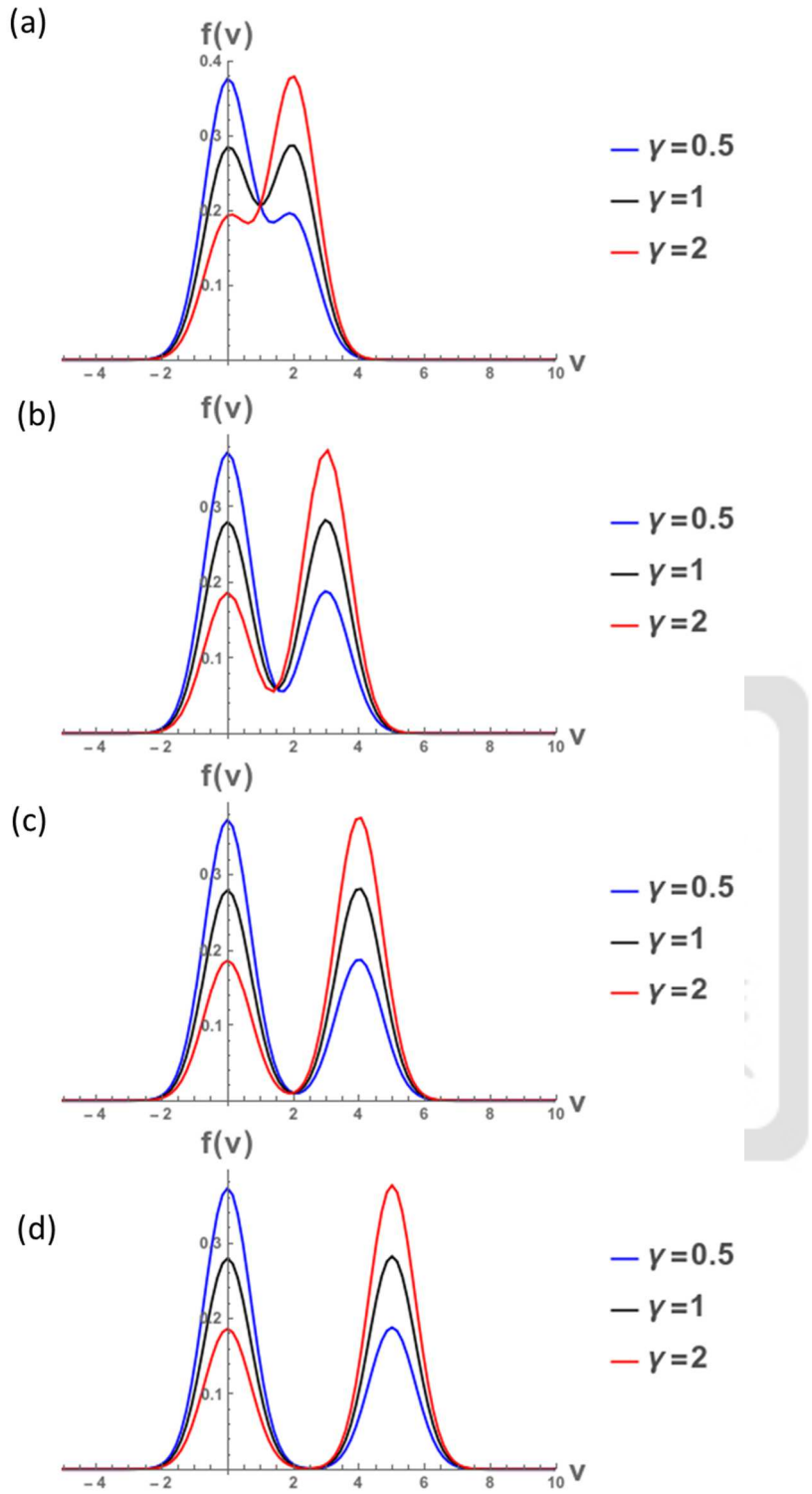

Figure 3-2 Initial distribution in v with different γ when (a) v_b=2. (b) v_b=3. (c) v_b=4. (d) v_b=5.

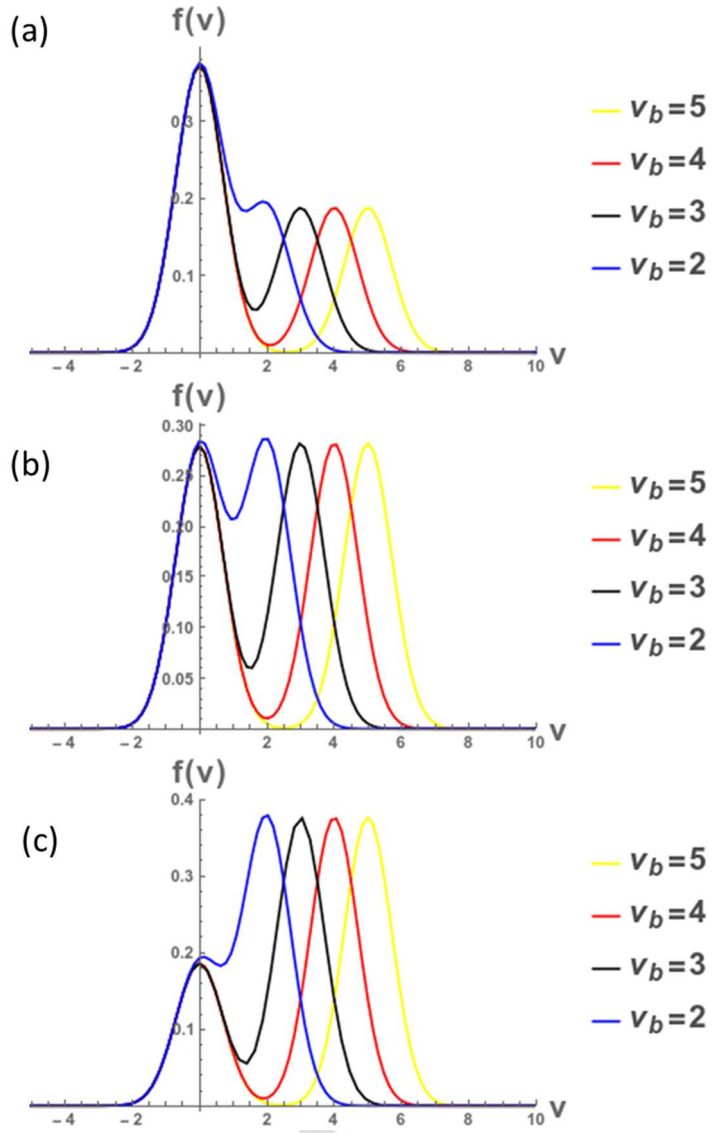

Figure 3-3 Initial distribution in v with different beam velocity v_b when (a) γ=0.5. (b) γ=1. (c) γ=2.

The initial state of Eq.(3-1) is set with v_{th} = 1 and using different v_b and γ to see the different effects of free streaming electron beams in different beam velocity and intensity.

3.2 Simulation results of free-streaming electrons

The simulation results at t = 0 ω_p^{-1} (initial condition), t = 20 ω_p^{-1} (linear growth region), and t = 100 ω_p^{-1} (nonlinear growth region) are shown in this section.

3.2.1 $\gamma = 0.5$

The initial condition are

$$f(x,v,0)=\frac{1}{1.5\sqrt{\pi}}\left(e^{-\frac{v^2}{1}}+0.5e^{-\frac{(v-2)^2}{1}}\right)(1+0.01\cos(0.5x)). \quad (3\text{-}2)$$

$$f(x,v,0)=\frac{1}{1.5\sqrt{\pi}}\left(e^{-\frac{v^2}{1}}+0.5e^{-\frac{(v-3)^2}{1}}\right)(1+0.01\cos(0.5x)) \quad (3\text{-}3)$$

$$f(x,v,0)=\frac{1}{1.5\sqrt{\pi}}\left(e^{-\frac{v^2}{1}}+0.5e^{-\frac{(v-4)^2}{1}}\right)(1+0.01\cos(0.5x)). \quad (3\text{-}4)$$

$$f(x,v,0)=\frac{1}{1.5\sqrt{\pi}}\left(e^{-\frac{v^2}{1}}+0.5e^{-\frac{(v-5)^2}{1}}\right)(1+0.01\cos(0.5x)) \quad (3\text{-}5)$$

The initial conditions and the simulation results are shown in Figure 3-4 to Figure 3-7.

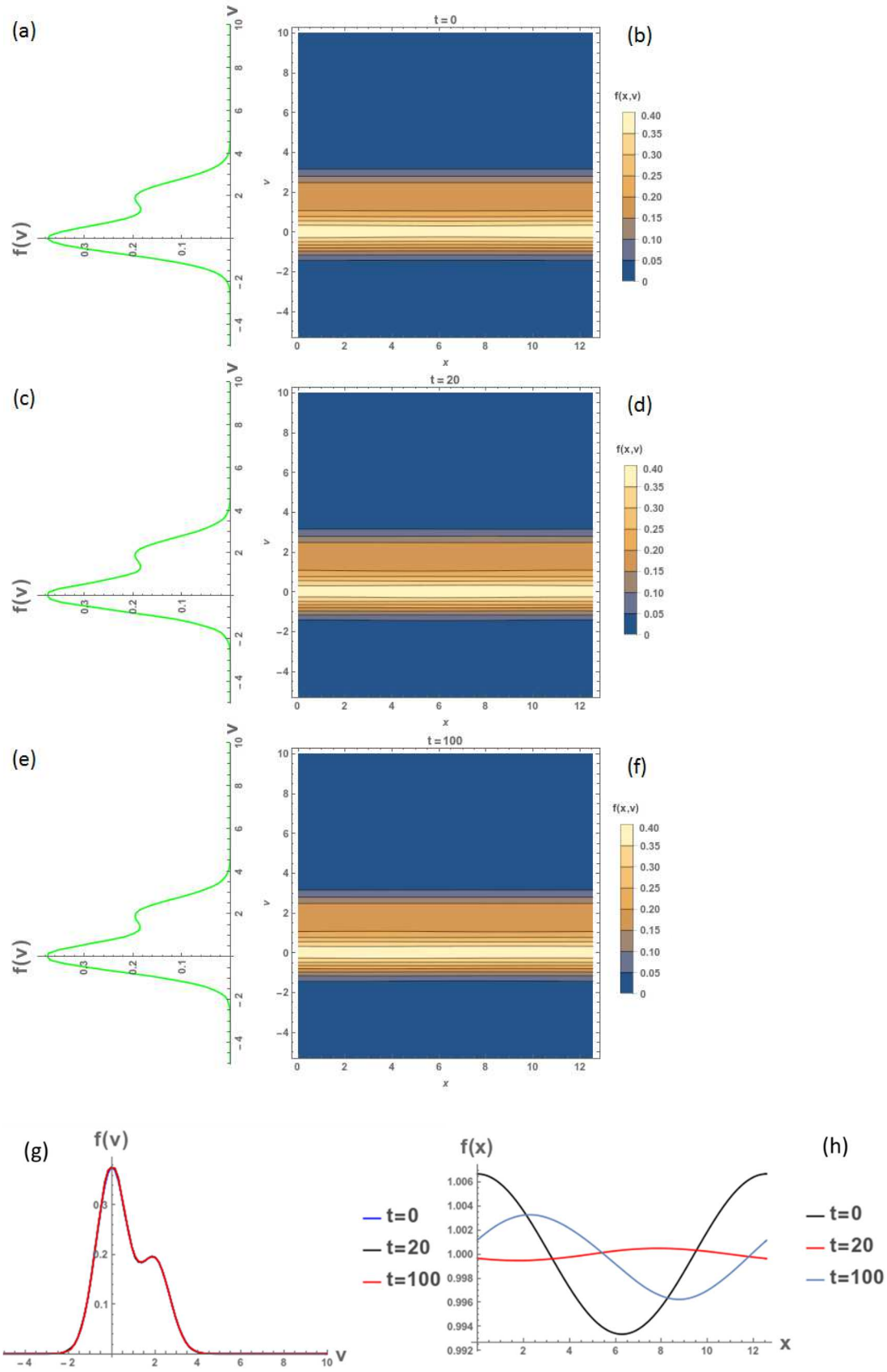

Figure 3-4 Free streaming electrons of Eq.(3-2). (a) Velocity distribution in t = 0 ω_p^{-1}.

(b) Phase space diagram in t = 0 ω_p^{-1}. (c) Velocity distribution in t = 20 ω_p^{-1}. (d) Phase space diagram in t = 20 ω_p^{-1}. (e) Velocity distribution in t = 100 ω_p^{-1}. (f) Phase space diagram in t = 100 ω_p^{-1}. (g) Velocity distribution in different time t. (h) Number density in different time t.

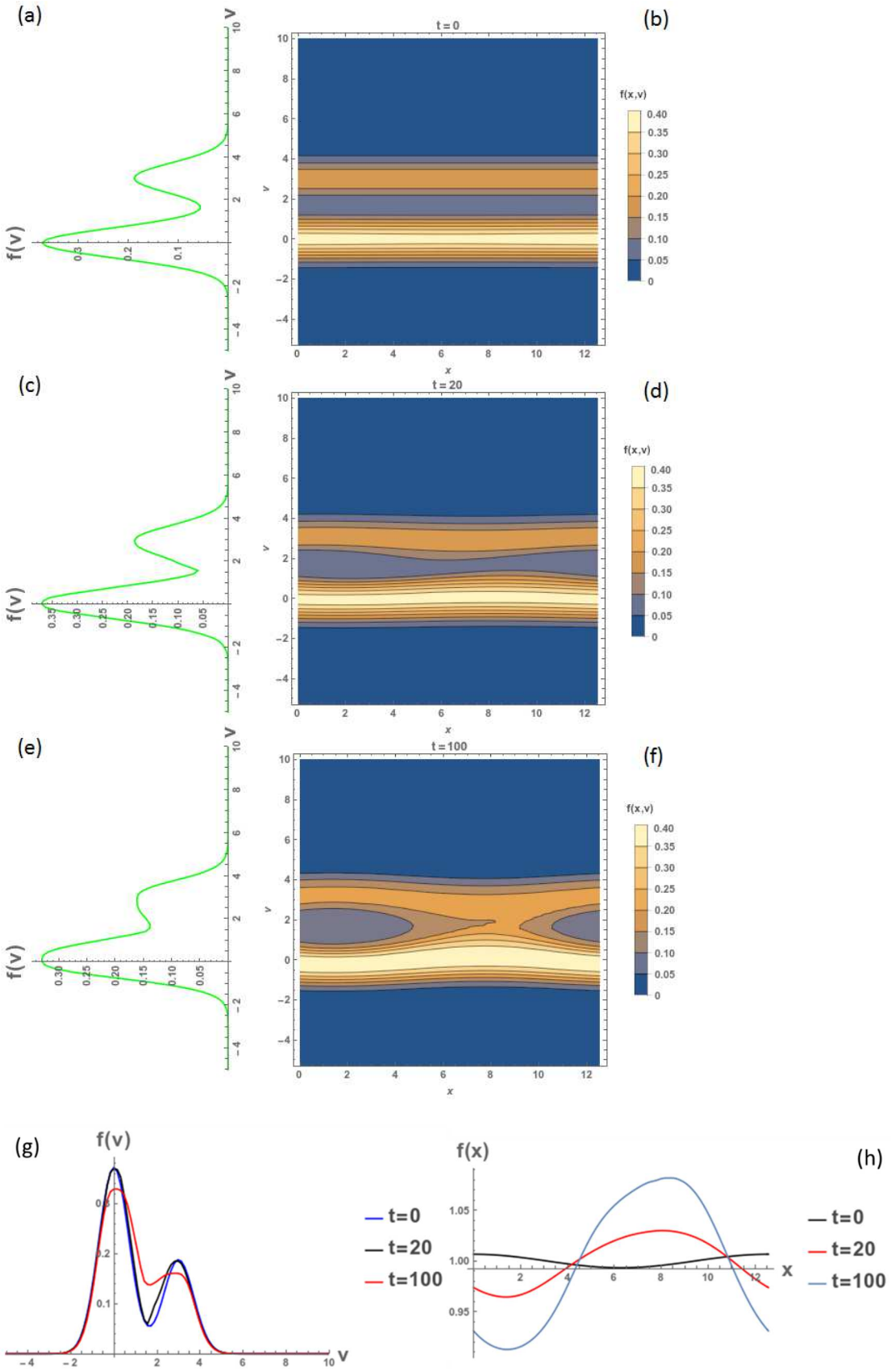

Figure 3-5 Free streaming electrons of Eq.(3-3). (a) Velocity distribution in t = 0 ω_p^{-1}.

(b) Phase space diagram in t = 0 ω_p^{-1}. (c) Velocity distribution in t = 20 ω_p^{-1}. (d) Phase space diagram in t = 20 ω_p^{-1}. (e) Velocity distribution in t = 100 ω_p^{-1}. (f) Phase space diagram in t = 100 ω_p^{-1}. (g) Velocity distribution in different time t. (h) Number density in different time t.

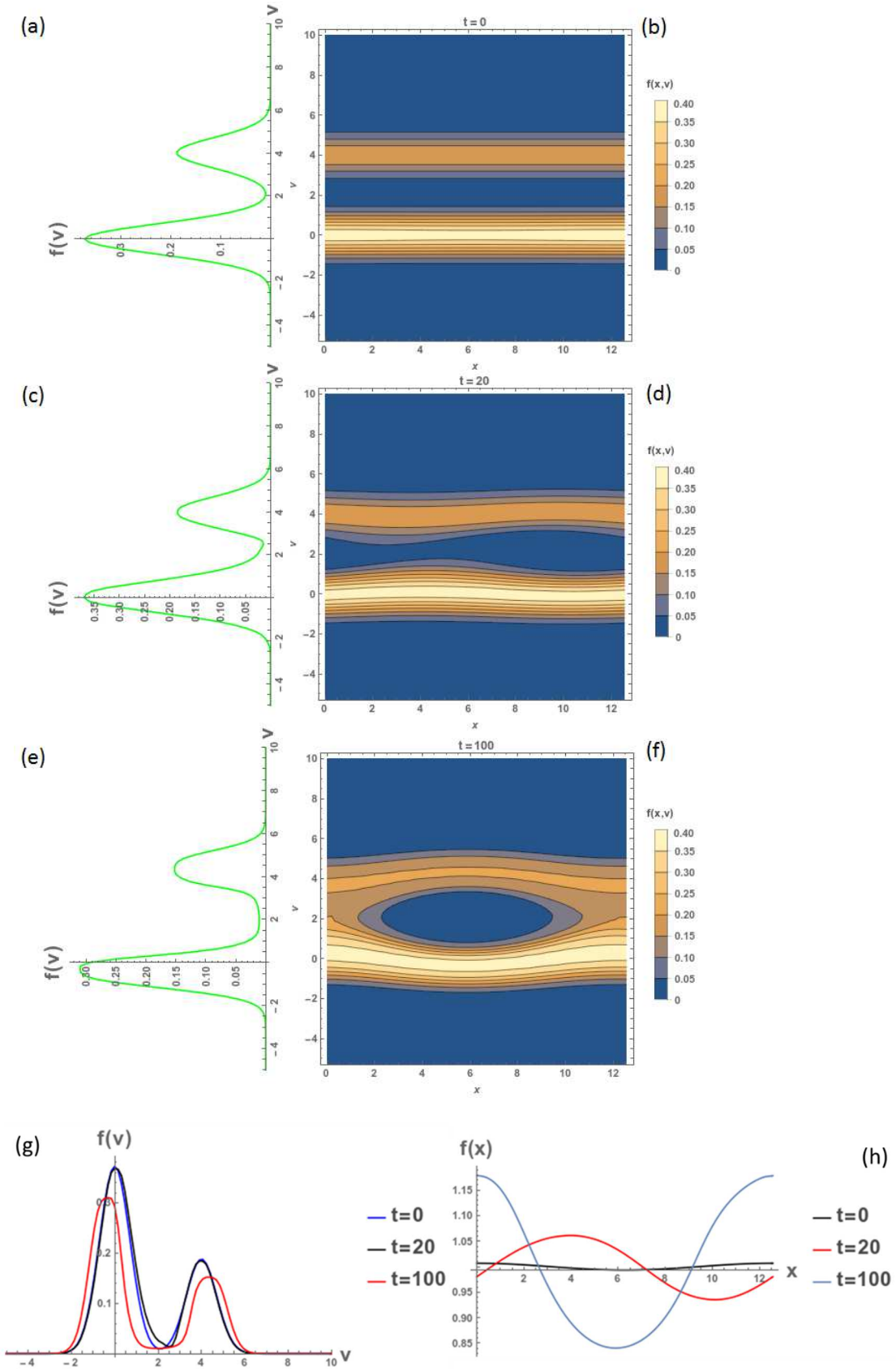

Figure 3-6 Free streaming electrons of Eq.(3-4). (a) Velocity distribution in t = 0 ω_p^{-1}.

(b) Phase space diagram in t = 0 ω_p^{-1}. (c) Velocity distribution in t = 20 ω_p^{-1}. (d) Phase space diagram in t = 20 ω_p^{-1}. (e) Velocity distribution in t = 100 ω_p^{-1}. (f) Phase space diagram in t = 100 ω_p^{-1}. (g) Velocity distribution in different time t. (h) Number density in different time t.

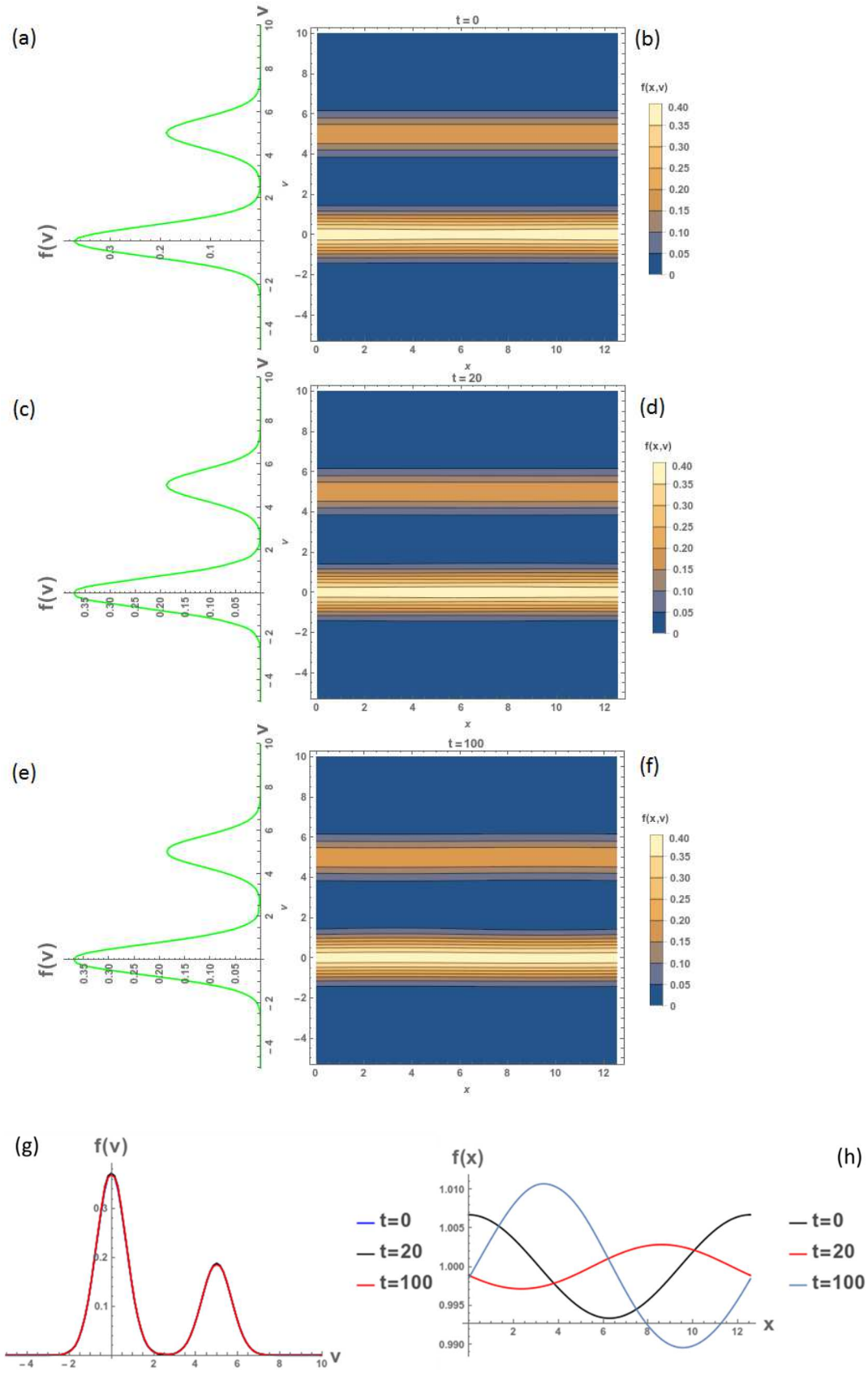

Figure 3-7 Free streaming electrons of Eq.(3-5). (a) Velocity distribution in t = 0 ω_p^{-1}.

(b) Phase space diagram in t = 0 ω_p^{-1}. (c) Velocity distribution in t = 20 ω_p^{-1}. (d) Phase space diagram in t = 20 ω_p^{-1}. (e) Velocity distribution in t = 100 ω_p^{-1}. (f) Phase space diagram in t = 100 ω_p^{-1}. (g) Velocity distribution in different time t. (h) Number density in different time t.

3.2.2 $\gamma = 1$

The initial condition are

$$f(x,v,0)=\frac{1}{2\sqrt{\pi}}\left(e^{-\frac{v^2}{1}}+e^{-\frac{(v-2)^2}{1}}\right)(1+0.01\cos(0.5x)). \quad (3\text{-}6)$$

$$f(x,v,0)=\frac{1}{2\sqrt{\pi}}\left(e^{-\frac{v^2}{1}}+e^{-\frac{(v-3)^2}{1}}\right)(1+0.01\cos(0.5x)) \quad (3\text{-}7)$$

$$f(x,v,0)=\frac{1}{2\sqrt{\pi}}\left(e^{-\frac{v^2}{1}}+e^{-\frac{(v-4)^2}{1}}\right)(1+0.01\cos(0.5x)). \quad (3\text{-}8)$$

$$f(x,v,0)=\frac{1}{2\sqrt{\pi}}\left(e^{-\frac{v^2}{1}}+e^{-\frac{(v-5)^2}{1}}\right)(1+0.01\cos(0.5x)) \quad (3\text{-}9)$$

The initial conditions and the simulation results are shown in Figure 3-8 to Figure 3-11.

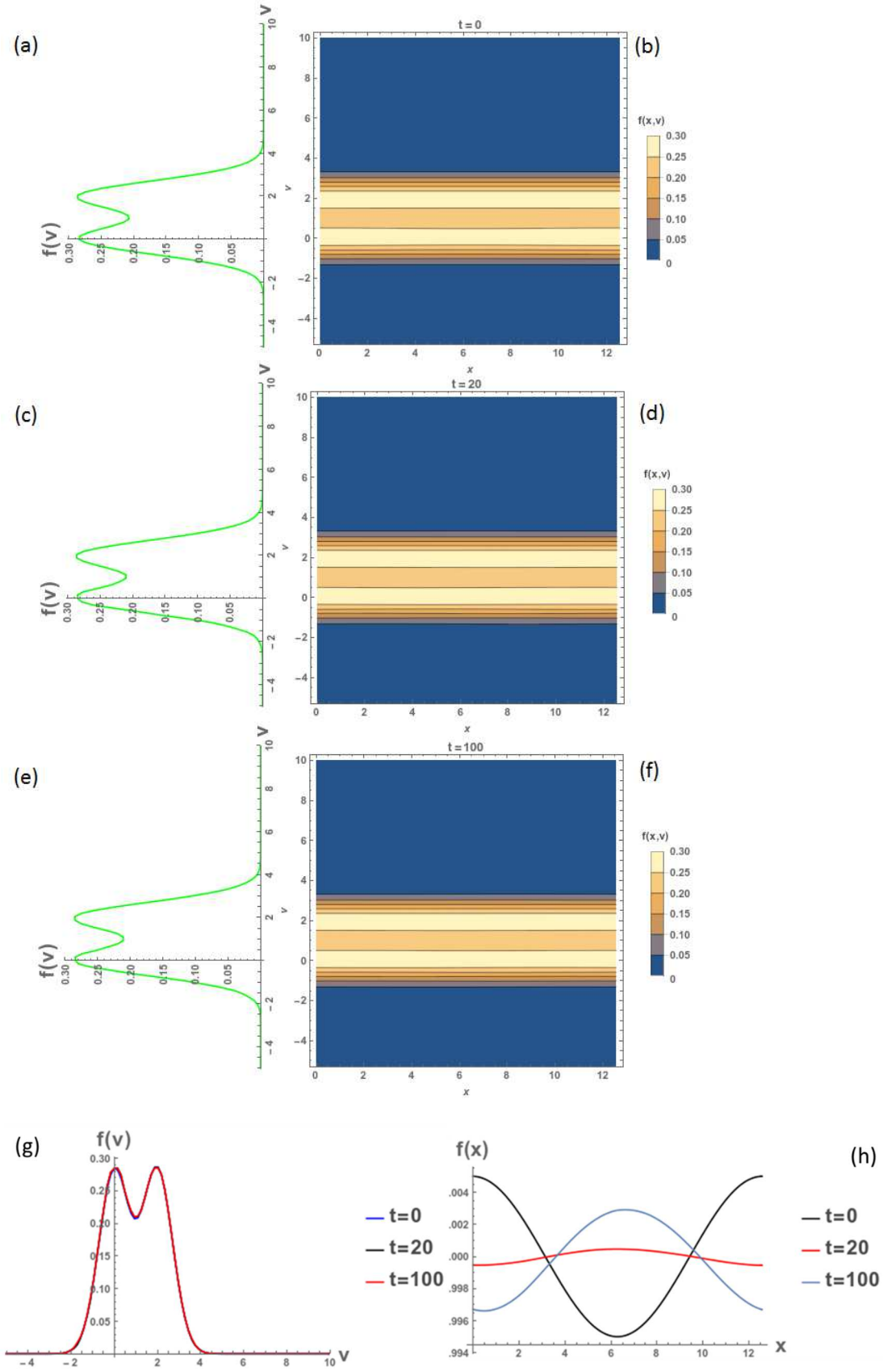

Figure 3-8 Free streaming electrons of Eq.(3-6). (a) Velocity distribution in t = 0 ω_p^{-1}.

(b) Phase space diagram in t = 0 ω_p^{-1}. (c) Velocity distribution in t = 20 ω_p^{-1}. (d) Phase space diagram in t = 20 ω_p^{-1}. (e) Velocity distribution in t = 100 ω_p^{-1}. (f) Phase space diagram in t = 100 ω_p^{-1}. (g) Velocity distribution in different time t. (h) Number density in different time t.

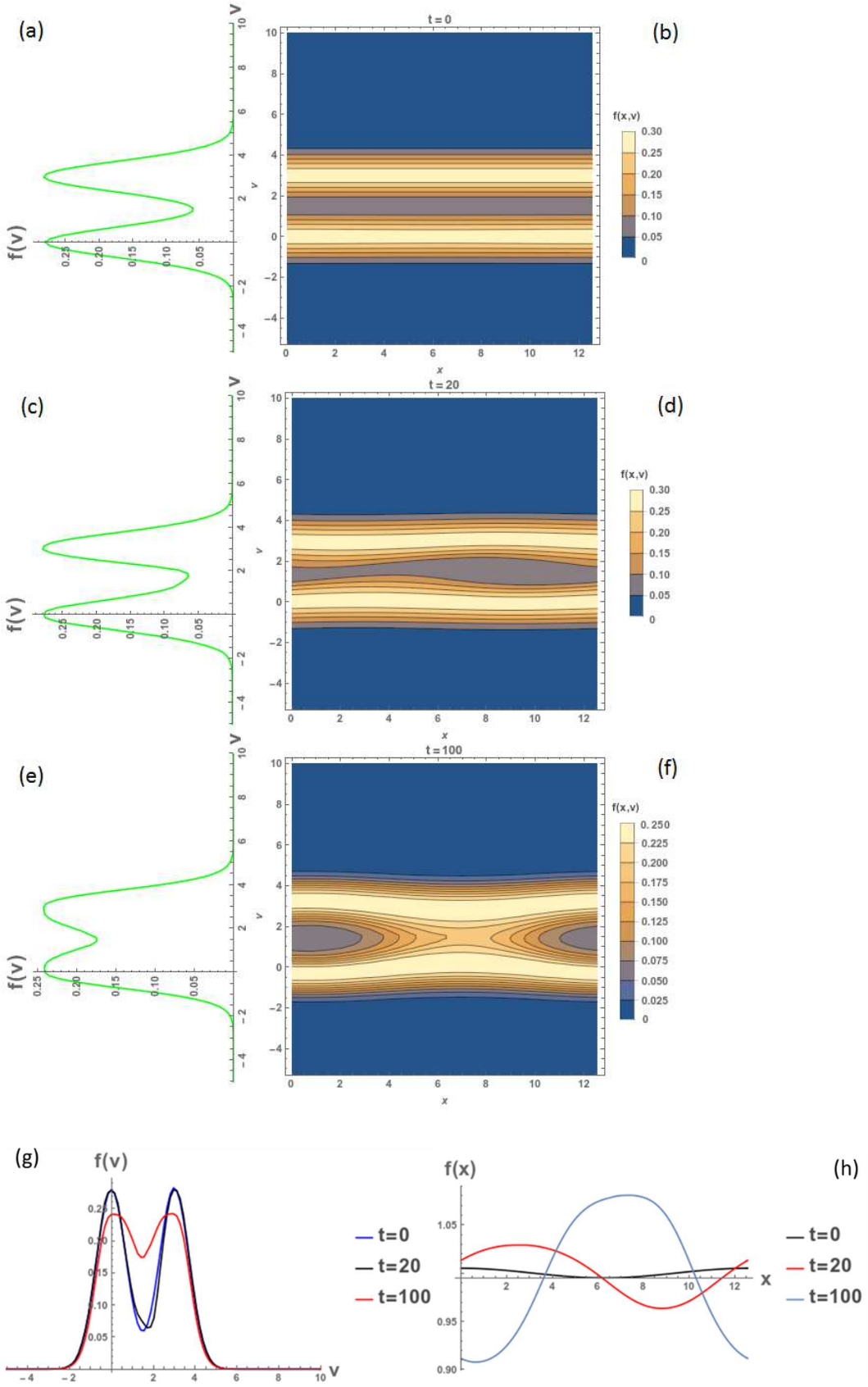

Figure 3-9 Free streaming electrons of Eq.(3-7). (a) Velocity distribution in t = 0 ω_p^{-1}.

(b) Phase space diagram in t = 0 ω_p^{-1}. (c) Velocity distribution in t = 20 ω_p^{-1}. (d) Phase space diagram in t = 20 ω_p^{-1}. (e) Velocity distribution in t = 100 ω_p^{-1}. (f) Phase space diagram in t = 100 ω_p^{-1}. (g) Velocity distribution in different time t. (h) Number density in different time t.

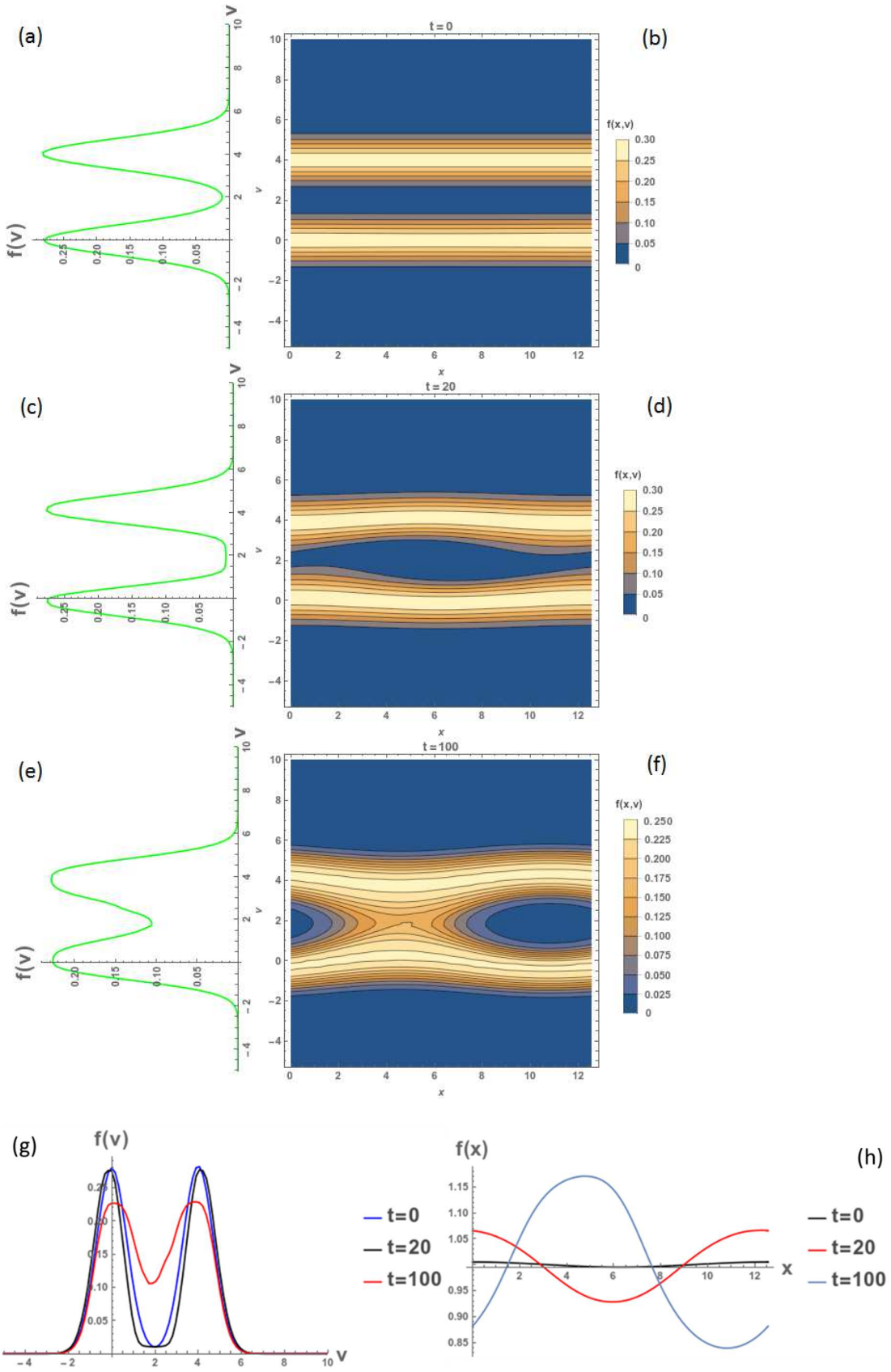

Figure 3-10 Free streaming electrons of Eq.(3-8). (a) Velocity distribution in t = 0 ω_p^{-1}.

(b) Phase space diagram in t = 0 ω_p^{-1}. (c) Velocity distribution in t = 20 ω_p^{-1}. (d) Phase space diagram in t = 20 ω_p^{-1}. (e) Velocity distribution in t = 100 ω_p^{-1}. (f) Phase space diagram in t = 100 ω_p^{-1}. (g) Velocity distribution in different time t. (h) Number density in different time t.

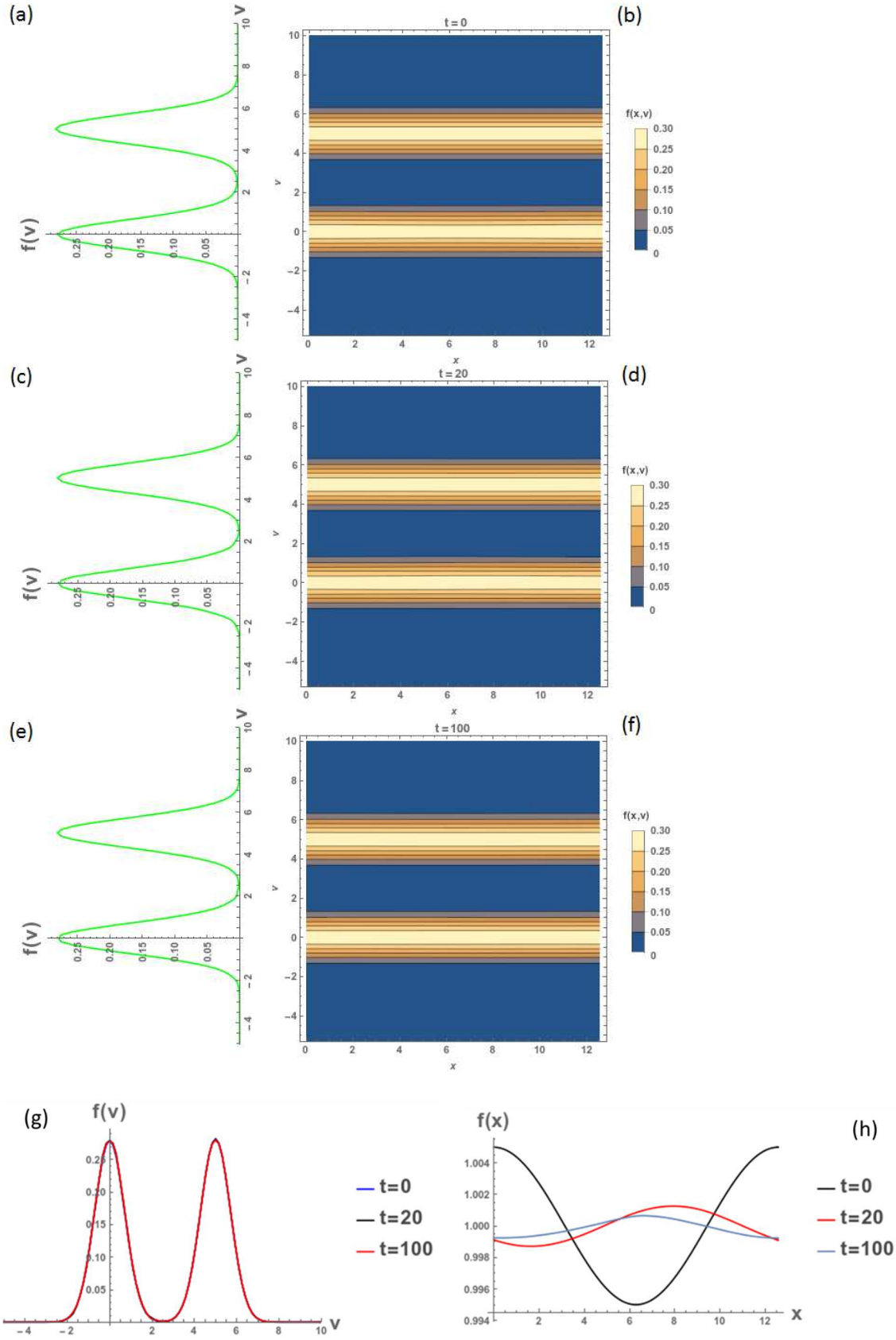

Figure 3-11 Free streaming electrons of Eq.(3-9). (a) Velocity distribution in t = 0 ω_p^{-1}.

(b) Phase space diagram in t = 0 ω_p^{-1}. (c) Velocity distribution in t = 20 ω_p^{-1}. (d) Phase space diagram in t = 20 ω_p^{-1}. (e) Velocity distribution in t = 100 ω_p^{-1}. (f) Phase space diagram in t = 100 ω_p^{-1}. (g) Velocity distribution in different time t. (h) Number density in different time t.

3.2.3 $\gamma = 2$

The initial condition are

$$f(x,v,0)=\frac{1}{3\sqrt{\pi}}\left(e^{-\frac{v^2}{1}}+2e^{-\frac{(v-2)^2}{1}}\right)(1+0.01\cos(0.5x)). \quad (3\text{-}10)$$

$$f(x,v,0)=\frac{1}{3\sqrt{\pi}}\left(e^{-\frac{v^2}{1}}+2e^{-\frac{(v-3)^2}{1}}\right)(1+0.01\cos(0.5x)) \quad (3\text{-}11)$$

$$f(x,v,0)=\frac{1}{3\sqrt{\pi}}\left(e^{-\frac{v^2}{1}}+2e^{-\frac{(v-4)^2}{1}}\right)(1+0.01\cos(0.5x)). \quad (3\text{-}12)$$

$$f(x,v,0)=\frac{1}{3\sqrt{\pi}}\left(e^{-\frac{v^2}{1}}+2e^{-\frac{(v-5)^2}{1}}\right)(1+0.01\cos(0.5x)) \quad (3\text{-}13)$$

The initial conditions and the simulation results are shown in Figure 3-12 to Figure 3-15.

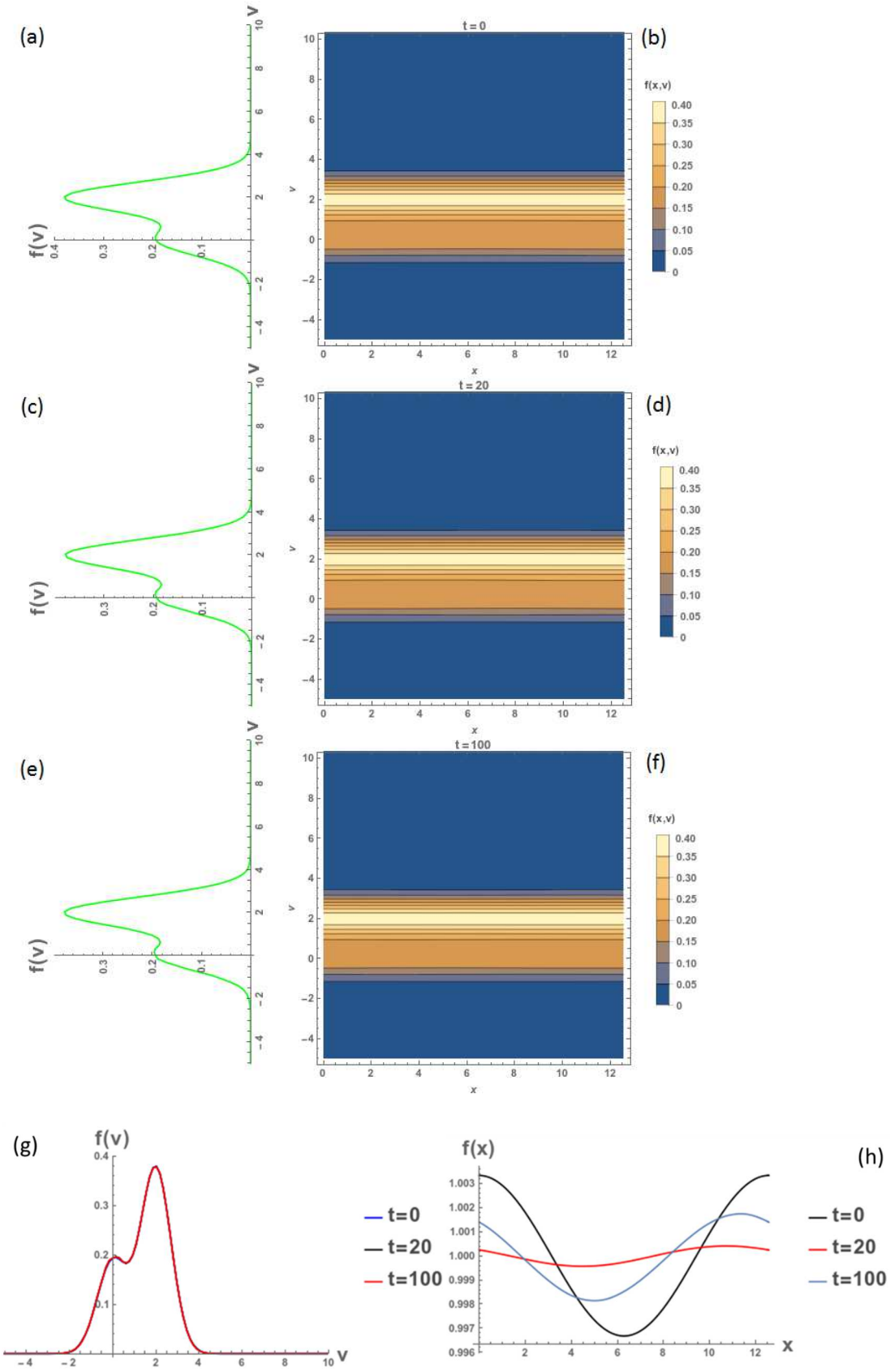

Figure 3-12 Free streaming electrons of Eq.(3-10). (a) Velocity distribution in t = 0 ω_p^-

[1]. (b) Phase space diagram in t = 0 ω_p^{-1}. (c) Velocity distribution in t = 20 ω_p^{-1}. (d) Phase space diagram in t = 20 ω_p^{-1}. (e) Velocity distribution in t = 100 ω_p^{-1}. (f) Phase space diagram in t = 100 ω_p^{-1}. (g) Velocity distribution in different time t. (h) Number density in different time t.

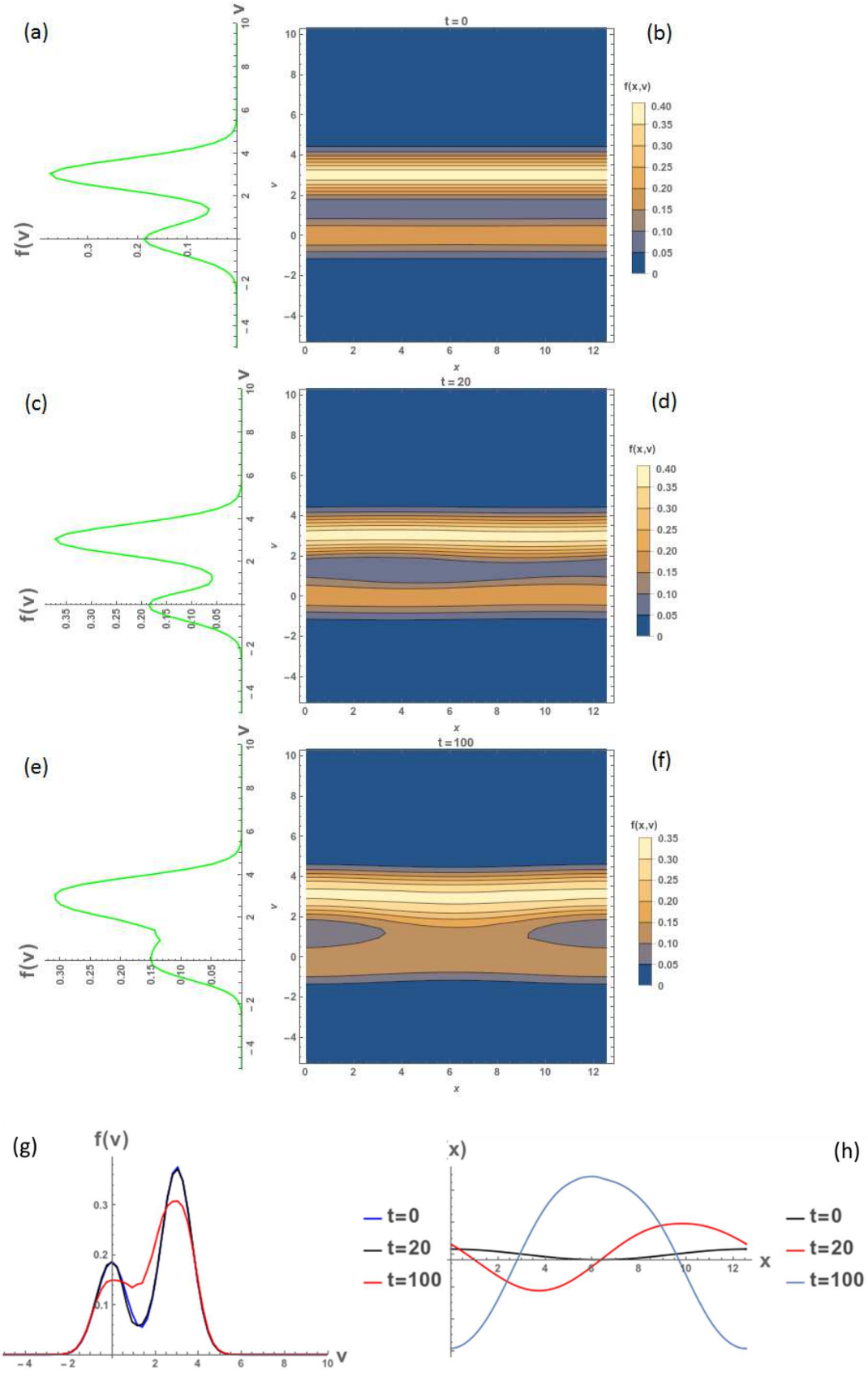

Figure 3-13 Free streaming electrons of Eq.(3-11). (a) Velocity distribution in t = 0 ω_p^-

[1]. (b) Phase space diagram in t = 0 ω_p^{-1}. (c) Velocity distribution in t = 20 ω_p^{-1}. (d) Phase space diagram in t = 20 ω_p^{-1}. (e) Velocity distribution in t = 100 ω_p^{-1}. (f) Phase space diagram in t = 100 ω_p^{-1}. (g) Velocity distribution in different time t. (h) Number density in different time t.

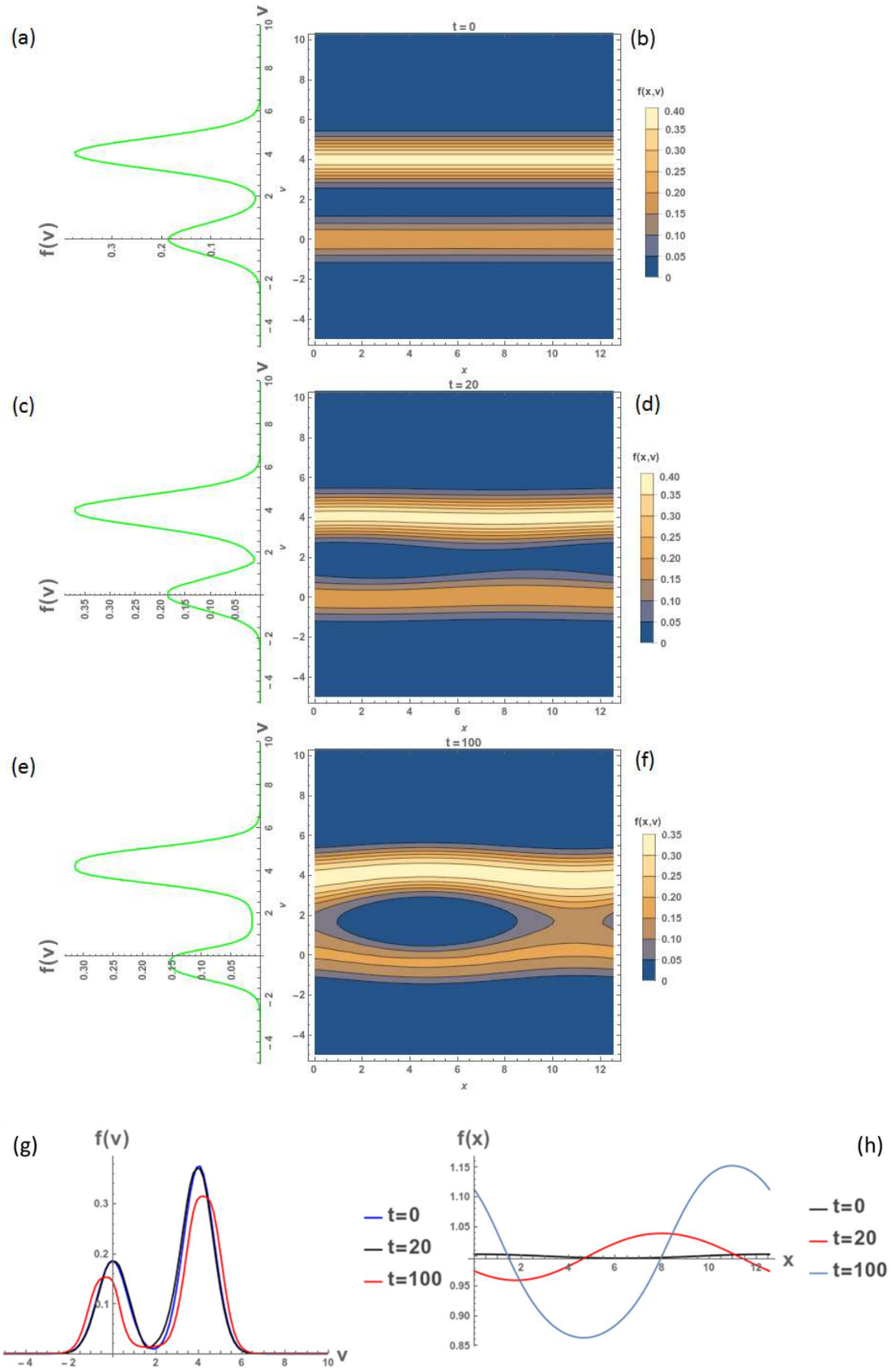

Figure 3-14 Free streaming electrons of Eq.(3-12). (a) Velocity distribution in t = 0 ω_p^-

[1]. (b) Phase space diagram in t = 0 ω_p^{-1}. (c) Velocity distribution in t = 20 ω_p^{-1}. (d) Phase space diagram in t = 20 ω_p^{-1}. (e) Velocity distribution in t = 100 ω_p^{-1}. (f) Phase space diagram in t = 100 ω_p^{-1}. (g) Velocity distribution in different time t. (h) Number density in different time t.

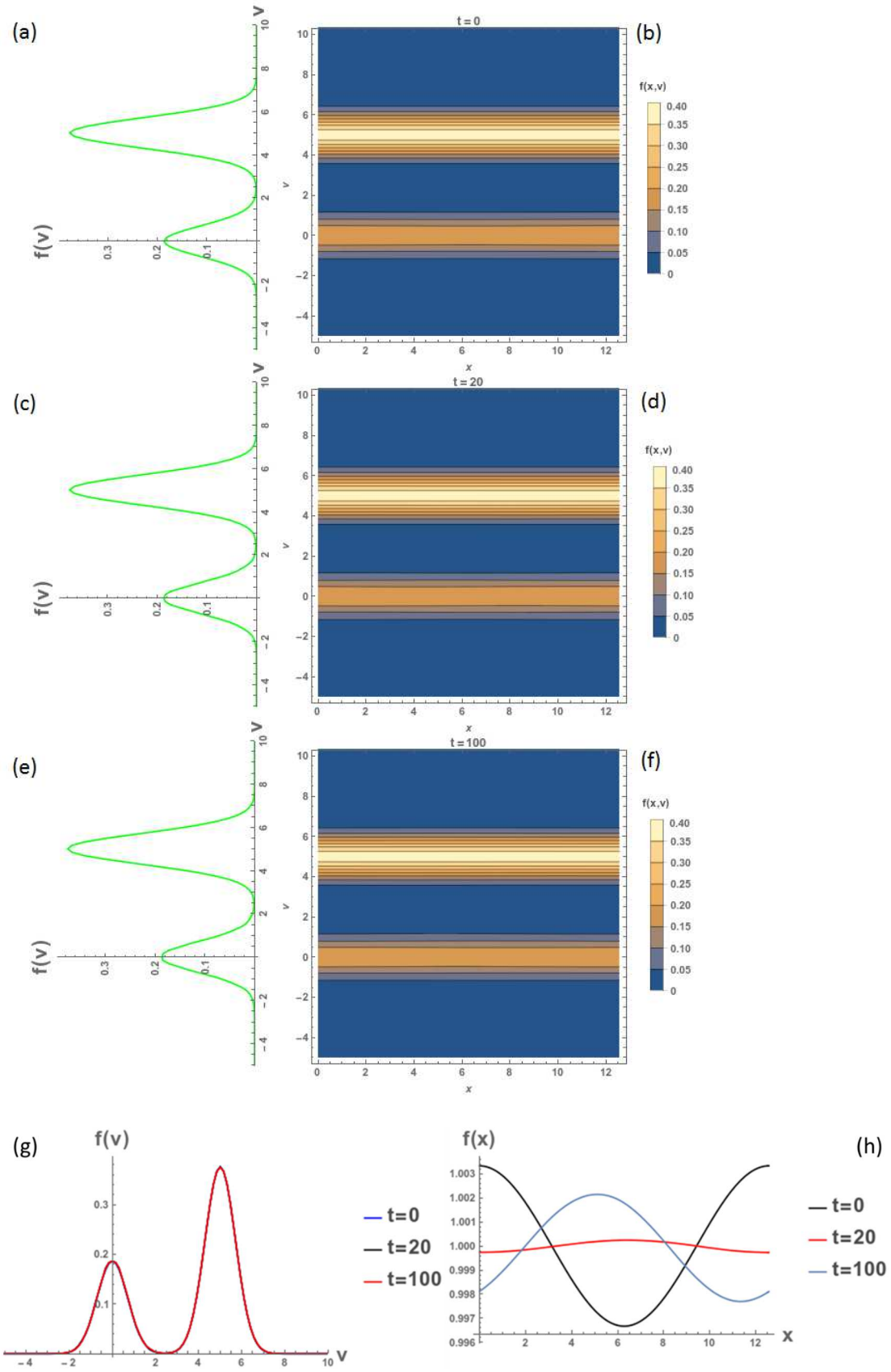

Figure 3-15 Free streaming electrons of Eq.(3-13). (a) Velocity distribution in t = 0 ω_p^-

[1]. (b) Phase space diagram in t = 0 ω_p^{-1}. (c) Velocity distribution in t = 20 ω_p^{-1}. (d) Phase space diagram in t = 20 ω_p^{-1}. (e) Velocity distribution in t = 100 ω_p^{-1}. (f) Phase space diagram in t = 100 ω_p^{-1}. (g) Velocity distribution in different time t. (h) Number density in different time t.

3.3 Discussion of results

The energy conservation should be checked in simulating free streaming electron beams. The calculation methods of total energy, kinetic energy, and electrical energy are shown in section 2.6.2. The simulating free-streaming electrons with initial condition in Eq.(3-11) is used to verify the energy conservation. The energy of simulating free-streaming electrons are shown in Figure 3-16. The total energy variation is less than 1.012% after 100 ω_p^{-1}. The energy conservation test on our simulations show that the results are convincing.

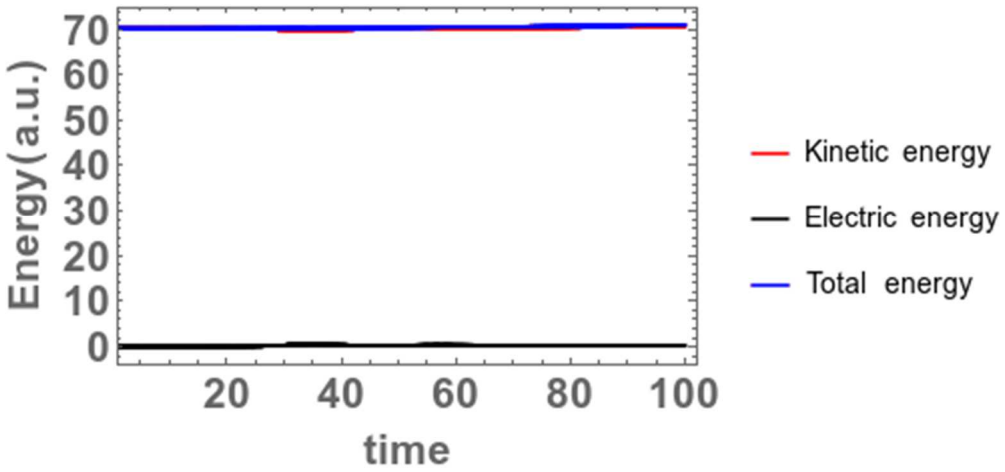

Figure 3-16 Checking of energy conservation of free-stream electrons simulation.

Figure 3-4, Figure 3-8, and Figure 3-12, are the simulation results for $v_b = 2$ and $v_{th} = 1$ but with different γ. The three figures show that no instability appeared. Due to the thermal velocity v_{th} for both groups of electrons, the instability is diffused and doesn't grow. In Figure 3-7, Figure 3-11, and Figure 3-15, $v_b = 5$. The three figures show that the electron beams are

too fast, i.e., the centers of their distribution function are far away to have any effect. As a result, only when $v_b = 3$ and $v_b = 4$ the instability occurred. The growth rate of electric energy is shown in Figure 3-17 for $v_b = 3$ and Figure 3-18 for $v_b = 4$. The growth rate of electric field with different v_b and γ are shown in Appendix B. Table 3-1 shows the simulation growth rate in different initial conditions.

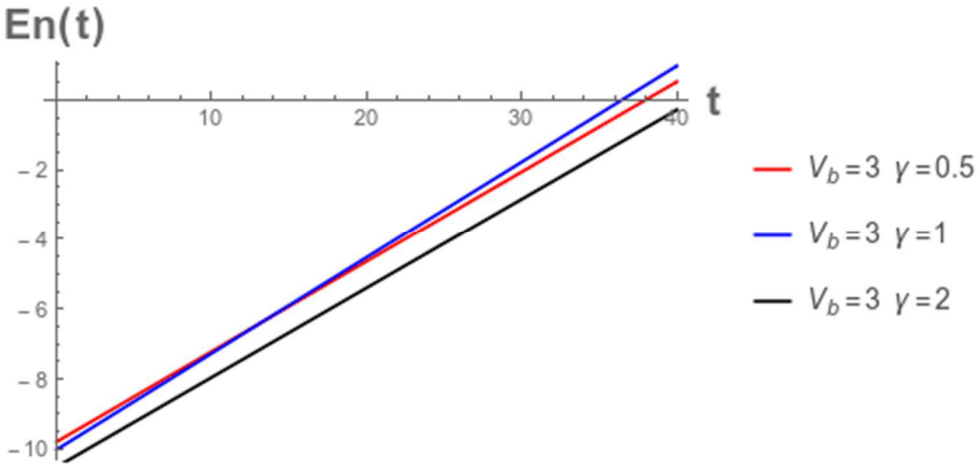

Figure 3-17 Growth rate of electric energy in $v_b = 3$.

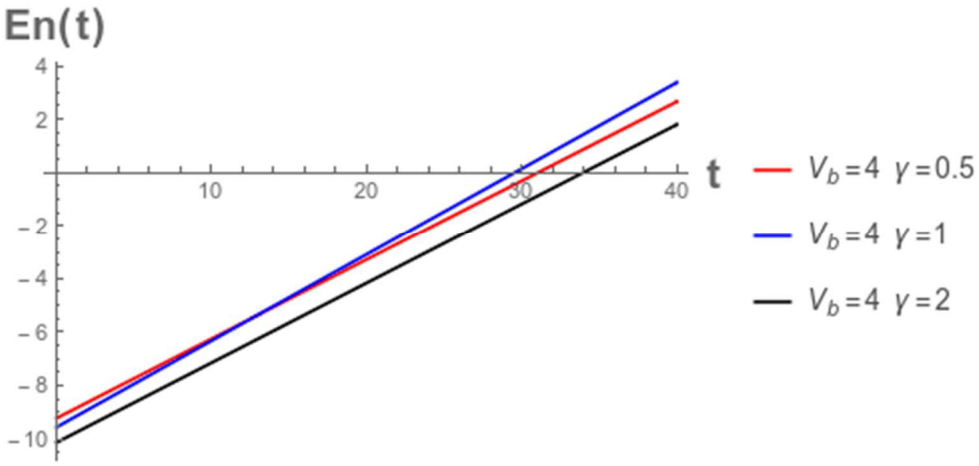

Figure 3-18 Growth rate of electric energy in $v_b = 4$.

There are no instability occurred for $v_b = 2$ and $v_b = 5$, so their electric energy doesn't change. For $v_b = 3$ and $v_{0b} = 4$, the electric energy grows. Both for $v_b = 3$ and $v_b = 4$, the maximum growth rate happened when $\gamma = 1$. For $v_b = 3$, growth rate of $\gamma = 1$ is 6.5% and 7.3% higher

than $\gamma = 0.5$ and $\gamma = 2$, respectively. For $v_b = 4$, growth rate of $\gamma = 1$ is 8% and 7.7% higher than $\gamma = 0.5$ and $\gamma = 2$, respectively. The growth rate in different γ doesn't change over 10%, and the largest growth rate appeared when $\gamma = 1$.

Table 3-1 growth rates in different initial conditions.

Initial condition	Growth rate(ω_p)
$v_b = 3$, $\gamma = 0.5$	0.258
$v_b = 3$, $\gamma = 1$	0.275
$v_b = 3$, $\gamma = 2$	0.255
$v_b = 4$, $\gamma = 0.5$	0.297
$v_b = 4$, $\gamma = 1$	0.323
$v_b = 4$, $\gamma = 2$	0.298

Chapter 4 Conclusion and summary

In this thesis, free-streaming electrons was simulated by using Vlasov solver in kinetic regime. The plasma simulation program was developed and benchmarked. The simulation code is developed to study the potential experiment on our pulsed-power system where free-streaming electrons can be generated by the strong electric field. Vlasov solver was benchmarked by simulating the two-stream instability and studying the growth rate. The total energy was calculated and ensured being conserved in our simulation. After the code is benchmarked, we used it to simulate the instability of free-streaming electrons in a background plasma. Free-streaming electrons with thermal velocity v_{th}, different beam velocity v_b, and different ration between the number density of the free-streaming electrons to the background electrons γ were simulated. The energy conservation was ensured in simulation. The growth of instability occurs between $v_b < 2$ in two-stream instability. In free-streaming electrons, growth of instability occurs when beam velocity $v_b = 3$ and $v_b = 4$. No instability occurs for $v_b = 2$ and $v_b = 5$. For $v_b = 3$, the growth rate is 0.258, 0.275, and 0.255 for $\gamma = 0.5$, $\gamma = 1$, and $\gamma = 2$, respectively. For $v_b = 4$, growth rate was 0.297, 0.323, and 0.298 for $\gamma = 0.5$, $\gamma = 1$, and $\gamma = 2$, respectively. The highest growth rate of $v_b = 3$ and $v_b = 4$ occurred when $\gamma = 1$. For $v_b = 3$, growth rate of $\gamma = 1$ was 6.5% and 7.3% higher than $\gamma = 0.5$ and $\gamma = 2$, respectively. For $v_b = 4$, growth rate of $\gamma = 1$ was 8% and 7.7% higher than $\gamma = 0.5$ and $\gamma = 2$, respectively. Nevertheless, the growth rate in different γ doesn't change over 10%.

Notice that if the total number density of electrons n_e including free-streaming electrons and the background electrons are not the same as number density of ions n_i, total charge isn't zero. In that case, Poisson's equation may not be solved with periodic boundary condition. To solve this kind of problems, we can set a huge simulation length L in real space x and apply other kinds of boundary conditions to solve this problem, such as Neumann boundary

condition setting differential of any quantities being zero on the boundary. An electron source or sink on the boundary is an alternative solution.

Vlasov solver can be used in simulation plasma phenomena widespread in both laboratory and space plasmas so it can be used in simulating and compared with experiment results or observation data. In the near future, the boundary condition can be changed as described previously to simulate free-streaming electrons with nonzero total charge density in plasma. Furthermore, Vlasov solver will be expanded to a two-dimensional program. Adding magnetic field in it so that it can be used to solve a problem in electromagnetic field. Depending on what experiments are constructed in our lab, different extensions of the code will be developed in the future.

Reference

[1]Balsara, Dinshaw S., Higher-order accurate space-time schemes for computational astrophysics—Part I: finite volume methods. Living Rev. Comput. Astrophys. **3:2**, 2017.

[2]Burden, Richard L., Faires, J. Douglas, Numerical Analysis (9th ed.). Brooks/Cole, 2011.

[3]Cheng, C. Z., Knorr, G., The integration of the Vlasov equation in configuration space. J. Comput. Phys. **22**, 330-351, 1976.

[4]Colella P., Woodward P., The piecewise parabolic method (PPM) for gas-dynamical simulations. J. Comput. Phys. **54**, 174–201, 1984.

[5]Colella P., Sekora Michael D., A limiter for PPM that preserves accuracy at smooth extrema. J. Comput, Phys, **227:7069**, 2008.

[6]Filbet, Francis, Sonnendrücker, Eric, Comparison of Eulerian Vlasov Solvers. J. Comput. Phys. **150:3**, 247-266, 2002.

[7]Godunov, S. K., A Difference Scheme for Numerical Solution of Discontinuous Solution of Hydrodynamic Equations. Math. Sbornik. **47**, 271–306, 1959

[8]LeVeque, Randall J., Finite Volume Methods for Hyperbolic Problems. Cambridge university press, 2004.

[9]Ustyugov, Sergey D., Piecewise parabolic method on a local stencil for magnetized supersonic turbulence simulation. J. Comput. Phys. **228**, 7614–7633, 2009.

[10]van Leer, B., Towards the ultimate conservative difference scheme V. A second-order sequel to Godunov's method. J. Comput. Phys. **32**, 101–136, 1979.

Appendix A Calculation of integration in PPM

To determine this third-degree polynomial, $f(x_i)$ is considered in the range between i-2 to i+1 for $f_{i,-}$.

$$f(x)=a_0+a_1(x-x_{i-\frac{1}{2}})+a_2(x-x_{i-\frac{1}{2}})^2+a_3(x-x_{i-\frac{1}{2}})^3. \tag{A-1}$$

Eq.(A-1) can be solved in the following integration.

$$\begin{aligned}
\bar{f}^n_{i-2}&=\frac{1}{\Delta x}\int_{i-\frac{5}{2}}^{i-\frac{3}{2}} f(x)dx\,,\\
\bar{f}^n_{i-1}&=\frac{1}{\Delta x}\int_{i-\frac{3}{2}}^{i-\frac{1}{2}} f(x)dx,\\
\bar{f}^n_{i}&=\frac{1}{\Delta x}\int_{i-\frac{1}{2}}^{i+\frac{1}{2}} f(x)dx,\\
\bar{f}^n_{i+1}&=\frac{1}{\Delta x}\int_{i+\frac{1}{2}}^{i+\frac{3}{2}} f(x)dx\,.
\end{aligned} \tag{A-2}$$

The indefinite integral of Eq.(A-1) is

$$\int f(x)dx=a_0x+\frac{a_1}{2}(x-x_{i-\frac{1}{2}})^2+\frac{a_2}{3}(x-x_{i-\frac{1}{2}})^3+\frac{a_3}{4}(x-x_{i-\frac{1}{2}})^4. \tag{A-3}$$

Therefore, the integration in Eq.(A-2) become

$$\begin{cases}
\bar{f}^n_{i-2}\Delta x=a_0\Delta x-\dfrac{a_1}{2}(3\Delta x)^2+\dfrac{a_2}{3}(7\Delta x)^3-\dfrac{a_3}{4}(15\Delta x)^4\\
\bar{f}^n_{i-1}\Delta x=-a_0\Delta x+\dfrac{a_1}{2}\Delta x^2-\dfrac{a_2}{3}\Delta x^3+\dfrac{a_3}{4}\Delta x^4\\
\bar{f}^n_{i}\Delta x=a_0\Delta x+\dfrac{a_1}{2}\Delta x^2+\dfrac{a_2}{3}\Delta x^3+\dfrac{a_3}{4}\Delta x^4\\
\bar{f}^n_{i+1}\Delta x=a_0\Delta x+\dfrac{a_1}{2}(3\Delta x)^2+\dfrac{a_2}{3}(7\Delta x)^3+\dfrac{a_3}{4}(15\Delta x)^4
\end{cases}. \tag{A-4}$$

These four equation in Eq.(A-4) can be calculated using simple algebra.

$$f_{i,-}=\left[\frac{7}{12}\left(\bar{f}^n_{i-1}+\bar{f}^n_{i}\right)-\frac{1}{12}\left(\bar{f}^n_{i+1}+\bar{f}^n_{i-2}\right)\right]. \tag{A-5}$$

To determine this third-degree polynomial, $f(x_i)$ is considered in the range between i-1 to i+2 for $f_{i,+}$.

$$f(x)=a_0+a_1(x-x_{i+\frac{1}{2}})+a_2(x-x_{i+\frac{1}{2}})^2+a_3(x-x_{i+\frac{1}{2}})^3. \tag{A-6}$$

Eq.(A-6) can be solved in the following integration.

$$\begin{aligned}
\vec{f}^{n}_{i-1}&=\frac{1}{\Delta x}\int_{i-\frac{3}{2}}^{i-\frac{1}{2}} f(x)dx,\\
\vec{f}^{n}_{i}&=\frac{1}{\Delta x}\int_{i-\frac{1}{2}}^{i+\frac{1}{2}} f(x)dx,\\
\vec{f}^{n}_{i+1}&=\frac{1}{\Delta x}\int_{i+\frac{1}{2}}^{i+\frac{3}{2}} f(x)dx,\\
\vec{f}^{n}_{i+2}&=\frac{1}{\Delta x}\int_{i+\frac{3}{2}}^{i+\frac{5}{2}} f(x_i)dx.
\end{aligned} \tag{A-7}$$

The indefinite integral of Eq.(A-6) is

$$\int f(x)dx=a_0x+\frac{a_1}{2}(x-x_{i+\frac{1}{2}})^2+\frac{a_2}{3}(x-x_{i+\frac{1}{2}})^3+\frac{a_3}{4}(x-x_{i+\frac{1}{2}})^4. \tag{A-8}$$

Therefore, the integration in Eq.(A-7) become

$$\begin{cases}
\vec{f}^{n}_{i-1}\Delta x=a_0\Delta x-\frac{a_1}{2}(3\Delta x)^2+\frac{a_2}{3}(7\Delta x)^3-\frac{a_3}{4}(15\Delta x)^4\\
\vec{f}^{n}_{i}\Delta x=-a_0\Delta x+\frac{a_1}{2}\Delta x^2-\frac{a_2}{3}\Delta x^3+\frac{a_3}{4}\Delta x^4\\
\vec{f}^{n}_{i+1}\Delta x=a_0\Delta x+\frac{a_1}{2}\Delta x^2+\frac{a_2}{3}\Delta x^3+\frac{a_3}{4}\Delta x^4\\
\vec{f}^{n}_{i+2}\Delta x=a_0\Delta x+\frac{a_1}{2}(3\Delta x)^2+\frac{a_2}{3}(7\Delta x)^3+\frac{a_3}{4}(15\Delta x)^4
\end{cases}. \tag{A-9}$$

These four equation in Eq.(A-9) can be calculated using simple algebra.

$$f_{i,+}=\left[\frac{7}{12}\left(\vec{f}^{n}_{i}+\vec{f}^{n}_{i+1}\right)-\frac{1}{12}\left(\vec{f}^{n}_{i+2}+\vec{f}^{n}_{i-1}\right)\right]. \tag{A-10}$$

To determine this third-degree polynomial, $f(x_i)$ is considered in the range between i-3 to i for $f_{i-1,-}$.

$$f(x)=a_0+a_1(x-x_{i-\frac{3}{2}})+a_2(x-x_{i-\frac{3}{2}})^2+a_3(x-x_{i-\frac{3}{2}})^3. \tag{A-11}$$

Eq.(A-1) can be solved in the following integration.

$$\vec{f}^{n}_{i-3}=\frac{1}{\Delta x}\int_{i-\frac{7}{2}}^{i-\frac{5}{2}} f(x_i)dx, \tag{A-12}$$

$$\vec{f}^{n}_{i-2}=\frac{1}{\Delta x}\int_{i-\frac{5}{2}}^{i-\frac{3}{2}} f(x)dx\,,$$

$$\vec{f}^{n}_{i-1}=\frac{1}{\Delta x}\int_{i-\frac{3}{2}}^{i-\frac{1}{2}} f(x)dx,$$

$$\vec{f}^{n}_{i}=\frac{1}{\Delta x}\int_{i-\frac{1}{2}}^{i+\frac{1}{2}} f(x)dx.$$

The indefinite integral of Eq.(A-1) is

$$\int f(x)dx=a_0x+\frac{a_1}{2}(x-x_{i-\frac{3}{2}})^2+\frac{a_2}{3}(x-x_{i-\frac{3}{2}})^3+\frac{a_3}{4}(x-x_{i-\frac{3}{2}})^4. \tag{A-13}$$

Therefore, the integration in Eq.(A-2) become

$$\begin{cases}\vec{f}^{n}_{i-3}\Delta x=a_0\Delta x-\frac{a_1}{2}(3\Delta x)^2+\frac{a_2}{3}(7\Delta x)^3-\frac{a_3}{4}(15\Delta x)^4\\ \vec{f}^{n}_{i-2}\Delta x=-a_0\Delta x+\frac{a_1}{2}\Delta x^2-\frac{a_2}{3}\Delta x^3+\frac{a_3}{4}\Delta x^4\\ \vec{f}^{n}_{i-1}\Delta x=a_0\Delta x+\frac{a_1}{2}\Delta x^2+\frac{a_2}{3}\Delta x^3+\frac{a_3}{4}\Delta x^4\\ \vec{f}^{n}_{i}\Delta x=a_0\Delta x+\frac{a_1}{2}(3\Delta x)^2+\frac{a_2}{3}(7\Delta x)^3+\frac{a_3}{4}(15\Delta x)^4\end{cases}. \tag{A-14}$$

These four equation in Eq.(A-4) can be calculated using simple algebra.

$$f_{i-1,-}=\left[\frac{7}{12}\left(\vec{f}^{n}_{i-2}+\vec{f}^{n}_{i-1}\right)-\frac{1}{12}\left(\vec{f}^{n}_{i}+\vec{f}^{n}_{i-3}\right)\right]. \tag{A-15}$$

To determine this third-degree polynomial, $f(x_i)$ is considered in the range between i-1 to i+2 for $f_{i,+}$.

$$f(x)=a_0+a_1(x-x_{i+\frac{3}{2}})+a_2(x-x_{i+\frac{3}{2}})^2+a_3(x-x_{i+\frac{3}{2}})^3. \tag{A-16}$$

Eq.(A-6) can be solved in the following integration.

$$\vec{f}^{n}_{i}=\frac{1}{\Delta x}\int_{i-\frac{1}{2}}^{i+\frac{1}{2}} f(x)dx,$$

$$\vec{f}^{n}_{i+1}=\frac{1}{\Delta x}\int_{i+\frac{1}{2}}^{i+\frac{3}{2}} f(x)dx\,, \tag{A-17}$$

$$\vec{f}^{n}_{i+2}=\frac{1}{\Delta x}\int_{i+\frac{3}{2}}^{i+\frac{5}{2}} f(x_i)dx,$$

$$\vec{f}^{n}_{i+3}=\frac{1}{\Delta x}\int_{i+\frac{5}{2}}^{i+\frac{7}{2}} f(x_i)dx.$$

The indefinite integral of Eq.(A-6) is

$$\int f(x)dx = a_0 x+\frac{a_1}{2}(x-x_{i+\frac{3}{2}})^2+\frac{a_2}{3}(x-x_{i+\frac{3}{2}})^3+\frac{a_3}{4}(x-x_{i+\frac{3}{2}})^4. \quad \text{(A-18)}$$

Therefore, the integration in Eq.(A-7) become

$$\begin{cases} \vec{f}^{n}_{i}\Delta x=a_0\Delta x-\frac{a_1}{2}(3\Delta x)^2+\frac{a_2}{3}(7\Delta x)^3-\frac{a_3}{4}(15\Delta x)^4 \\ \vec{f}^{n}_{i+1}\Delta x=-a_0\Delta x+\frac{a_1}{2}\Delta x^2-\frac{a_2}{3}\Delta x^3+\frac{a_3}{4}\Delta x^4 \\ \vec{f}^{n}_{i+2}\Delta x=a_0\Delta x+\frac{a_1}{2}\Delta x^2+\frac{a_2}{3}\Delta x^3+\frac{a_3}{4}\Delta x^4 \\ \vec{f}^{n}_{i+3}\Delta x=a_0\Delta x+\frac{a_1}{2}(3\Delta x)^2+\frac{a_2}{3}(7\Delta x)^3+\frac{a_3}{4}(15\Delta x)^4 \end{cases} . \quad \text{(A-19)}$$

These four equation in Eq.(A-9) can be calculated using simple algebra.

$$f_{i+1,+}=\left[\frac{7}{12}(\vec{f}^{n}_{i+1}+\vec{f}^{n}_{i+2})-\frac{1}{12}(\vec{f}^{n}_{i+3}+\vec{f}^{n}_{i})\right], \quad \text{(A-20)}$$

Appendix B Figures of the electrical energy of free-streaming electrons

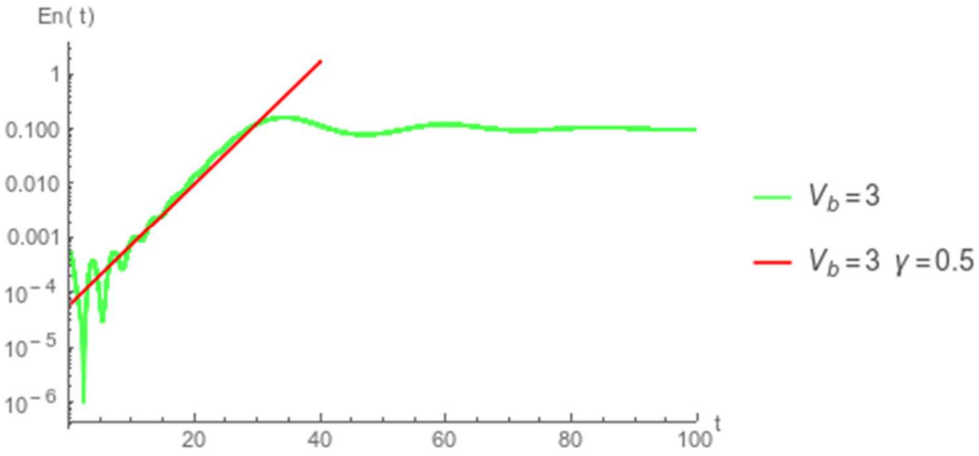

Figure B-1 Growth rate of free-streaming electrons with $v_b = 3$, $\gamma = 0.5$

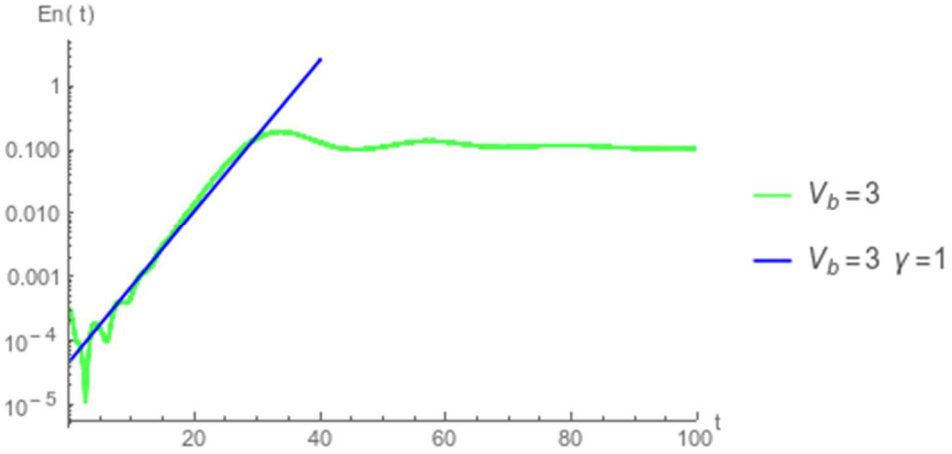

Figure B-2 Growth rate of free-streaming electrons with $v_b = 3$, $\gamma = 1$

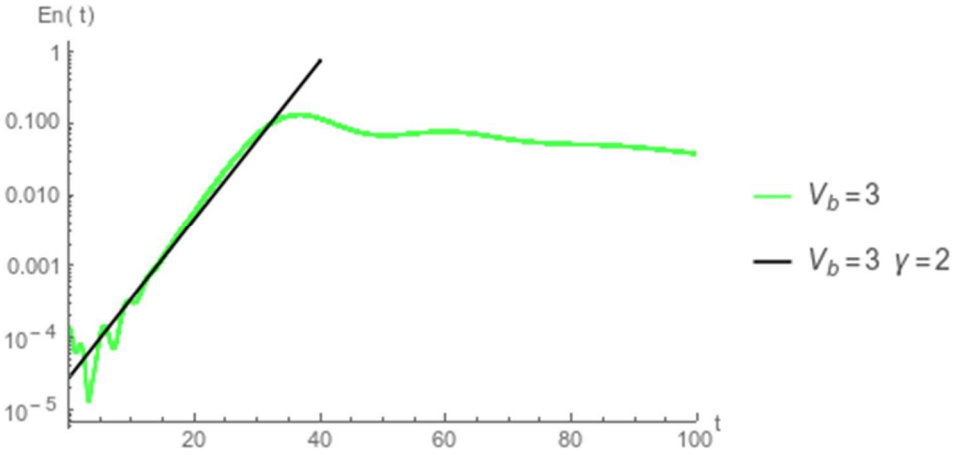

Figure B-3 Growth rate of free-streaming electrons with $v_b = 3$, $\gamma = 2$

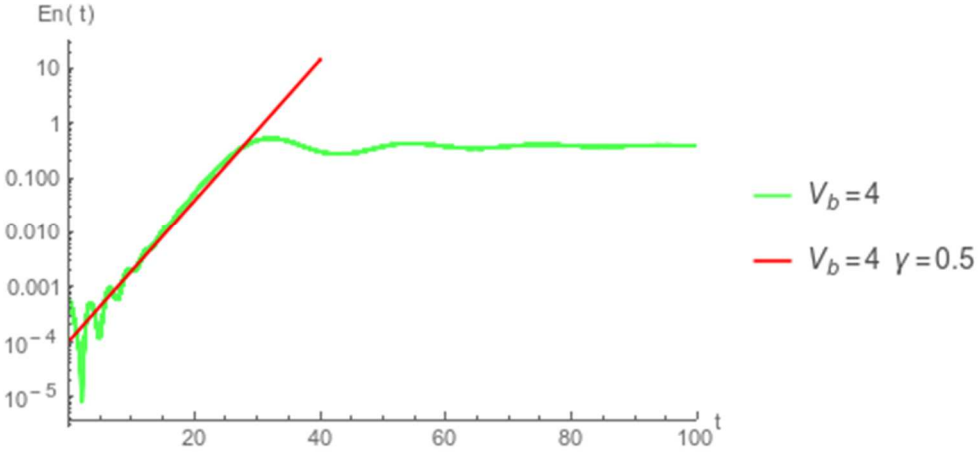

Figure B-4 Growth rate of free-streaming electrons with $v_b = 4$, $\gamma = 0.5$

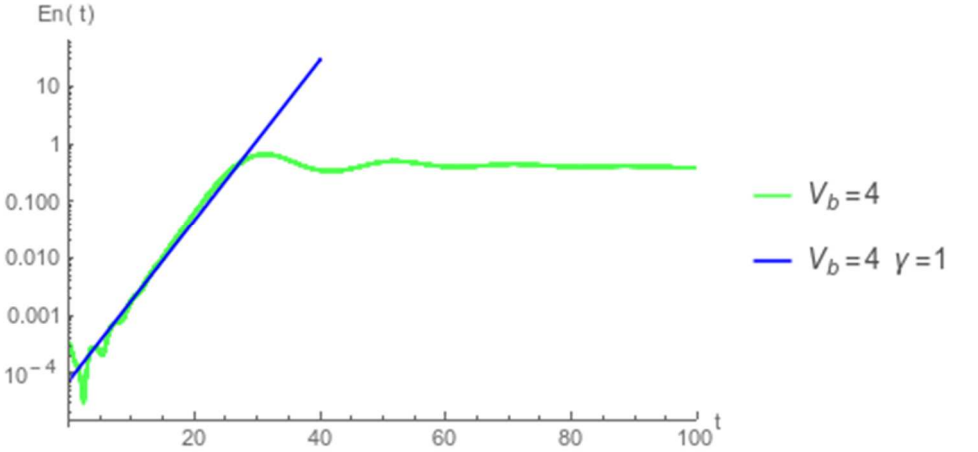

Figure B-5 Growth rate of free-streaming electrons with $v_b = 4$, $\gamma = 1$

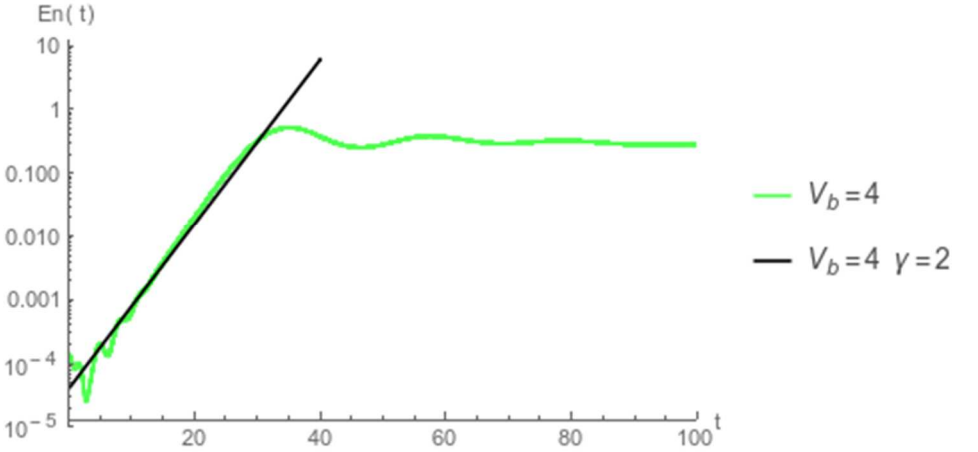

Figure B-6 Growth rate of free-streaming electrons with $v_b = 4$, $\gamma = 2$

Appendix C List of data films of Vlasov solver

The simulation data films are listed in this section, and the naming method are explained.
Naming method of folders:
In “two_stream_instability” folder,

“methods”_”vth value”_”vb value”_”grids in both x and v”_”perturbation value”

Ex:

If using PLM first and PPM second with β=0.5, v_{th}=0.3, $v_b=\sqrt{\frac{3}{2}}$, grids=128, perturbation=0.01*function, the folder name is “plmppm_vth0.3_vbrt1.5_128”

P.S. The folders using PPM first and PLM second with β=0.5 won’t show the methods in folder names, and the folders using perturb=0.01*function won’t show as well.

In “free_streaming_electrons” folder,

”vth value”_”γ””vb value”

Ex:

If using v_{th}=1, v_b=3, γ=0.5, the folder name is “vth1_0.5vb3”

P.S. All folders are used PPM first and PLM second with β=0.5, and grids=128.

Folder position:

Vlasovdata

- **two_stream_instability**
  - **plmppm_vth0.3_vbrt1.5_128**
  - **plm_vth0.3_vbrt1.5_128**
  - **plm_vth1_vbrt1.5_128**
  - **ppmplm_vth1_vbrt1.5_64**
  - **ppmplm_vth1_vbrt1.5_128**
  - **ppm_vth0.1_vbrt1.5_256**
  - **ppm_vth0.5_vbrt1.5_256**
  - **ppm_vth1_vbrt1.5_128**
  - **ppm_vth1_vbrt1.5_256**
  - **vth0.3_vb1.9**
  - **vth0.3_vb2.1**
  - **vth0.3_vbrt1.5_64**
  - **vth0.3_vbrt1.5_128**
  - **vth0.3_vbrt1.5_256**
  - **vth0.5_vb1.9_256**

vth0.5_vb2.1_256

vth1_vbrt1.5_0.1

vth1_vbrt1.5_64_0.1

vth1_vbrt1.5_128_0.1

vth1_vbrt1.5_256_0.1

vth1_vbrt1.5_512_0.1

free_streaming_electrons

vth1_0.5vb2

vth1_0.5vb3

vth1_0.5vb4

vth1_0.5vb5

vth1_1vb2

vth1_1vb3

vth1_1vb4

vth1_1vb5

vth1_2vb2

vth1_2vb3

vth1_2vb4

vth1_2vb5

The naming methods of films in each folder are shown in the following.

"***data#.txt***" phase space plot at t=#

"***rhodata#.txt***" number density at t=#

"***phidata#.txt***" electric potential at t=#

"***efxdata#.txt***" electric field at t=#

"***acldata#.txt***" acceleration at t=#

"***eedata.txt***" electric energy

"***kedata.txt***" kinetic energy

"***tedata.txt***" total energy